University of Louisville

ThinkIR: The University of Louisville's Institutional Repository

8-2005

Development of simplified models for crashworthiness analysis.

Yucheng Liu 1976-
University of Louisville

Follow this and additional works at: https://ir.library.louisville.edu/etd

DEVELOPMENT OF SIMPLIFIED MODELS FOR CRASHWORTHINESS ANALYSIS

By

Yucheng Liu
B.Sc. Hefei University of Technology, 1997
M.S. University of Louisville, 2003

A Dissertation
Submitted in partial fulfillment of the requirements for the degree of

Doctor of Philosophy

Department of Mechanical Engineering
University of Louisville
Louisville, Kentucky

August 2005

DEVELOPMENT OF SIMPLIFIED MODELS FOR CRASHWORTHINESS ANALYSIS

By

Yucheng Liu
B.Sc. Hefei University of Technology, 1997
M.S., University of Louisville, 2003

A Dissertation Approved on

July 7, 2005

by the following Dissertation Committee

Michael L. Day,   Director

Glen Prater, Jr.

Julius P. Wong

Ellen G. Brehob

J.P. Mohsen

DEDICATION

This dissertation is dedicated to my parents

Mr. Wenlong Liu

and

Mrs. Rong Jin

who have given me invaluable educational opportunities.

ACKNOWLEDGMENTS

I would first like to express my sincere gratitude to Dr. Michael L. Day, my dissertation committee chair, for his support and guidance during this research. Dr. Day has been a patient, supportive, and conscientious advisor during this process. I also would like to express my gratitude to Dr. Glen Prater for his guidance and support throughout the years during which I have had the privilege of working for him—especially during my dissertation. Very special thanks go to Dr. Julius P. Wong for his invaluable help through these years and for serving on my committee. I also would like to thank Dr. Ellen Brehob and Dr. J. P. Mohsen for serving on my committee. Thanks also go to the faculty and staff of the Department of Mechanical Engineering for their support.

I am deeply indebted to my parents, Wenlong Liu and Rong Jin, for all of their love, support, faith, and encouragement throughout this dissertation and my life. I could never be who I am today without them. I am also indebted to my uncle, my aunt, and all my family members for their unconditional support and caring. Particularly, I am forever grateful to my grandpa and grandma. Although they have passed away, I will never forget the selfless love they gave me, and the countless hours they spent with me during my childhood. My dear grandpa and grandma, I love you! I will always do my best to make you proud of me.

Last but not least, I would like to thank all of my friends, both in the U. S. and in China, for their support, advice, and friendship that have helped me to remain focused on

the ultimate objective and motivated to accomplish the mission. Many thanks are also expressed to Miss Samantha Bartels for her help in editing this dissertation.

ABSTRACT

DEVELOPMENT OF SIMPLIFIED MODEL FOR CRASHWORTHINESS ANALYSIS

Yucheng Liu

August 5, 2005

Simplified modeling generates a great deal of interest in the area of crashworthiness analysis. Modeling methods used to create simplified computer models for crashworthiness have been well developed. In advanced simplified models, researchers develop simplified elements that can correctly predict structure's crash behavior based on the existing collapse theories. These developed simplified elements then are applied to develop the simplified models.

Nevertheless, most of the exiting collapse theories are regarding the thin-walled box section beams. However, in addition to the box section member, the channel section member is another popular member and is widely used in engineering for architectural structures, vehicles, and etc. Therefore, to simplify the thin-walled channel section beams, new collapse theory is required to predict the crash behavior for such beams. This topic is the focus of this dissertation.

This dissertation develops a mathematical model to predict the crash behavior of the thin-walled channel section beams based on their real collapse mechanisms. The derived math formulae are verified through several basic applications. After that, both the existing collapse theories and the developed collapse theory regarding the thin-walled channel section beams are applied to simplify the detailed truck chassis model. The

developed simplified model is used for crashworthiness analysis and the results are compared to those from the detailed model. The developed theory and the modeling method are then validated through the comparison.

Additionally, in developing the simplified truck chassis model, the cross members that were modeled using coarse shell elements in previous simplified models are remodeled using simple elements. Two of the simplified modeling methods, the superelement method and the equivalent beam method, are utilized to generate the simplified models for the cross members of the truck chassis model. The principle of both methods is to use simple elements to transfer the original members' mass and stiffness matrices. The equivalent beam method is recommended after comparison of the results of the crashworthiness analyses of each method.

The primary contributions of this work are first, the derivation of crash theory that can predict the crash behavior of thin-walled channel section beams. The second is the use of equivalent beams to simplify the cross members within truck chassis models. Finally, a simplified modeling methodology is presented and evaluated.

All the theory and modeling method developed in this work are applied for creating simplified models. Both the simplified and detailed models are used for crashworthiness analyses, results show that the errors caused by the simplified models are fewer than 10% and the simplified models only take less than 10% of the computer time of the corresponding detailed models.

LIST OF TABLES

LIST OF FIGURES

TABLE OF CONTENTS

PAGE

CHAPTER

CHAPTER I

INTRODUCTION

1.1 Background

Crashworthiness is the ability of a vehicle to withstand a collision or crash and to prevent injuries to the occupants in the event of a vehicular accident. It is one of the most important criteria used in designing and evaluating a vehicle. Many manufacturers, research facilities and consumer protection groups need to perform crashworthiness analyses to test a vehicle's crash resistance ability and to better understand the vehicle's response during the crash. However, using real vehicles for the crashworthiness analysis is quite expensive because the crash test is a destructive test. Generally, in order to obtain qualified crashworthiness analysis results, multiple tests need to be conducted to assure the accuracy and the reproducibility of the test or to acquire the optimum design. Thus, numerous vehicle prototypes need to be produced and tested, which is extremely costly in terms of both time and money. Due to the necessity of crashworthiness analysis and the limitations of the real crash tests, computer analyses using finite element (FE) models, is warranted. This method can reasonably simulate the vehicle's crash process accurately at a reduced cost.

The FE method, first developed in the late 1950's, has evolved into a very useful tool available to engineers for solving problems in many different areas. In its early use, the FE method was primarily restricted to linear analyses. With the increased availability

1

of high performance computers, nonlinear finite analyses are increasingly being used in more applications, such as vehicle crashworthiness analyses. FEA has been integrated into many advanced CAD and CAE software programs to yield powerful computer tools such as ANSYS, NASTRAN, and LS-DYNA. These are extensively used in the area of dynamic and nonlinear analyses, including vehicle crashworthiness analysis. With the aid of these programs, the vehicle crash test can easily be simulated and observed on the computer, eliminating the need for producing and crushing numerous vehicle prototypes, thereby saving both time and money.

A standard procedure in conducting a crashworthiness analysis using engineering software is to create a FE model for the real structure, to define the crash test conditions, and to run the simulation. However, new problems arise because the crashworthiness analysis usually includes high-rate heavy loading, which requires a small time step size to simulate the load history. Meanwhile, as the vehicle structure becomes more complicated, the size of the respective FE model increases significantly. Thus, the computer simulation consumes a larger amount of computer resources and takes much longer to complete the crashworthiness analysis when using a detailed FE model that faithfully reflects the structure's physical geometry. Moreover, for some complicated models, the crash problems cannot even be effectively solved with current computational power. Therefore, it is necessary that new methods and modeling techniques be developed to decrease the size of the current detailed FE models, which reduces the calculations and saves computation time. One possible solution is simplified modeling, which chooses a coarse mesh or applies equivalent elements to build a simpler finite element model for crashworthiness analysis.

In addition, in an automotive design stage, designers usually need to attempt different schemes with different geometries and shapes to achieve an optimum design. In this case, to repeatedly generate detailed models with respect to each scheme appears unnecessarily time-consuming. Simplified modeling can effectively remove this inconvenience. With a basic simplified model, users may only need to make small changes or switch certain settings to achieve new models with different design schemes. Therefore, simplified models are also useful in an automotive design stage and can be used to replace the detailed models for approximately evaluating different designs.

1.2 Literature Review

In preparation for this research, previous literature on the subject of interest is reviewed to establish a solid background. The literature can be classified according to the following three areas:

1) Structural crashworthiness

2) Crashworthiness analysis

3) Development of simplified models

1.2.1 Structural Crashworthiness

In crashworthiness analysis, the response, or crash behavior, of the studied structures always receives the most attention.

Don O. Brush and Bo O. Almroth [1] demonstrate the classic buckling behavior of identical structural members subjected to axial crash loading in the book "Buckling of Bars, Plates, and Shells." In this book, the authors discuss common buckling problems

and develop the equilibrium and stability equations for bars, plates, and shells. The authors also provide some particular examples that demonstrate how to determine the critical load using the stability equations. They include the direct numerical solution of the governing nonlinear equations.

Ishiyama, Nishimura, and Tsuchiya [2] report a numerical study of the impact response of plane frame structures with thin-walled beam members to predict the deformation and absorbed energy of automobiles under crash loading. The researchers investigate the collapse characteristics of thin-walled beam members under crashing loads, describe the inelastic deformations of the frame structure, and verify the important assumptions and conclusions via crash tests.

E. Haug and A. De Rouvray [3] illustrate the numerical simulation and prediction of the crash response of metallic components and structures. The algorithms of the numerical crashworthiness simulation and prediction are developed in their research. To validate the developed numerical algorithms, a full car crash simulation is performed using the numerical method. The reliability of the numerical method is verified by comparing the results of the simulations and the experiments.

A. G. Mamalis, D. E. Manolakos, G. A. Demosthenous, and M. B. Ioannidis [4] study the crashworthy behavior of thin-walled structural components subjected to various loading conditions, i.e. static and dynamic axial loading and bending. The authors describe the loading and deformation characteristics of the collapsed shells and discuss the influence of the shell geometry and the material properties on these characteristics. Also, the structural features related to vehicle collisions are introduced and useful conclusions for vehicle design and manufacture are provided.

H. S. Kim and T. Wierzbicki [5] investigate the crush response of thin-walled prismatic columns under combined bending-compression collapse loading. They construct the initial and subsequent failure loci representing the interaction between the axial forces and the bending moment. In their work, the researchers formulate a problem in which rectangular cross-section beams with different aspect ratios are subjected to a prescribed translational and rotational displacement rate. They then generate numerical results after solving the problem. From the numerical results, they continue developing the corresponding initial and subsequent failure loci, which describe the anticipated crush behavior of thin-walled columns under combined loading.

A. A. A. Alghamdi [6] studies the buckling behavior of specific thin-walled aluminum frusta. The thin-walled aluminum frusta with different angles and differing thickness are axially crushed separately, and respective folding-crumpling mode is observed. In this paper, the load-displacement relationship between the frusta and the axially load and the final energy density of the frusta are selected to describe the frusta's buckling behavior. Also, the effect of its angle and thickness on the results is introduced. Then, the load-displacement curve and the energy density are specified as the functions of them.

From the reviewed crashworthiness literature, useful information is gained in the following areas:

1) Crash response of structural members including bars, plates, and thin-walled beams.

Crash response refers to the crash member's reaction to sudden damage or destruction on impact. In most cases, during the crashes, the crushing forces

that are transferred to the crash member, the energies absorbed by the crash member, and the displacement are the most important output parameters, and thus, typically used to describe the member's crash response.

For an identical crash response, the crushing force usually increases linearly with the displacement on the early stage of loading up to its maximum value and then decreases abruptly as the deformation proceeds. Additionally, the crashed member's displacement increases significantly right after the crash. Then, the rate of increase decreases as the deformation proceeds and goes to zero when the crashed member entirely stops. Finally, the characteristics of the absorbed energy are determined by the crushing force and the displacement.

Also, it is found from the above literature that many factors affect the member's crash response. The most important factors are the member's initial velocity, its thickness, and the material. From previous crash tests and numerical analyses, it is concluded that the maximum crushing force increases with the increasing of the initial velocity, thickness, or the crash member's yield stress.

2) The commonly used research methods that are applied to study the structure's crash behavior

From the literature mentioned in this section, it is found that the researchers usually use the experimental method and numerical analysis method to find the structure's crash response.

The experimental method involves acquiring the important crash outputs through real crash tests and then, studying the characteristics of the crashes based on the analysis of the acquired experimental data. The advantage of this method is that it is a direct way to describe the member's crash response. Another widely used method is the numerical analysis method. In this method, a numerical model is created for the crash member, current crash theories are applied to create its equations of motion and constitutive equations. Therefore, the crash member's crushing force and displacement are expressed by related formulae. After that, the crushing force and the displacement are solvable at successive instances of time using the integration method. This method is widely used to predict and estimate a single member's crash response. Due to the assumptions taken in building the equations and integrating over the time domain, the derived analytical solutions approximate the actual situation. As introduced above, both methods have their advantages and limitations, forcing researchers to apply both methods simultaneously to study and verify the crash problems.

1.2.2 Crashworthiness Analysis

1.2.2.1 Methods and Techniques Used for Crashworthiness Analysis

Computational technology, computer tools, and programs that can quickly perform complex calculations make complicated engineering problems easier to approach. With the evolution of the computer, numerous research methods are integrated into the

computer to help researchers study and simulate the structural crashworthiness analysis [7].

A. Toyama, K. Hatano, and E. Murakami [8] introduce an example of using numerical analysis to investigate vehicle crashworthiness. In their paper, the authors point out the limitations of the vehicle crash experiments. The crush characteristics and performance of a vehicle body can not be obtained experimentally due to the very short experimental time. Thus, the numerical analysis techniques using the finite element method can be applied to determine the behavior of vehicle components during the crash. A vehicle frontal crash simulation study is presented with the explicit FE code PAM-CRASH performing this simulation. The deformation modes, the transmitted force, and the internal energy are studied, and the detailed deformation mechanism of the vehicle body, which is impossible to make experimentally, is analyzed quantitatively.

U. N. Gandhi and S. J. Hu [9] build an analytical model directly from the crash test measurements using system identification techniques. The model is used for automotive crashworthiness analysis and for the parametric study. The analytical model includes two parts: a differential equation part consisting of mass, stiffness, and damping characteristics and a transfer function part consisting of an autoregressive moving average of white noise. The authors discuss a data-based approach in modeling automobile crashes with the procedure and numerical method of creating a data -based model being described intensively. To verify the approach they construct two simple models for frontal impact and for side impact. The comparison between the measured and the simulated results verifies that the data-based model developed in the research is

beneficial both when predicting the vehicle crash test results and when performing the parametric study.

C. Cosme, A. Ghasemi, and J. Gandevia (1999) [10] discuss the roles of different CAE tools in the design of heavy-duty truck frames and perform specific case studies to demonstrate how this technology is used. Two popular CAE tools, FEA and multi-body system simulation (MSS), along with a modal superposition technique known as component mode synthesis (CMS) are presented in the paper. The authors establish the possibility of using an FE model directly in a multi-body simulation with the help of CMS. The technique of FE mesh modeling is demonstrated clearly as well. Then, a detailed MSS heavy truck model is developed using the ADAMS software code. The truck model is analyzed, and all the changes to the truck frame in the event of impact are simulated successfully. Next, the CAD/CAE methodology described in the research is applied to several projects, which mainly concern the structural design and optimizations. Satisfactory results are obtained using this technique.

H. Nishigaki, S. Nishiwaki, T. Amage, Y. Kojima, and N. Kikuchi [11] propose a new variant of CAE, first order analysis (FOA) for automotive body design. The authors present the concept FOA and completely demonstrate the characteristics and advantageous of FOA. In applying the FOA to automotive body structures, they choose beam and panel elements for the structural analysis and use the beam elements for topology optimization. Also, a cross-section analysis is performed as a part of the FOA. The analysis process and its results are thoroughly illustrated, and the formulations of the elements used in these analyses are also explained. During the research, the Microsoft/Excel graphic interface is used to achieve these analyses.

1.2.2.2 Applying FEA for Crashworthiness Analysis

Among all the methods, FEA is the method most commonly used to solve engineering problems involving non-linearity. In O. C. Zienkiewicz's book [12], the author illustrates how to apply the classic FE method to nonlinear problems, including material non-linearity such as plasticity and creep and geometric non-linearity such as large displacement and structural instability. The differential equations governing the non-linearity are presented in addition to a demonstration of the classic FE method. Recently, due to integration with advanced computer programs, FEA is intensively applied to solving and to simulating the problems of structural analysis and other related fields. Also, the wide application of the FEA is stated.

B. G. Prusty and S. K. Satsangi [13] present a finite element buckling analysis of the laminated stiffened plates and the stiffened cylindrical shells using revised shell and stiffener modeling methods. Their work utilizes quadratic isoparametrics to model the shell and plate structures with a three-node curved stiffener element representing the stiffeners. Before starting the buckling analysis, the characteristics of the stiffened laminated structures subjected to small displacements are introduced, and finite element formulations are created to describe the stiffness matrix and geometric stiffness matrix for both the shell element and the stiffener element. Then, the buckling analysis commences on the identical stiffened laminated structures, which suffer from various loading cases. The final results are compared with the published ones, and an acceptable degree of correlation is obtained.

C. B. W. Pedersen [14] concentrates on the topology and the optimum design of the frame structures with respect to their crashworthiness. He creates the frame structures

using rectangular 2D-beam elements with plastic hinges, and chooses the height of each beam as the design variable that optimizes the design in order to control the energy absorption of the whole structure. A nonlinear FEA is combined with the topology optimization to solve the problem. Particularly, the Newmark method is used for time integration, the implicit backward Euler algorithm is applied to obtain the system solutions, and the direct differentiation method is used to evaluate the implicit sensitivities. With the optimum design achieved, the whole topology optimization procedure and the parametric study of the design variable presented in the work become a reference for this research.

An identical procedure of performing a vehicle crashworthiness analysis using FEA combined with advanced computer tools does the following: creates an eligible computer model, defines the appropriate crash conditions, runs the analysis, documents and analyzes the computational results, and enables the drawing of conclusions. Of the whole procedure, the computer modeling is the most important step, which directly relates to the accuracy of the final results. Researchers and engineers create many qualified computer crash models using different computer programs to perform crashworthiness analyses. Some previously published, fully developed computer models also involve the application of various computer programs.

The Silicon Valley Office of ARA [15] enabled crashworthiness simulations by developing a high fidelity computer model of a Ford Crown Victoria. Before creating the FE vehicle model, the researchers complete the measurement and digitization process that acquires complete and detailed vehicle geometries. When performing the crash simulations, the frontal impact and the side impact are considered, and the corresponding

impact conditions are defined. After finishing the computer simulations, the crash test data are collected, and the collision responses of different parts of the vehicle are described. Comparing the computer analysis results with those measured from real impact tests reveals a good correlation between the two results. The impact tests and the computer simulations of vehicle components are performed, and similar modeling and evaluation procedures are carried out on some of the important components such as the frame and the bumper.

J. M. Gonzalez, C. D. Kan, and N. E. Bedewi [16] present a highly detailed FE model of a 1997 Dodge Grand Caravan. The detailed modeling process and techniques are described in their work. This detailed vehicle model is used for different types of crash simulations, and a good correlation is established between the computer simulations and the real vehicle impact tests.

D. Lawver, L. Nicodym, D. Tennant, and H. Levine [17] predict the response of nonlinear, explicit, and FE aircraft impacting into concrete runaways and soil surfaces or reinforced concrete shelters. FLEX explicit finite element code is used to model the aircraft and the impacted structures; also, shell elements, hexahedral elements, and beam elements are used to model the fuselage, the concrete walls, and the aircraft stiffeners separately. The created FE models simulate the crash process, and the FEA results, such as the total forces and impulses acting on the target, are summarized to describe the responses of the rigid target and the aircraft during the crash. In this work, the theories and background of FE modeling are referenced along with the advantages of the explicit FE model in high-speed crash analysis in comparison to other existing models.

Z. Q. Cheng, J. G. Thacker, W. D. Pilkey, W. T. Hollowell, S. W. Reagan, and E. M. Sieveka [18] validate a finite element model for a four-door sedan that can be successfully used in computational simulations of different car-to-car impact conditions. In the project, a detailed finite element model of a four-door sedan is provided. The main tasks of the researchers are to modify and to refine the model to improve its computational performance. This performance is based on computational impact simulations and ensures that the computer results are concordant with the test data of actual vehicles. The pre-processing software, HyperMesh, reviews the model before the simulation, and the LS-DYNA executes the computational simulations. The researchers describe the experiences encountered during the modification and refinement of the finite element model. Some common issues associated with LS-DYNA and the model are addressed, which include the negative volume of solid elements, shooting nodes, energy balance, and calculation of accelerative forces. Several different car-to-car impact tests are simulated on a computer with an acceptable congruency between the results of the computational simulations and the actual test data.

Dr. A. Eghlimi and Dr. J. D. Yang [19] perform a crash analysis to simulate a car impacting a collapsible signpost using ANSYS and LS-DYNA. The objective of the project is to predict the behaviors of the thin-walled signposts under wind load, self-weight, and crash conditions. Then, they optimize the design of the signpost to achieve better performance under both the static and the dynamic load conditions. The whole project includes the static analysis of the signpost when subjected to the wind load and self-weight and the crash analysis of impact from a vehicle. ANSYS is used for the static analysis, and the LS-DYNA is used for the crash simulation. The work displays different

applications of ANSYS and LS-DYNA and beneficial examples of how to use the postprocessor of LS-DYNA to record and to plot all the important data. In addition, the buckling behavior and the response of the signpost during the crash simulation are recorded in terms of the displacement, the velocity, and the acceleration history at certain monitored nodes. These monitored nodes serve as indicators representing the entire buckling process of the signpost.

Y. M. Jin [20] develops the analysis and evaluation of vehicle body structure using FE methods. He uses MSC products such as Patran, Nastran, and NVH_Manager to perform the FE modeling and calculation. In his research, the target body structure model undergoes static analysis, dynamic analysis, and noise-velocity-harshness (NVH) analysis. The performance of the vehicle body is evaluated, and the full body crash is simulated on the computer. This project demonstrates the effective application of finite element methods when combined with the advanced CAD/CAE programs in vehicle crashworthiness analysis. The computer results are verified by real tests.

To create a valid FEA crash model, the modeling method must be considered first; the original CAD model must be correctly meshed. Additionally, appropriate crash conditions such as boundary conditions and initial conditions should be selected to guarantee the accuracy of the analysis results. Some projects pertaining to these areas are reviewed for later research.

M. H. Ray [21] describes the typical impact conditions in side-impact collisions with fixed roadside objects. He defines the impact conditions by specifying four parameters: the vehicular mass, the impact velocity, the impact angle, and the impact point. The author examines the data of numerous accidents from police-reported side-

impact collisions and summarizes the effects of each parameter on the severity of the collisions. Then, the worst-case impact conditions that result in fatal consequences are determined and as possible, selected as the conditions for the full-scale crash test. The conclusions obtained in this work are adopted to determine the impact conditions for a vehicle crash computer simulation.

J. A. Zukas and D. R. Scheffler [22] focus on the effects of the computational mesh on the computational simulations of problems that involve fast and transient loading such as, impact problems and crash analysis. The researchers discuss various factors related to the mesh that might cause discrepancies between the computer results and the experiment results. They also provide suggestions on how to decrease the effects of these factors and guarantee the reliability of the finite element model used for the simulations. This work is very instructive and is usable as a reference for how to generate the meshes for a finite element model appropriately.

B. Canaple, G. P. Rungen, E. Markiewicz, P. Drazetic, J. H. Smith, B. P. Chinn, and D. Cesari [23] develop a new methodology in modeling the motorcycle accidents in which a motorcycle impacts a stationary car. The objective of the research is to evaluate the head injuries of the riders involved in motorcycle accidents, but the modeling method in the paper is very creative. The researchers use a "multi-body" model to represent the motorcycle and the target vehicle. They divide the full physical model into several components with specific joints that connect them together. Using the understanding of the possible relative motions between the components and the characteristics of their joints, the corresponding multi-body models are created. It is verified that the developed model can simulate the responses of the original model very well.

15

The reviewed literature on crashworthiness analysis using finite element analysis is summarized into three areas:

1) Introduction of the methods and techniques usually applicable to crashworthiness analysis

   These methods mainly include the numerical analysis method and the experimental method. With the development of computational technology, some powerful CAE tools such as FEA, MSS, and FOA are proposed and applied to solve such problems quickly and efficiently. Also, new techniques in system identification and component mode synthesis are introduced to aid users in building high quality analytical crash models for the numerical analysis.

2) Explaining how to apply FEA to solve crashworthiness analysis and describing the normal steps

   From the above literature, the normal steps used to apply FEA to solve crashworthiness analysis are briefly summarized as:

   - Creating an eligible FEA computer model

   - Determining the appropriate crash conditions and boundary conditions

   - Applying these conditions to the FEA model

   - Running the crashworthiness analysis

   - Obtaining and analyzing the computer results

   - Drawing conclusions

3) Presenting several FE vehicle models that are used for crashworthiness analysis and illustrating the modeling methods

A typical FE vehicle model is generated based on the geometries and shapes of the prototype vehicle, which is usually composed of solid elements, shell elements, and beam elements. The number of elements depends upon the meshing method used and determines the overall size of the model. Different computer software packages create such models and run the analysis. Some examples are LS-DYNA, ANSYS, PAM-CRASH, MSC products, HyperMesh.

1.2.3 The Development of Simplified Models

Because of the advantages of the simplified FEA model in crashworthiness analysis, some previous researchers search for valid simplified models to replace the existing detailed models. Only a few such models are published because simplified modeling is a relatively new subject and is not developed as fully as other fields.

P. Drazetic, E. Markiewicz, and Y. Ravalard [24] develop kinematic models to analytically determine the resistance to collapse of thin-walled structures of simple geometric shapes subjected to compression or bending loading. Then, based on the kinematic models, a simplified model for an "S" frame is created that is composed of beams and nonlinear springs. Both the simplified model and the detailed model undergo crashworthiness analyses. The results are compared with each other as well as with the results of an experimental test. The comparison reveals that the simplified model is a promising tool for rapid estimates of the crash behavior of simple structures and can model vehicle structures.

In the Ford Motor Company's manual book "Guidelines for Modeling an Automobile Body for NVH Analysis – Simplified Models" [25], researchers present the concept of simplified models in contrast to the detailed models. They describe the characteristics of the simplified model and demonstrate the advantages of using the simplified model as opposed to the detailed model. The series of simplified modeling techniques and methodologies in creating different members and components of Ford vehicles are documented in this book and are very beneficial to later research.

R. J. Brooks and A. M. Tobias [26] review the related studies on model simplification techniques and develop an instructive guideline of how to choose the best model for a mathematical or computer modeling study. They evaluate the performance of a model and explain the meaning of the level of detail and complexity. In their work, they focus on the relationship between the model performance and the level of detail or complexity of the model. Then, they assert comparing and choosing the alternative model based on its level of detail and complexity.

H. S. Kim, S. Y. Kang, I. H. Lee, S. H. Park, and D. C. Han [27] create simplified vehicle structures using beam elements and nonlinear springs for crashworthiness analysis. They introduce the method that uses nonlinear springs and beam elements to model the major parts of a vehicle, while shell elements model the plate parts and rigid parts. Also, they verify that the nonlinear spring and beam element can simulate both the axial and the bending collapse behaviors involved in crashes very well. In their work, the same crashworthiness analysis is performed on two full car models. One is mainly modeled by nonlinear springs and beam elements (almost 75%), and the other one is modeled by shell elements. After checking the results and computer times, it is shown

that compared to the detailed vehicle model (the shell element model), the simplified model (the beam-spring model) provides an approximate result (with 15% error) while only requiring 16% of the computing time of the shell element model.

A. K. Aaouk, N. E. Bedewi, C. D. Kan, and D. Marzougui [28] develop a multi-purpose finite element model of a 1994 Chevrolet C-1500 pick-up truck and use it for impact simulations. A detailed model and a simplified model are created; the procedures of the modeling generation and simplification are described, and the features of each model is thoroughly demonstrated and compared. They use the detailed model and the simplified model for the crash simulations separately. They compare the simulation results with those of real impact tests in terms of overall impact deformation, component failure modes, and the velocity and the acceleration at various locations of the vehicle. The impact modes include frontal and side impact, and both of them are discussed in the paper. The LS-DYNA performs the computer simulations; the results are gathered and analyzed. Also, the simulation results of the simplified model are compared with those of the detailed model and the real impact test; a good correlation among these results is achieved. Thus, the advantages and the possibility of using the simplified model to replace the detailed models are confirmed. This project exemplifies how to develop a simplified model from detailed model used for crash simulations. The main technique in this work is to fully increase the element size while maintaining the accuracy of the results. However, some advanced techniques can still be developed in future work.

Since the simplified computer modeling is a relatively new technique, there are not many articles on this issue, but current papers address two possible ways of simplifying a detailed model:

19

1) Using a coarse mesh for the unimportant components and increasing the overall element size to simplify the detailed model

In this method, the impact region of the vehicle model is defined as the high impact zone. This is extremely important in representing the global crash characteristics because it cannot be coarsely meshed. For the none-impact regions a coarse mesh is applied to reduce the overall number of elements. Generally, the farther the components are away from the impact regions, the higher the degree of accuracy with which they can be coarsely meshed.

2) Developing new simplified elements to replace the current elements and developing the simplified model using the new elements

As illustrated in Kim's article [27], the detailed model consists of 10912 shell elements, which requires more than 10 hours to run the crashworthiness analysis due to the complicated formulations of the shell elements. In the simplified model, which uses beam and spring elements to replace most of the shell elements, the computer time is significantly reduced to less than 2 hours. The simple formulations of the beam and spring elements require fewer calculations than the shell elements during the analysis.

1.3 Motivation

Simplified modeling generates a great deal of interest in the area of crashworthiness analysis. Researchers study the possibilities and methods of developing eligible simplified models, and some effective ones are developed. Examples of these models and the corresponding modeling methodologies are introduced and reviewed in

the previous section. Below, in more detail, is a model of great interest, which reveals the intentions of this research and provides its foundation.

1.3.1 The Existing Simplified Vehicle Model

H. S. Kim, S. Y. Kang, and coworkers create a simplified vehicle model and use it for crashworthiness analysis [27]. The results are compared with those obtained from a detailed model. An acceptable correlation is achieved between these results, and the required computing time of the simplified model is significantly reduced. In this research, the theories of axial and bending collapse are applied to the development of modeling methods. After separately calculating the spring element's $F - \delta$ curve and $M - \theta$ curve in relation to the axial and bending response, the researchers use nonlinear spring elements and beam elements to build the simplified model. The existing detailed car model is composed of 10912 shell elements, but in the new model, it only has 2310 elements and 70% is modeled using nonlinear springs and beam elements. For this revised model, the researchers use nonlinear springs and beam elements to model the major parts (usually thin-walled closed section members) that absorb most of the crash energy. They still use shell elements to model the plate parts and the rigid parts. One example is the single S-shaped member. Figure 1 and Figure 2 illustrate the detailed and simplified models of this member, while Figure 3 plots their deformed shapes. It is clear that the member is modeled using shell elements for the detailed model, and the simplified model only uses a 2D beam element with nonlinear springs at both ends.

Figure 1. S-Shaped Member [27] – Isometric View
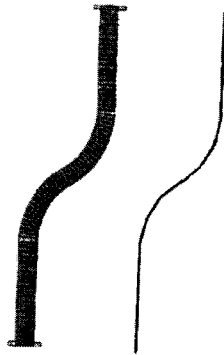
Figure 2. Original Shapes of Detailed and Simplified Models [27] – Side Views
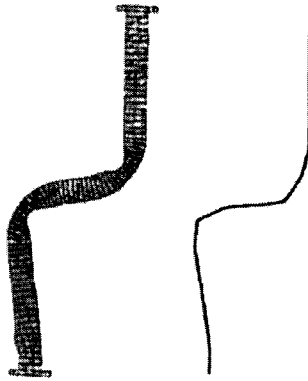
Figure 3. Deformed Shapes of Detailed and Simplified Models [27] – Side Views

In Kim's simplified vehicle model [27], the researchers remove all the

components that do not significantly contribute to the impact load and replace them with

lumped masses to reduce the simplified model's size. Both the detailed and simplified

models undergo crashworthiness analysis. The computing time is 41900 seconds for the

detailed model and 6660 seconds for the simplified model. From the comparison of

results, it is found that the simplified model generates only a 15% error when compared to the detailed model. Thus, the objective of their research is achieved. Figures 4 to 8 display related full car models and results plots. The researchers create another simplified model which only uses beam elements to model those thin-walled closed section members. A comparison of the results shows the effects of the nonlinear spring elements in simulating the vehicle model's crash behavior. Their paper includes a comparison of the displacement, the crushing force, and the absorbed energy, which are most important in reflecting a structure's crash behavior. Figures 9 and 10 plot the comparisons of the crushing force and the absorbed energy. Table 1 displays the summary of the comparisons between the models.
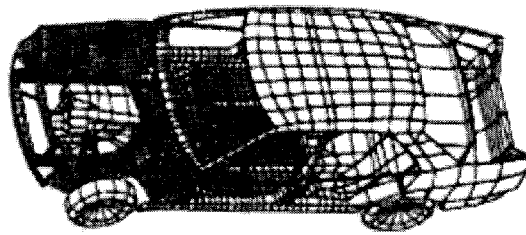
Figure 4. Full car model [27]
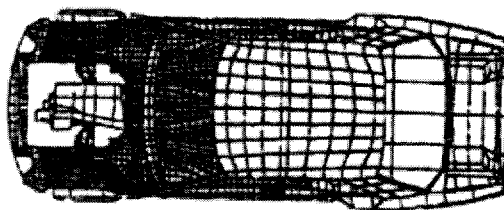
Figure 5. Full car detailed model, before crash [27]
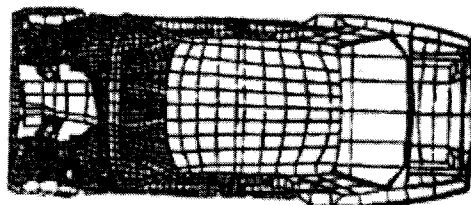
Figure 6. Full car detailed model, after crash [27]
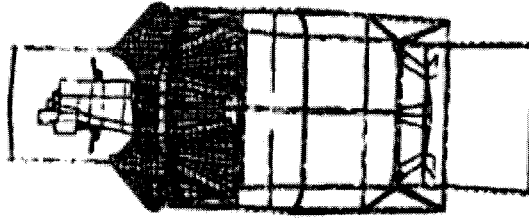
Figure 7. Full car simplified model, before crash [27]
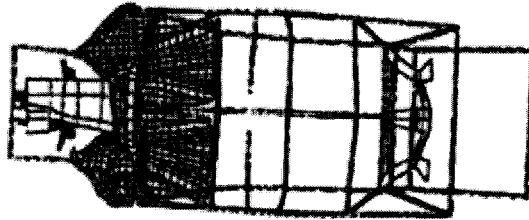
Figure 8. Full Car Simplified Model, after Crash [27]
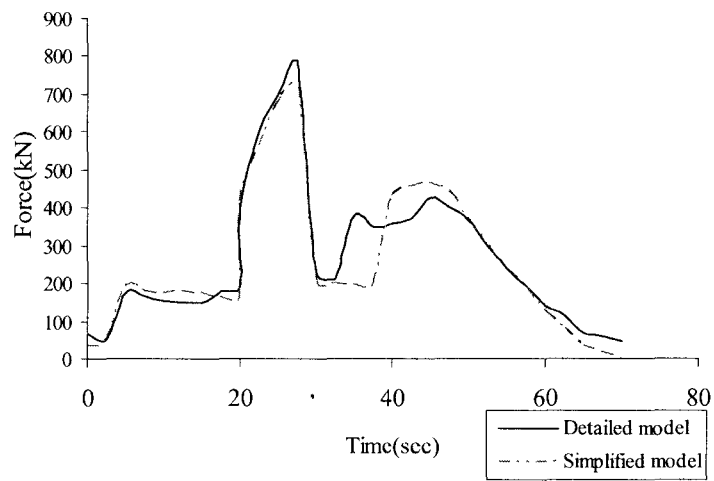
Figure 9. Peak crushing force [27]

24
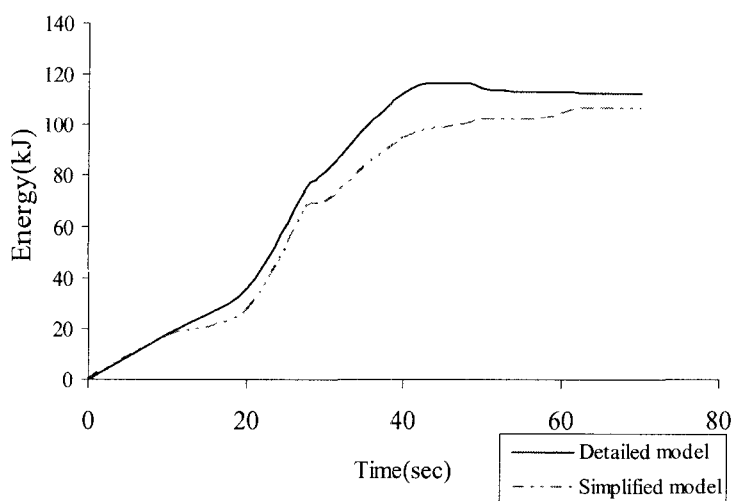
Figure 10. Absorbed energy [27]

Table 1. Comparison between Detailed and Simplified Car Models [27]

	Detailed model	Simplified model	Difference (%)
Peak crushing force (kN)	780	720	-7.7
Absorbed energy (kJ)	113	107	-5.3
No. of elements	10912	2310	-78.8
Computer time (sec)	41900	6660	-84.1

1.3.2 Limitations of Current Work

H. S. Kim, S. Y. Yang, and coworkers provide a good simplified modeling

method, which is to use simple elements to replace the complex elements, and thereby,

reduces the entire finite element model's size. In their vehicle model, the beam elements

model the body of the thin-walled members, and the nonlinear springs model the plastic

hinges that can correctly simulate the member's crash behavior under axial and bending

collapse. Among them, the beam elements are extensively used in modeling, while the

nonlinear springs are developed based from the existing collapse theories regarding the

thin-walled box section beams. However, in addition to the box section member, the channel section member is becoming increasingly more popular and is widely used in engineering for architectural structures, vehicles, and etc. Thus, a valid simplified crash model is required for such structures to perform the crashworthiness analysis effectively and for replacing the existing detailed model in the early design stages. Unfortunately, the nonlinear spring in this paper cannot be applied to the simplification of the channel section beam model due to the absence of related collapse theories. Therefore, to acquire an eligible simplified model of a structure composed of thin-walled channel section members, the collapse behavior of channel section member requires investigation, and the development of new elements to simulate the behavior is necessary.

Kim's simplified vehicle still contains shell elements, which model the components that do not significantly contribute to the impact load (i.e. plate parts and rigid parts). The shell element parts still increase the overall model size and still require considerable computer resources to accomplish crashworthiness analysis. Thus, to fully simplify a crash model, a new modeling method is required that does not use shell elements to model the unimportant components. The superelement method or the equivalent beam method is considered for the achievement of this goal.

In summary, the proposed research follows the direction set forth in the existing research and continues to develop a new element that can simulate the collapse behavior of thin-walled channel section members and use it to simplify the structures that contain such members. Also, the superelement and the equivalent beam element are implemented to model the components previously modeled using shell elements.

Combining the existing beam element and the new element builds an improved simplified model.

1.4 Research Objectives and Description

1.4.1 Problem Description

This research focuses on developing a simplified FE model that is useful for vehicle crashworthiness analysis and that can be applied in early vehicle design stages. Moreover, after the simplified model is created, the relevant methodology of simplified modeling is summarized. All the crashworthiness analyses and dynamic analyses in this research (unless otherwise specified) are performed using the explicit computer software package: LS-DYNA. LS-DYNA is an explicit code very capable of solving high-speed impact problems that require small time steps. Appendix A illustrates the principle of LS-DYNA and compares the two analysis procedures: explicit analysis (used by LS-DYNA) and implicit analysis (used by ANSYS).

Because of the extensive application of thin-walled channel section members in the automobile industry, it is necessary to develop a new element to simulate the crash behavior of the channel section beam in order to acquire a qualified simplified model for vehicle structures. Specifically, it is necessary to develop a new type of nonlinear spring element to model the plastic hinges of the longitudinal vehicle members, which can correctly express their response to axial and bending collapse during crashes. As introduced in earlier sections, the motivation of this research is derived from a previous study on simplified crash modeling [27]. In that work, the existing theories about axial

and bending collapse of thin-walled box section beam are applied to the development of a new spring element that can express the collapse behavior of plastic hinges. Then, the researchers continue to develop a simplified vehicle model using this spring element and other known elements. In that paper, due to the lack of related collapse theories, the researchers did not mention the simplified modeling of the channel section beam, which is widely used in vehicle structures including the chassis. One objective is to minimize this weakness.

In defining the properties of the new spring element, the crash responses of the thin-walled channel section beam under different loading conditions are determined. W. Abramowicz [29, 31, 32, 33, 34], D. Kecman [30], and T. Wierzbicki [31, 32, 33, 34] study the crash behavior of the thin-walled box section beam and derive mathematical equations to predict its bending and axial resistance. These equations are later referred to in the development of the nonlinear spring that can successfully simulate the corresponding plastic hinges, which appear during the crash. In the present research, following the published methods of derivation, the crash behavior of the channel section beam is studied, and the corresponding mathematical equations are derived to describe the bending resistance. This is necessary to define the characteristics of the new spring element.

After the new spring element is developed, it is combined to the beam element to create the simplified model for channel section beam. Similar to the presented simplified model, the whole channel section beam is divided into two parts: the first suffers large plastic deformation and absorbs most of the crash energy, and the second undergoes a rigid body motion or elastic deformation [28]. Thus, the beam element models the elastic

or rigid part, and the new developed spring element models the part that undergoes plastic deformation, called "plastic hinges."

An existing detailed truck chassis FE model is involved in this research. A simplified model is created from it, and the same crashworthiness analysis is performed on both models. The results of both are compared to validate the newly developed simplified model. The reason for choosing this truck chassis model is because its longitudinal members are composed of channel section members. This enables the application of the newly developed spring element of this research to the simplification of those members. Meanwhile, the chassis is an important component within the full vehicle crash response, and current research reveals that approximately one-half of the vehicle's frontal collision response is attributable to the chassis collapse behavior [6].

As described in an earlier section, the basic idea of simplified modeling is to use beam elements and nonlinear spring elements to replace the current shell elements in modeling the longitudinal members that absorb most of the crash energy. The plate members of the chassis model, which are modeled using shell elements in the referenced simplified model, are replaced by superelements and equivalent beam elements instead of the original shell elements to completely reduce the overall model's size.

Finally, the simplified chassis model is accomplished by integrating all of the simplified members together, and crashworthiness analyses are performed to validate this model. The advantages and limitations of the superelement method and the equivalent beam element method are discussed. Then, an effective methodology of simplified modeling is summarized and presented that can promote further study and can be applied to the building of a simplified crash model for other complicated structures.

1.4.2 Research Objectives

As demonstrated in previous sections, the objectives of this research are summarized as follows: 1) to develop a new element that can correctly express the bending collapse of the thin-walled beam with channel section; 2) to find a way to simplify the transverse plate members that are modeled with shell elements even in previous simplified models; 3) to continue to develop simplified models applying the new element and the developed simplified plate members, and ensure that the developed simplified model is eligible for the vehicle crashworthiness analysis; and 4) to present a methodology of simplified modeling which is applicable to the crash modeling of further structures using the present research.

1.5 Preview of the Remaining Chapters

Of the remaining chapters, chapter 2 introduces how to apply existing theories to the development of simplified crash models for the thin-walled beams with box section. Simplified models are presented for the straight beam, the "Z" shaped beam, and the "S" shaped beam. Chapter 3 derives the bending resistance of the thin-walled beams with channel sections based on current literature and applies the derived bending resistance to the development of a simplified model for single channel section beams to verify their efficiency. With all the preparation work completed, chapter 4 starts to develop the final simplified model for the truck chassis; the superelement method and the equivalent beam element method are also described in this chapter. After the completion of the modeling and validation, chapter 5 reviews all the modeling work and presents a common

simplified modeling methodology that is applicable to other engineering problems.

Finally, chapter 6 summarizes and evaluates this entire research project and completes

this dissertation.

CHAPTER II

SIMPLIFIED MODELING OF THIN-WALLED BOX SECTION BEAMS

2.1 Introduction

In this chapter, theoretical works about collapse theories of thin-walled box section beams are reviewed from published papers. Nonlinear spring elements, simplified models, and crash analyses are developed and performed to verify and illustrate the existing theories. Section 2.2 reviews the collapse mechanisms of straight thin-walled beams and introduces building simplified models for such beams based on their axial collapse mechanisms. Because of its straight outline, the nonlinear spring element used for such simplified models only reflects the axial crushing behavior. The purpose of section 2.3 is to delineate how to create simplified models for curved beams with a "Z" shape, which are commonly used in many different vehicle structures. Classic theories about the crash behavior of curved beams are reviewed and applied. The nonlinear spring element is used in the resulting simplified models to simulate the bending and rotating behaviors. Section 2.4 studies the curved beams with an "S" shape, which contain arc segments instead of only straight segments. The modeling method and the nonlinear spring element presented in section 2.3 are applied to create the simplified model for the "S" shaped beams. A series of simplified models dependent upon the varying amounts and locations of the nonlinear spring elements are created to find the best way to represent the crash behavior of the arc segments. In each section, detailed

models for the box section beams are presented first. Next, similar crash analyses are performed on both the simplified and the detailed models via computer simulation. The efficiency of the simplified models is then verified by comparing the results.

2.2 Simplified Modeling of Straight Beams

In this section, a detailed model for a straight thin-walled beam with a square cross section is created using shell elements. Then, a simplified model is developed based on the detailed model composed only of beam and nonlinear spring elements. The same crash analysis is performed on both models. A good correlation is obtained when they are compared using the crash results. After that, a similar process is repeated for the straight thin-walled beam with a rectangular cross section to verify the validity of the modeling method for different kinds of box sections. Wierzbicki and Abramowicz's theories [31, 32] about the thin-walled column that is subjected to axial loading are applied in determining the characteristics of the nonlinear spring elements. Their classic collapse mechanism of the thin-walled column is also referenced during the simplified modeling.

2.2.1 Detailed Model

The detailed model for the thin-walled straight beam with a square cross section used in a crashworthiness analysis is shown in Figure 11. The detailed model uses the full integration shell element: 4-node Belytschko-Tsay shell element with 5 integration points through the thickness. This shell element is based on a combined co-rotational and velocity-strain formulation. Because of its computational efficiency, it is usually the

shell element formulation of choice and has become the default shell element formulation of LS-DYNA (for more details, see [35]).

As shown in the figure, during the crash analysis, the beam model is fully constrained at one end. The initial velocity is applied on the other end to make the model move along the Z direction. Table 2 lists all the related conditions and information about the thin-walled straight beam. After analysis, the dynamic results are documented and compared with those from the simplified model. These are presented in the latter section.

Table 2. Thin-Walled Straight Beam Input Data

Material Properties	
Young's modulus (E)	2.07E5MPa
Density (ρ)	7830kg/m^3
Yield Stress (σ_y)	200MPa
Ultimate Stress (σ_u)	448MPa
Hardening modulus (E_{sn})	630MPa
Poisson's ratio (ν)	0.3

Geometries	
Total length (L)	300mm
Cross section (a,b)	60mm×60mm
Wall thickness (t)	1.5mm

Crash conditions	
Added mass (m)	400kg
Initial velocity (v_0)	15m/s
Crash time (t_c)	0.01sec
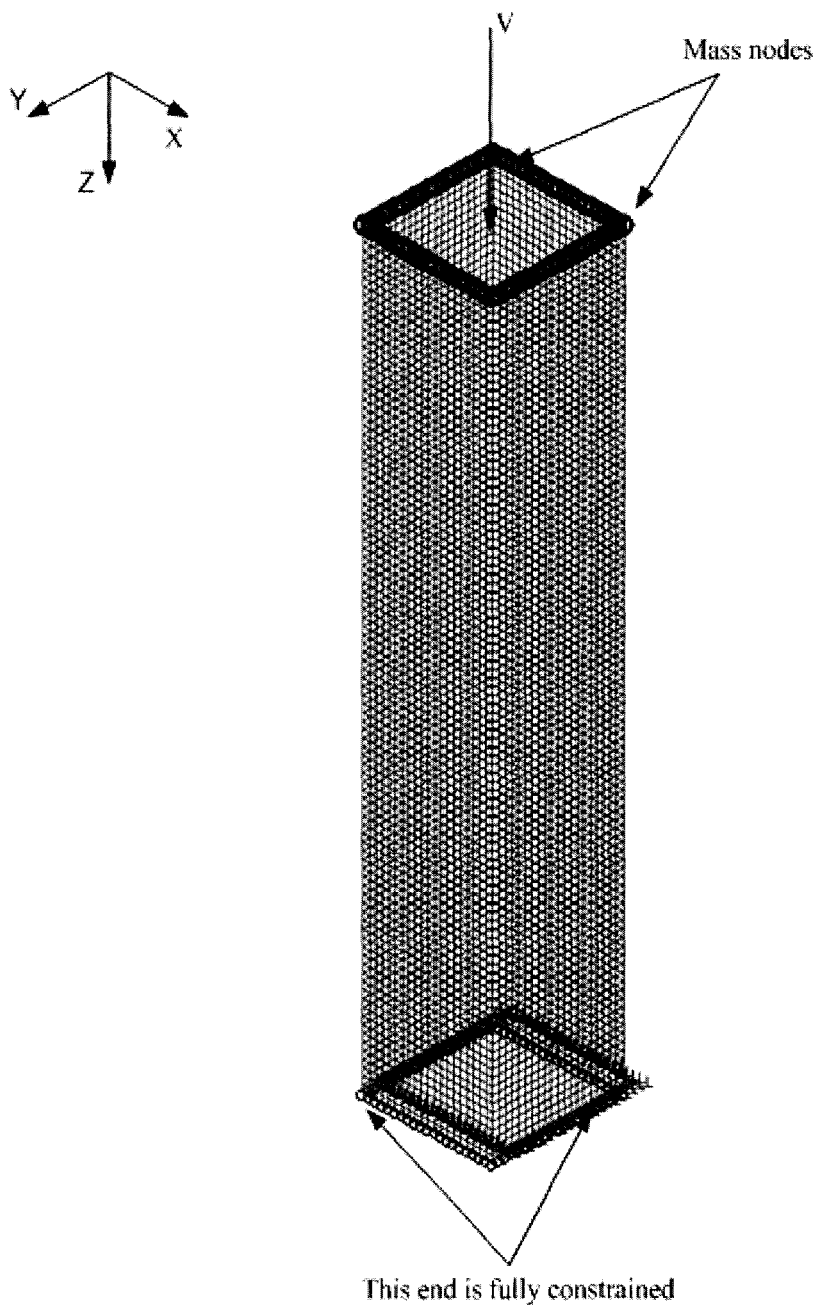
Figure 11. The detailed model for thin-walled straight beam with square section

2.2.2 Collapse Mechanisms of Straight Thin-walled Beams

The collapse mechanisms of straight thin-walled columns were thoroughly

studied by T. Wierzbicki and W. Abramowicz [31, 32, 33]. In these papers, it is assumed

that the crumpling process of a rectangular tube is progressive with each new fold being

formed after the previous one is completed. This phenomenon is also verified by the

computer simulation. Figure 12 displays the configuration of the square beam at different

times during the crash—clearly reflecting the progressive crushing process of the model.

The figure demonstrates that during the crash the detailed beam model buckled and

generated the first fold at about 3msec. Then the entire fold moved down together with

the second and third folds occurring sequentially. The nodes at the middle of each fold

are traced for later comparison with the corresponding nodes in the simplified model

(where the spring elements are defined). Those nodes are indicated in Figure 12 as nodes

1, 2, and 3.
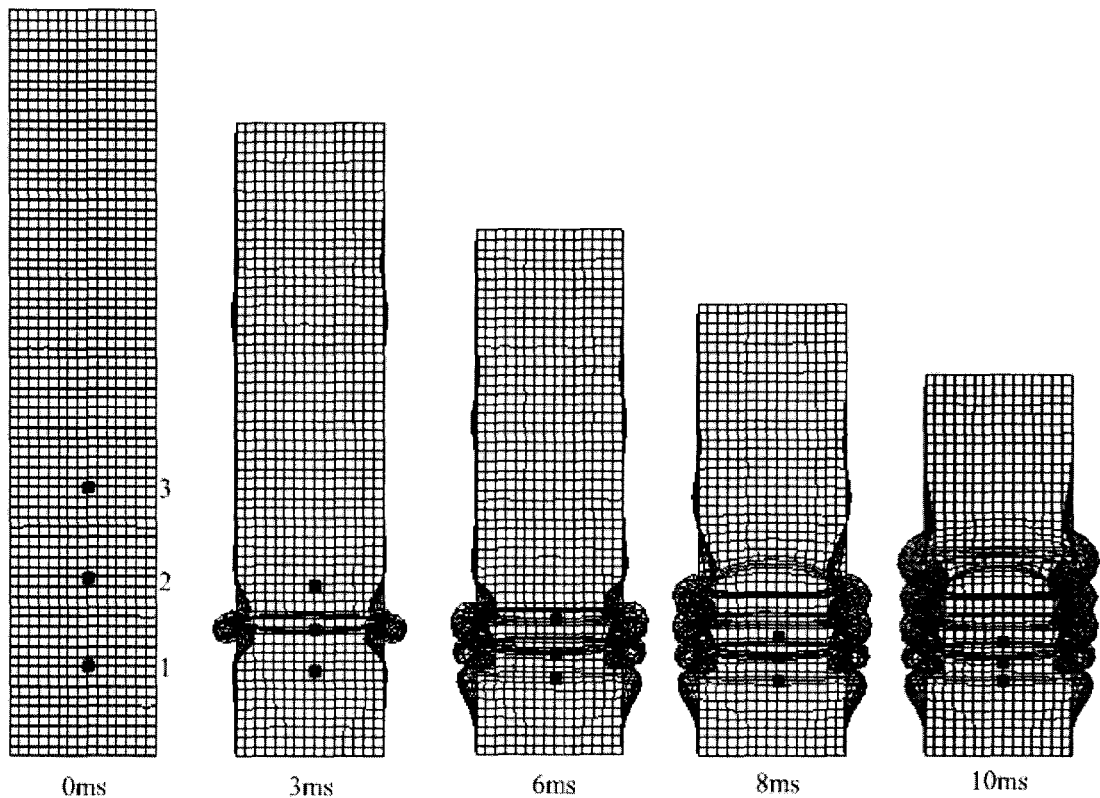
Figure 12. Configurations of a Detailed Straight Square Beam Model in a Series of Time

2.2.3 Nonlinear Spring Characteristics

As illustrated in section 2.2.2, the buckling of the thin-walled box section beam model during the crash is realized through the generation of the consecutive folds, which have a "spring-like" characteristic. Therefore, it is possible to have several nonlinear spring elements simulate the beam's axial collapse mechanisms in the simplified model. The force-shortening characteristics of the nonlinear spring elements have been published in previous papers [31, 32]. According to those papers, the length of the half plastic fold that was generated during the beam crushing, H (as shown in Figure 13), and the mean crushing force P_m can be calculated as

$$H = 0.98\sqrt[3]{tC^2}$$
<div align="right">2-1</div>

$$P_m = 9.56\sigma_0 t^{5/3} C^{1/3}$$
<div align="right">2-2</div>
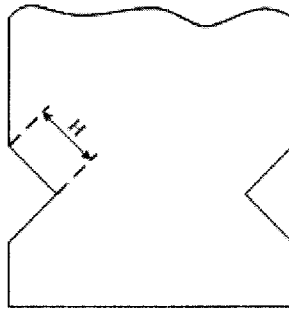
Figure 13. Length of half plastic fold, H

Also, from [31, 32], the σ_0 is the material's energy equivalent flow stress which can be estimated based on the material's ultimate stress σ_u using the formula

$$\sigma_0 = 0.92\sigma_u$$
<div align="right">2-3</div>

t is the thickness of the thin-walled beam. C is the average edge length of the cross section's depth a and width b, which can be calculated using the equation

$$C = \frac{1}{2}(a + b) \qquad\qquad 2\text{-}4$$

Applying equations 2-1 through 2-4 and substituting the material properties given in section 2.2.1, the calculated length of one plastic fold is $2H = 34.4$mm, and the mean crushing force is $P_m = 30.3$kN.

The nonlinear spring element for the straight beam can be entirely determined from the mean crushing force and the length of the plastic fold. In the referenced paper, the authors defined the F − δ curve starting directly at $(0, P_m)$ and continuing as a horizontal line as shown in figure14. As a nonlinear spring, it should have an initial portion to define its displacement when the applied force is increased from 0 to P_m, where the P_m is 30.3KN. To solve this problem, an initial linear portion is added onto the current F − δ curve. Because the nonlinear spring has a high stiffness before the force reaches 30.3KN, the linear part needs a high slope. Thus, one more point (0.01, 30.3) is added to redefine the modified F − δ curve. The new F − δ curve first increases from (0, 0) to (0.01, 30.3). Then, it becomes the horizontal line (as shown in Figure 15). As the initial linear portion of the nonlinear spring element is not discussed in those published literatures, an assumed initial straight line is applied here. In later chapters, the determination of the initial F − δ is further presented and discussed.

With this property, the spring begins to deform when the crushing force reaches 30.3KN. After its deformation reaches 34.4mm, the spring fails and stops deforming.
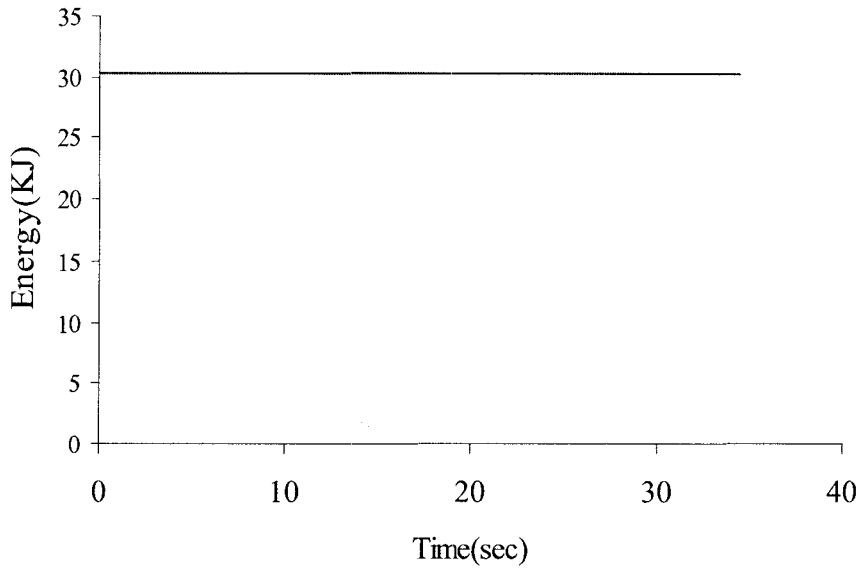
Figure14. Original F – δ curve of nonlinear spring element for straight box section beam
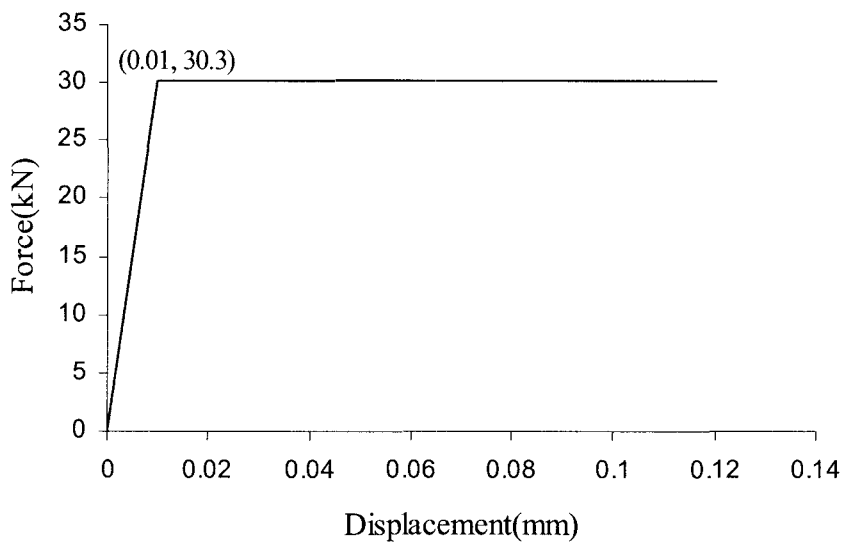
Figure15. Initial portion of modified F – δ curve

2.2.4 Development of Simplified Model

After determining the characteristics of the nonlinear spring element, the

simplified crash model for the straight beam can be created. With the given geometry

information, a pure beam-element model is created using the Hughes-Liu beam elements;

appropriate cross section information is also specified for the beam. Similar to the Belytschko-Tsay shell element, the Hughes-Liu beam element is selected as the default beam element of LS-DYNA because of its computational efficiency and robustness. Moreover, this beam element includes transverse shear strains. The added computations needed to retain this strain component are insignificant compared to those for the assumption of no transverse shear strain (for more details, see [35]).

To determine the arrangements of the nonlinear spring elements, refer to the approximate collapse model shown in Figure 12. Accordingly, the spring elements are arranged evenly along the beam with each element being defined between two coincident nodes. Each pair of nodes is spaced at a distance of 34.5mm, which is the length of one plastic fold. Thus, the 300mm-long beam is divided into 9 equal segments of 34.5mm each starting from the clamped end. Additionally, the LS-DYNA allows user to define a nonlinear spring by inputting a displacement – force table. For example, the nonlinear spring element used here can be defined by typing (0, 0), (0.01, 30.3), and (34.4, 30.3). To ensure that the simplified model only deforms along its length, suitable boundary conditions are applied on corresponding nodes. Figure 16 shows the developed simplified model.
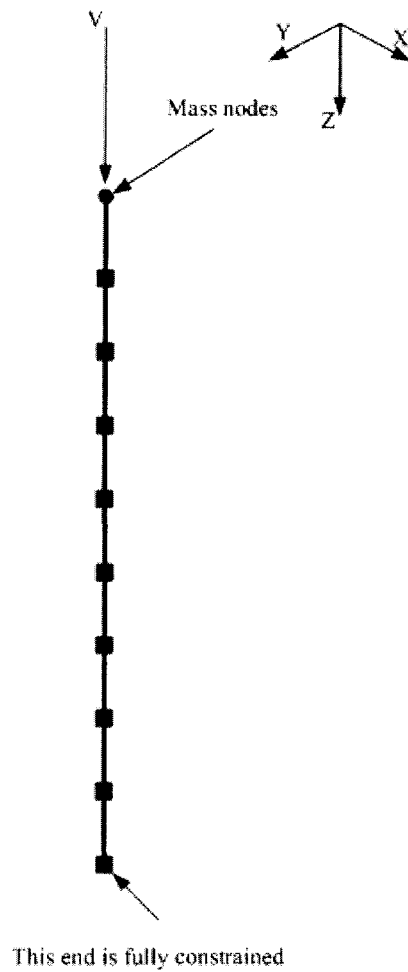
Figure 16. Simplified model for thin-walled straight beam with square section

2.2.5 Dynamic Results and Comparisons

After the completion of the modeling, the simplified model undergoes the same

crash analyses that have been performed on the detailed model. The dynamic results

from both models are compared. Table 3 and Figures 17 through 19 display all the

results from the comparisons.
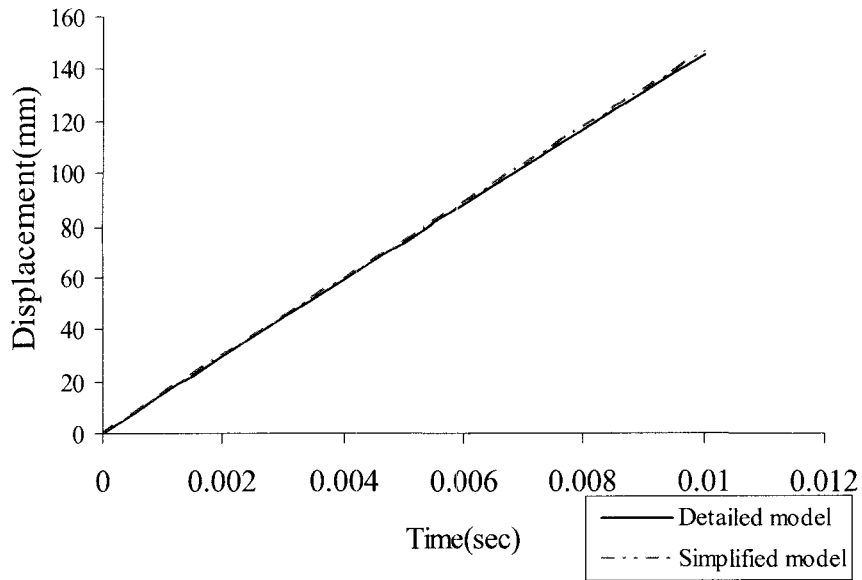
Figure 17. Displacements at end of straight square section beam models

Figure 18. Crushing forces for straight square section beam models

Figure 19. Absorbed energies for straight square section beam models

Table 3. Comparisons of Dynamic Results from Detailed and Simplified Straight Square Section Beam Models

	Detailed model	Simplified model	Difference (%)
Global displacement (mm)	145.5	146.6	0.8
Peak crushing force (kN)	82.6	70.5	-14.6
Absorbed energy (kJ)	4.83	4.37	-9.5
Computer time (sec)	3544	193	-94.6

Upon examination of the results, it is found that the simplified model can generate good results while saving much more computer time (it only took about 5% of the computer time required by the detailed models. Table 3 shows that the errors of all the important crash results are within 15%. The crushing force is below 15%; the final deformation is almost the same as the amount obtained from the detailed model. The error of the absorbed energy is under 10%.

43

Simple calculations can test the validity of the computer results. For example, if this straight thin-walled beam is assumed to be linearly elastic, then its stiffness is $K = \dfrac{EA}{L} = \dfrac{2.07 \times 10^5 \times \left[60^2 - (60 - 2 \times 1.5)^2\right]}{300} \approx 2.42 \times 10^5 (N/mm)$. Therefore, under the applied load 82.6KN, which is obtained by running analyses on the detailed model, the static displacement can be calculated as $\delta_{static} = \dfrac{F}{K} = \dfrac{82.6 \times 10^3}{2.42 \times 10^5} = 0.34 (mm)$. In comparing the crash results, it is found that the δ_{static} is far small than the yielded displacement. This verifies that during the crash analysis, the thin-walled beam did buckle instead of deforming statically. On another hand, under the external load 82.6KN, the resultant static stress $\sigma_{static} = \dfrac{F}{A} = \dfrac{82.6 \times 10^3}{60^2 - (60 - 2 \times 1.5)^2} = 235 (Mpa)$ is found to be higher than the material's yield stress while still below the ultimate stress. This static stress value indicates that during the analysis, the thin-walled beam experienced plastic deformation, but did not fail. Also, the same conclusions can be drawn from the crash results of the simplified model. Thus, through the simple estimations, the crash analysis results are assumed to be reasonable for a buckling beam model.

Additionally, to investigate how the nonlinear spring elements worked in the simplified model, the nodes defining the first three spring elements are studied and compared with the previous nodes indicated in Figure 12. It demonstrates how the nonlinear springs simulated the behavior of the folds. Figure 20 lists the series of the deformed simplified model on which the three spring nodes are indicated. Figures 21 through 23 plot the displacements at the specified nodes for both the detailed and the

simplified models. The numerical values of the displacements at different times are listed

in tables 4 through 6.
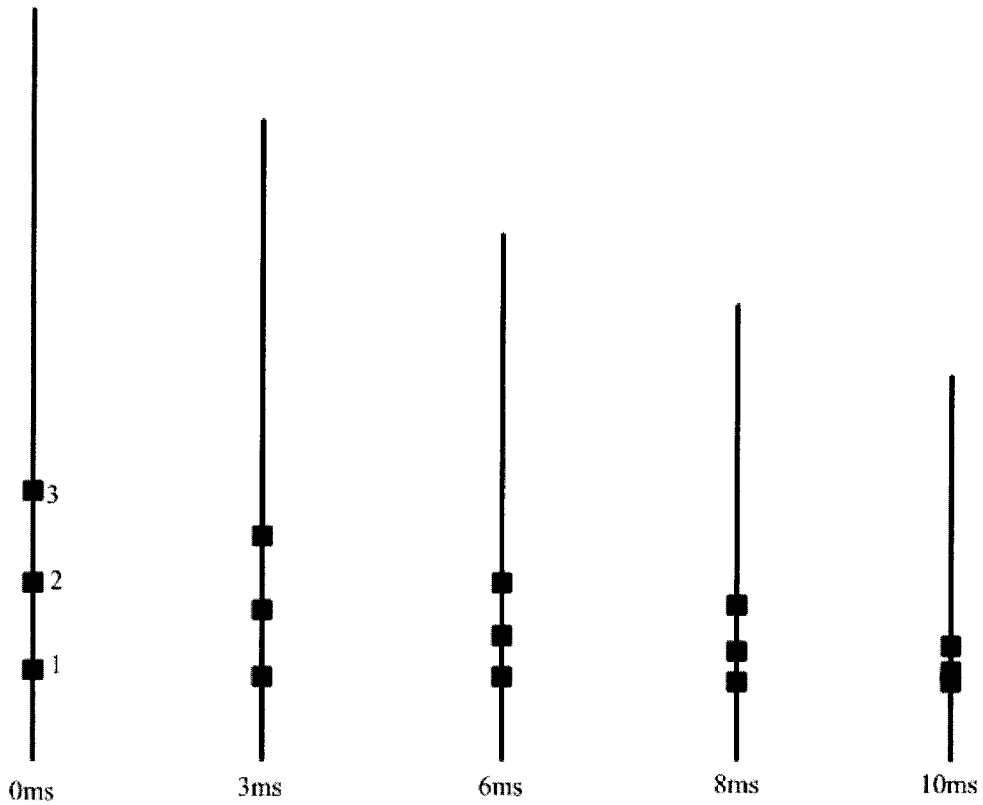
Figure 20. Configurations of simplified straight square beam model at specific times
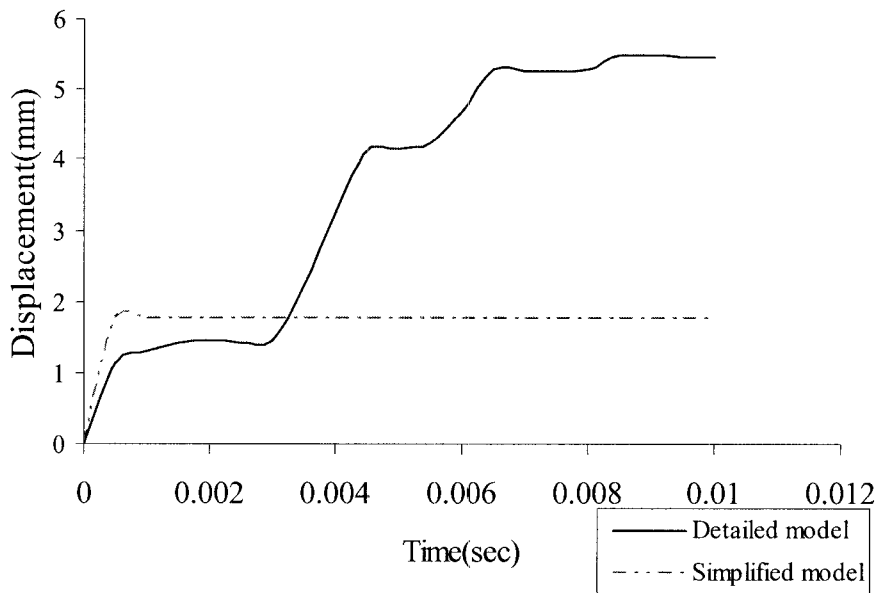
Figure 21. Displacements at node1

Table 4. Comparison of Displacements at Node1

	Detailed model	Simplified model	Difference (%)
Displacement at time 3ms (mm)	1.45	1.76	21.4
Displacement at time 6ms (mm)	4.70	1.76	-62.6
Displacement at time 8ms (mm)	5.28	1.76	-66.7
Displacement at time 10ms (mm)	5.47	1.77	-67.6
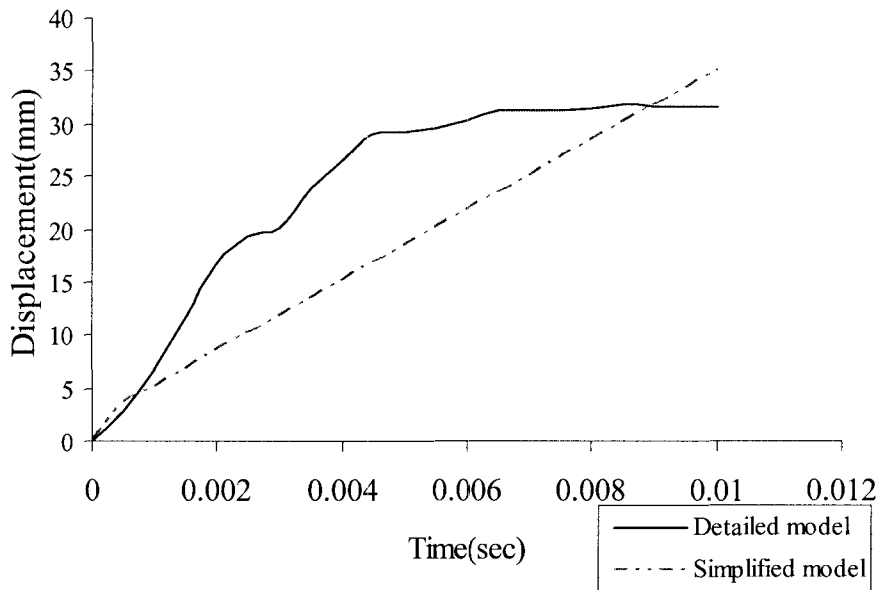
Figure22. Displacements at node2

Table 5. Comparison of Displacements at Node2

	Detailed model	Simplified model	Difference (%)
Displacement at time 3ms (mm)	20.1	11.8	-41.3
Displacement at time 6ms (mm)	30.3	21.8	-28.1
Displacement at time 8ms (mm)	31.4	28.4	-9.6
Displacement at time 10ms (mm)	31.7	35.1	10.7
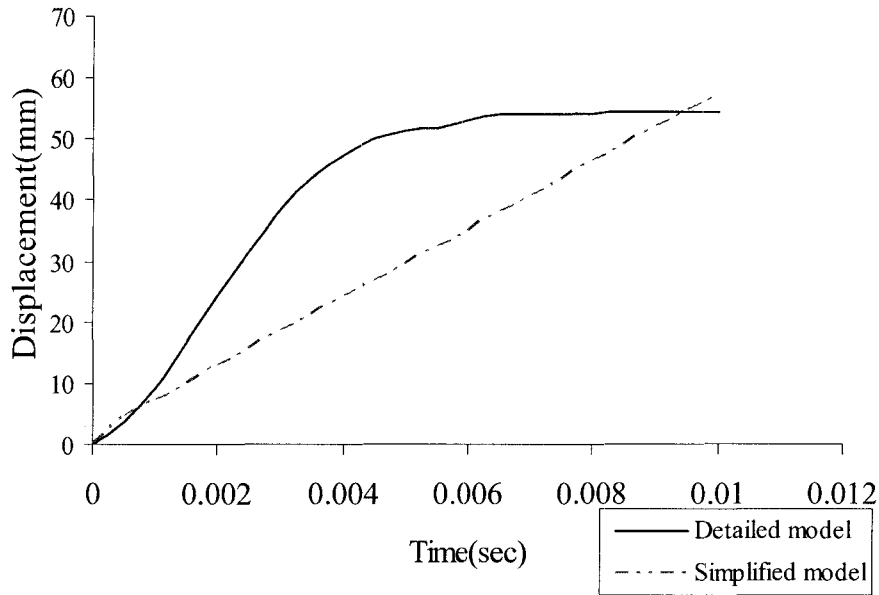
Figure23. Displacements at node3

Table 6. Comparison of Displacements at Node3

	Detailed model	Simplified model	Difference (%)
Displacement at time 3ms (mm)	38.3	18.5	-51.7
Displacement at time 6ms (mm)	53.1	35.2	-33.7
Displacement at time 8ms (mm)	54.0	46.4	-14.1
Displacement at time 10ms (mm)	54.3	57.5	5.9

The above tables and Figures show that the corresponding nodes 1, 2, and 3 in the different models experienced different displacement histories during the crash analysis. Also, from the results of the comparisons, it can be found that except for node1, nodes 2 and 3 of both models reached similar final displacements at the end of the analysis. Considering the good correlation between both models' end displacements, it can be concluded that in the simplified model, even though an individual spring can not truly

reflect the crash behavior of the plastic folds, the entire model can correctly simulate the detailed beam model's crash process with the help from the developed nonlinear springs.

2.2.6 Application of the Simplified Modeling Method

In last section, the simplified model was created for a straight square section beam. The same modeling method should be applied to modeling more straight box section beams with different geometries. In this section, a detailed model for a straight thin-walled beam with a rectangular section is presented, and a simplified model is then created following the same steps validating the presented modeling method. In the rectangular section beam model, all the conditions and geometries are exactly the same as the earlier square section beam model, except that its cross section is 40mm×60mm. With all the given parameters, the mean crushing force P_m and the length of one plastic fold $2H$ can be calculated as 28.5KN and 30.6mm respectively using equations 2-1 through 2-4. Then, the characteristics of the nonlinear spring element can be determined as well as the arrangements of the spring elements in the new simplified model. Similar to the earlier model, the new simplified model is composed of 100 beam elements and the 9 spring elements that were just determined. Both the detailed and the simplified models are analyzed by the same crash analyses described in previous sections. The dynamic results are compared and displayed through the following Figures and table.

This end is fully constrained
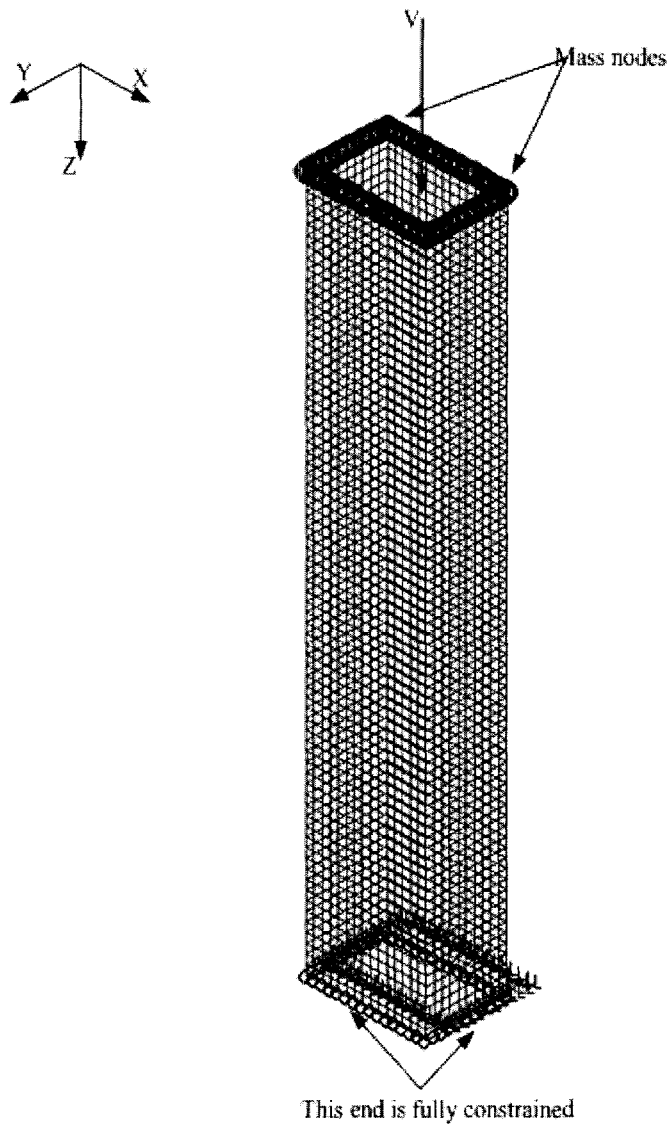
Figure 24. Detailed model for thin-walled straight beam with rectangular section
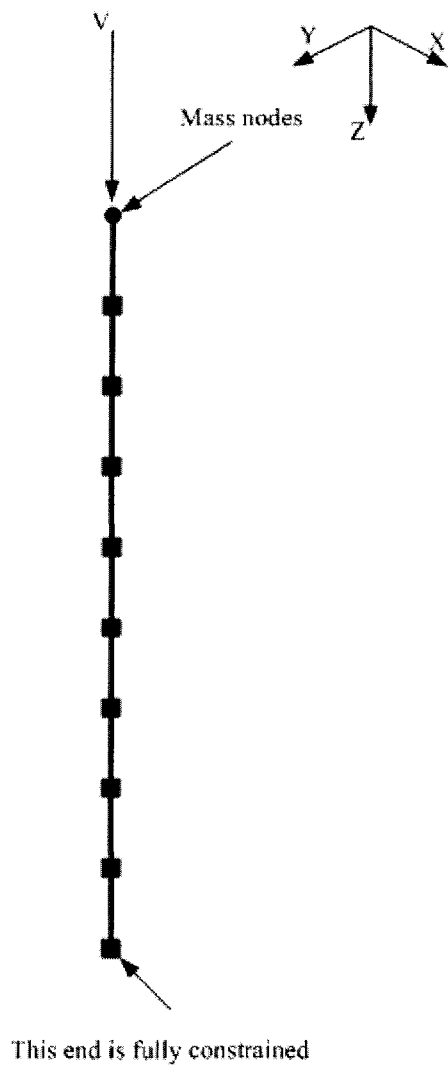
Figure 25. Simplified model for thin-walled straight beam with rectangular section
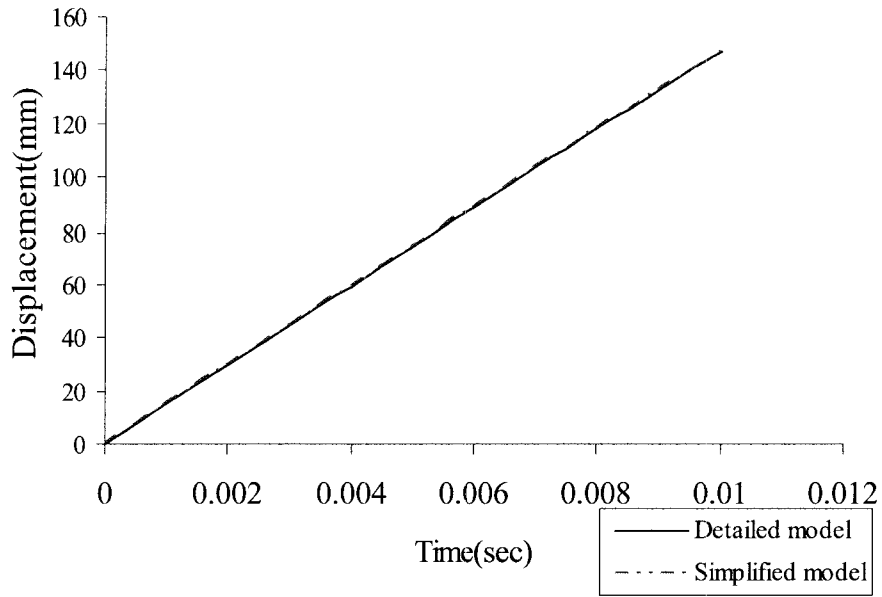
Figure 26. Displacement at end of straight rectangular section beam models
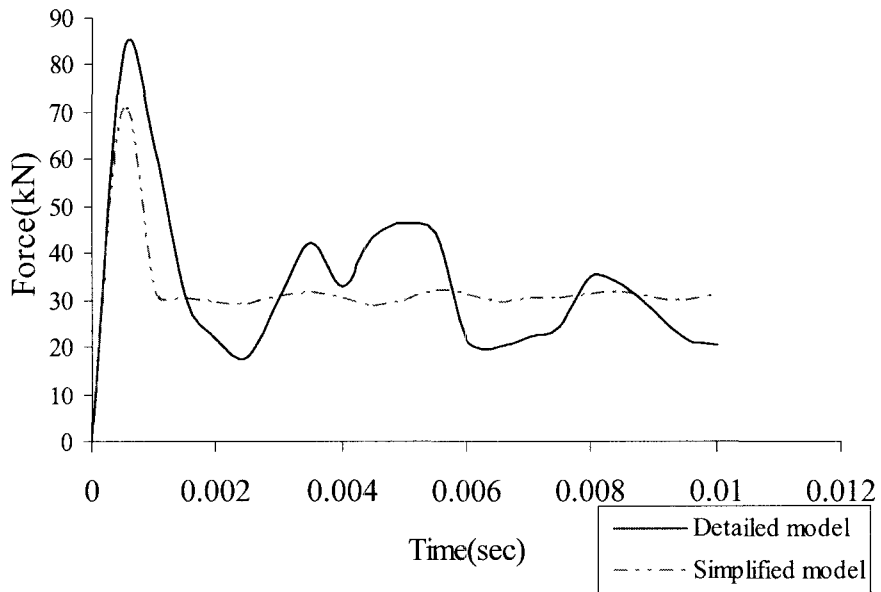

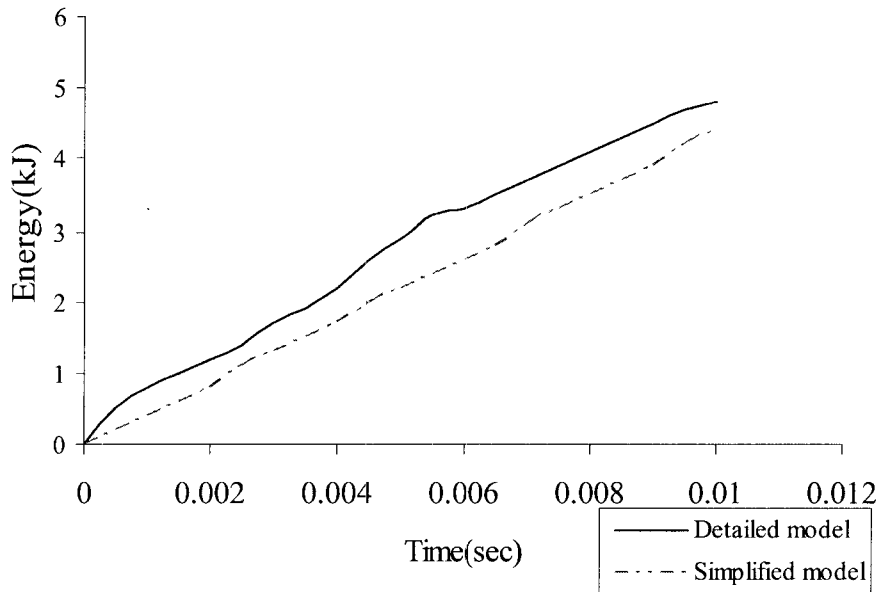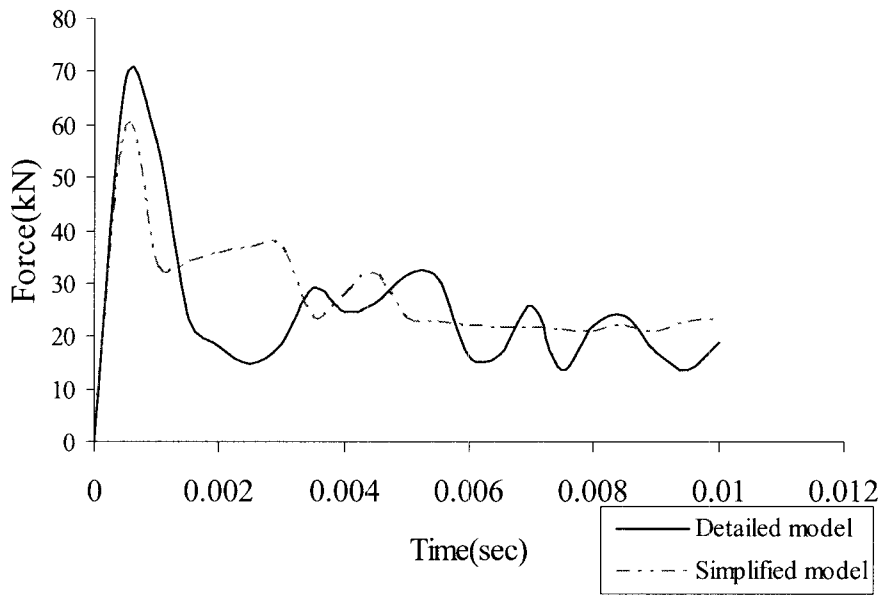Figure 27. Crushing forces for straight rectangular section beam models
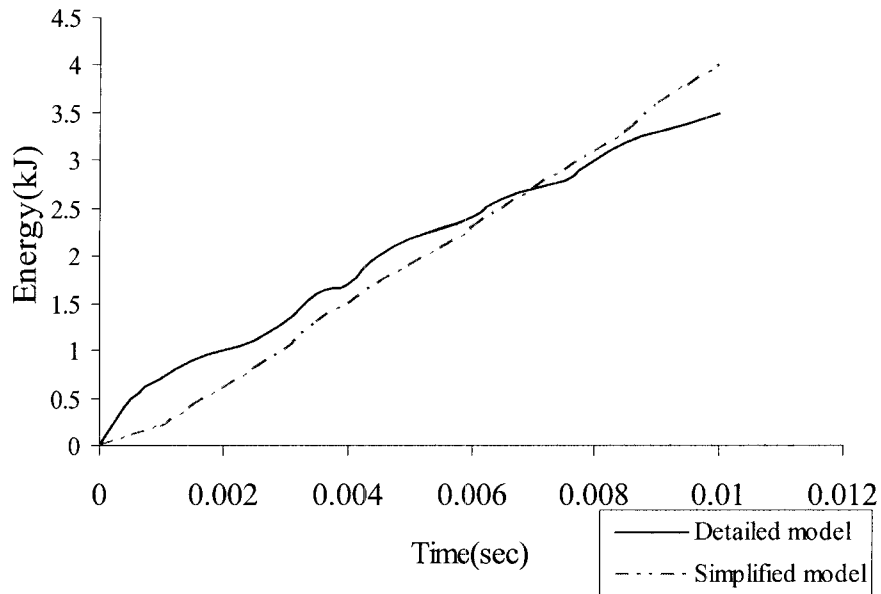
Figure 28. Absorbed energies for straight rectangular section beam models

Table 7. Comparison of Dynamic Results from Detailed and Simplified Straight Rectangular Section Beam Models

	Detailed model	Simplified model	Difference (%)
Global displacement (mm)	147.3	147.1	-0.1
Peak crushing force (kN)	68.8	59.4	-13.7
Absorbed energy (kJ)	3.54	3.97	12.1
Computer time (sec)	3453	173	-95

From the above Figures and table, similar results can be obtained as that of the straight thin-walled rectangular beam. The errors between the crash results of the simplified and the detailed models are within 15%. The simplified model only took about 5% of the computer time required by the detailed models.

2.2.7 Conclusions

From the analyses and comparisons, it is shown that the simplified models created in this section can be efficiently used for crash analysis while saving a large amount of computer time. Therefore, a valid method to develop the simplified model for straight thin-walled box section beams, which are subjected to axial loading during the crashes, can be summarized by the following steps:

- Apply existing equations to determine the mean crushing force P_m and the length of one plastic fold $2H$

- Based on these results, define the force-deflection characteristic of the nonlinear spring element, as shown in figure19

- Divide the entire beam into a certain number of segments with equal length $2H$;

- Use the beam element with the correct cross section information to model those segments. Then use the defined spring element to connect those segments with the remaining part.

2.3 Simplified Modeling of "Z" Shaped Beams

In this section, simplified models for thin-walled curved beams are developed by applying some of the existing collapse theories. Unlike the straight beam, the thin-walled curved beam experiences more bending and rotation during the crash instead of crushing axially. T. Wierzbicki and W. Abramowicz's theories [34, 35] about the thin-walled beam subjected to its bending moment are applied to creating the simplified models. Their theories about the collapse mechanisms of the curved beam are also referenced. Similar to the previous studies, simplified modeling begins with a detailed model for a

simple "Z" shaped beam, which is composed of three straight segments and has square cross section.

2.3.1 Detailed Model

Figure 29 shows the detailed model of the thin-walled "Z" shaped beam with a square cross section, which is used for crash analysis. All the related conditions and information are listed and shown below. The dynamic results will be recorded and compared with those from the simplified model, which will be presented in later sections.
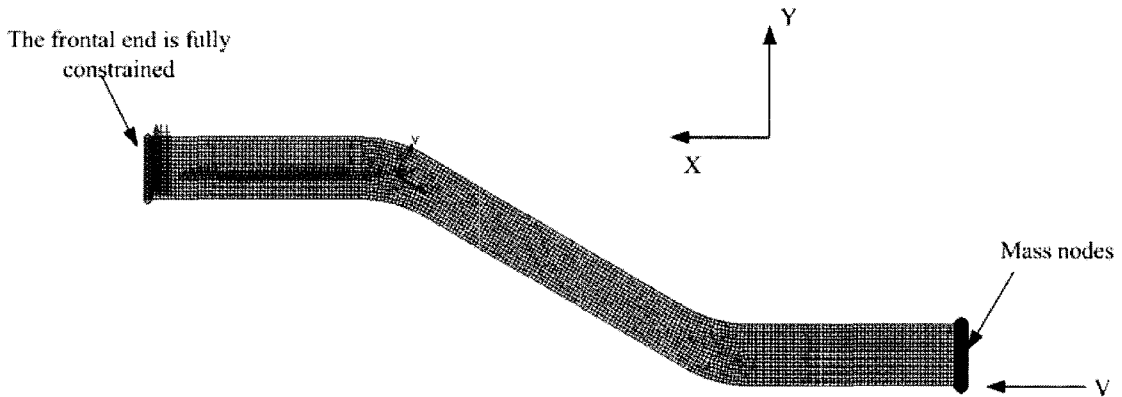
Figure 29. Detailed model for thin-walled "Z" shaped beam with square section

Also, as shown in this figure, during the crash analysis, the beam model is fully constrained at its frontal end. The initial velocity is applied on the other end to make the model move along the X direction. All the related conditions and information about this thin-walled "Z" shaped beam are listed in table 8. The important dynamic results are documented and compared with those from the simplified model after the analysis, which will be presented in a later section.

Table 8. Thin-Walled "Z" Shaped Beam Input Data

Material Properties	
Young's modulus (E)	2.07E5MPa
Density (ρ)	7830kg/m^3
Yield Stress (σ_y)	200MPa
Ultimate Stress (σ_u)	448MPa
Hardening modulus (E_{sn})	630MPa
Poisson's ratio (ν)	0.3

Geometries	
Total length (L)	1084mm
Cross section (a,b)	80mm×80mm
Wall thickness (t)	1.6mm

Crash conditions	
Added mass (m)	640kg
Initial velocity (v_0)	15m/s
Crash time (t_c)	0.01sec
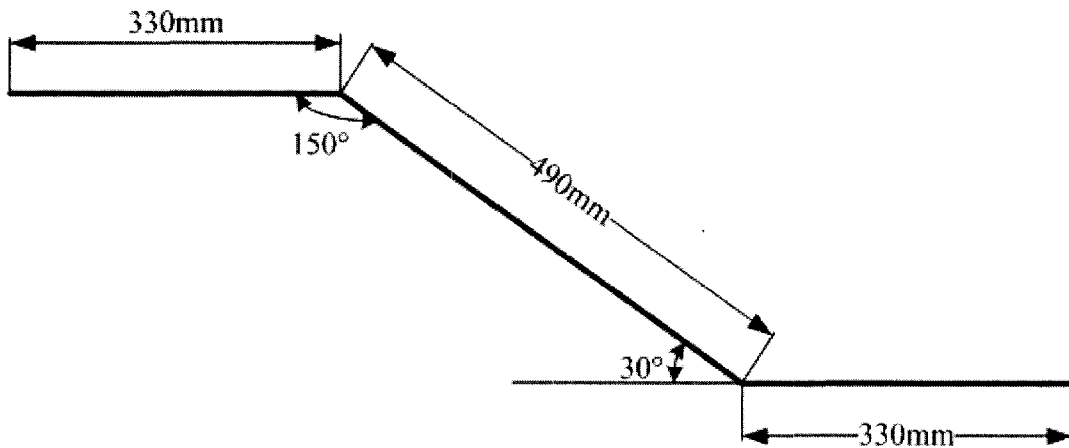
Figure 30. Geometries of detailed thin-walled "Z" shaped beam model

2.3.2 Collapse Mechanisms of "Z" Shaped Thin-walled Beams

Due to its curved shape, the crash of the "Z" shaped beam will generate a bending moment in addition to the axial crushing force. The effect of the bending moment is the rotation of each segment of the beam around its local plastic hinge. One published paper [36] concluded that during the crash of the thin-walled "Z" shaped beams, the collapse or large shape distortion of the beams is localized over relatively narrow zones while the remainder of the structure undergoes rotations around the local plastic hinges. This phenomenon is verified by the results of the computer simulation. Figure 31 plots the deformed shape at 50msec, and Figures 30 and 32 compare the dimensions of the original and the deformed models.

Figures 31 and 32 reveal that during the crash analysis, all the segments of the "Z" shaped beam rotated around the local plastic hinges and that the axial deformations mainly concentrate on these plastic hinges. When comparing Figures 30 and 32 at time 50msec, the axial deformations along each segment equal $330 - 323.3 = 6.7$mm, $490 - 472.7 = 17.3$mm, and $330 - 326.4 = 3.6$mm. The global displacement caused by rotations are calculated from the geometrical relationships as $[330 + 490\cos(30°) + 330] - [323.3\cos(4.2°) - 472.7\cos(4.2° + 50.1°) + 326.4\cos(4.2° + 50.1° - 30.7°)] = 735.4$mm. The results indicate that the displacements caused by the axial deformations are very small compared to those caused by rotations. The global displacement 735.4mm is estimated from the approximate deformed geometries of the "Z" model. In later sections, this value will be validated through comparison with the computer results.
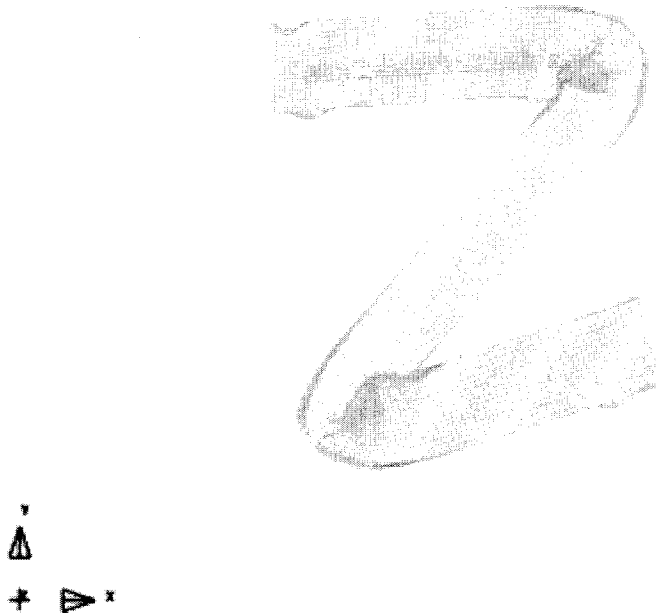
Figure 31. Deformed shape of detailed thin-walled "Z" shaped beam model, t = 50msec
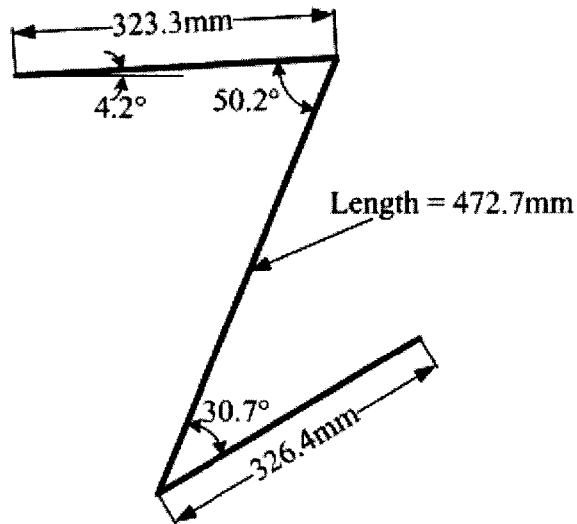
Figure 32. Geometries of deformed detailed "Z" shaped beam model, t = 50msec

2.3.3 Nonlinear Spring Characteristics

According to Figures 30 through 32, the "Z" shaped beam can be decomposed into three straight segments, which are connected by three plastic hinges (as shown in

Figure 33). Also, as demonstrated earlier, it can be assumed that during the crash, the three straight segments only rotate about the local plastic hinges. Thus, the key problem of the simplified modeling becomes how to correctly represent the plastic hinge's behavior during the entire crash process.

As discussed in a previous article [29], during the crash, the plastic hinge works as a nonlinear rotational spring. Its general $M(\theta) - \theta$ characteristic has also been developed in the same paper. $M(\theta)$ is the bending moment that was applied on the spring, and the θ is the spring's rotation angle (as shown in Figure 34).
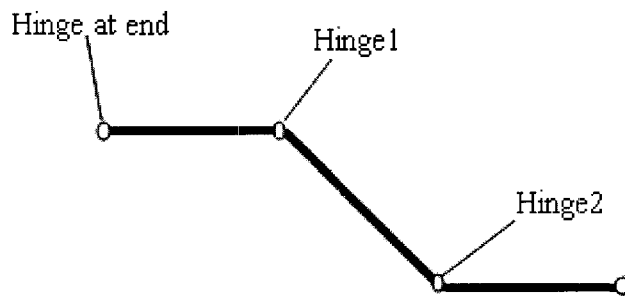
Figure 33. Three plastic hinges of "Z" shaped beam
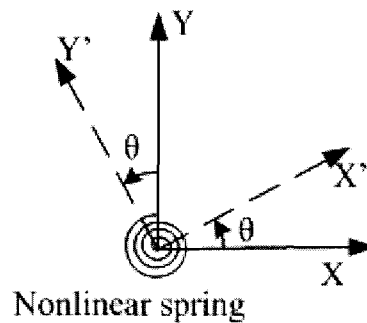
Figure 34. Rotation angle of nonlinear spring

From the published conclusions ([29]), the bending resistance of the rotational spring is defined using following formulae:

$$\frac{M(\theta)}{M_0 a} = (A-1)\left[6 + \cos\alpha\left(\frac{2}{(2-\sin\alpha)\sqrt{1-\sin\alpha}} + 2\phi + 26.2\right)\right] + 2A(1+\sin\alpha) + 2 \qquad 2\text{-}5$$

where

$$M_0 = (\sigma_0 t^2)/4 \qquad 2\text{-}6$$

is a fully plastic moment per unit length of the section wall, and

$$A = \frac{\lambda\cos\left(\theta/2\right)}{\sqrt{\lambda\sin\left(\theta/2\right) - \lambda^2\sin^2\left(\theta/2\right)}} \qquad 2\text{-}7$$

$$\phi = \arccos\left(1 - 2\lambda\sin\left(\theta/2\right)\right) \qquad 2\text{-}8$$

$$\lambda = \frac{a}{b} \qquad 2\text{-}9$$

$$\alpha = \phi - \theta/2 \qquad 2\text{-}10$$

a is the width of the cross section (web) and the b is the depth of the cross section (flange).

Equation 2-5 shows that the moment ratio $\dfrac{M(\theta)}{M_0 a}$ is a function of λ, and Figure 35

plots different $\dfrac{M(\theta)}{M_0 a}$ curves with respect to $\lambda = 0.5$, 1, and 1.5. The value of

$\dfrac{M(\theta)}{M_0 a}$ increases as λ increases.
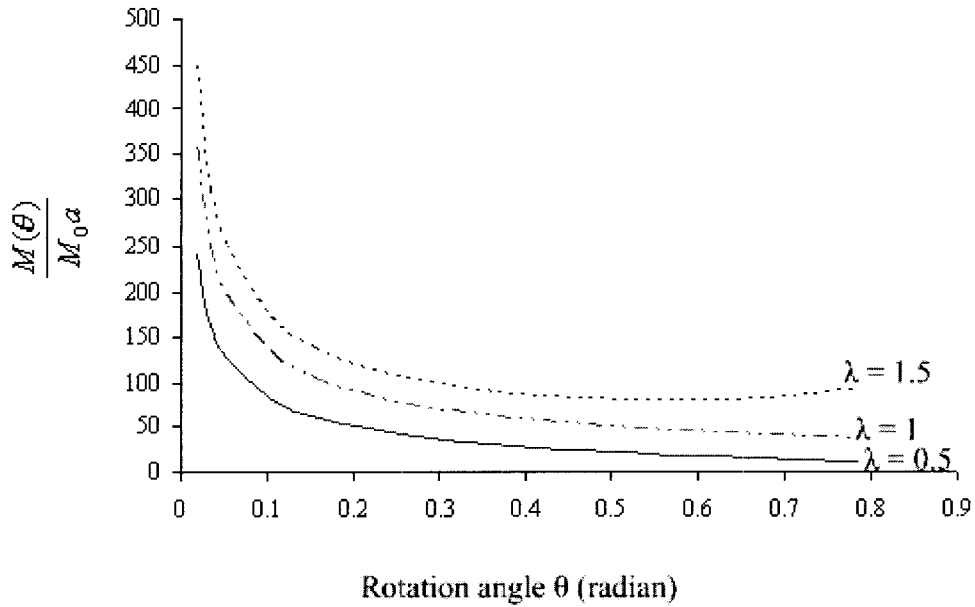
Figure 35. $\dfrac{M(\theta)}{M_0 a}$ vs. θ for various λ, box section beam

Nevertheless, the above equations cannot correctly predict the $M(\theta) - \theta$ relationship for very small θ, and from equation 2-5 and 2-7 it is inferred that the $M(\theta)$ tends toward infinity as θ approaches zero. Thus, another equation is required to describe the $M(\theta) - \theta$ relationship when θ approaches zero. Previous literature [30] and [34] discusses this problem. In those articles, the moment $M(\theta)$ under very small θ is described as linearly increasing from zero to its fully plastic moment M_p (2-11), and then decreasing to follow the relationship defined by equation 2-5. Thus, the entire $M(\theta) - \theta$ relationship is composed of two parts: the linear relationship where the moment increases from 0 to M_p and the relationship defined by equation 2-5 for the increasing θ.

According to reference [30], the fully plastic moment of a rectangular section M_p is:

$$M_p = \sigma_0 t[a(b-t) + \frac{1}{2}(b - 2t)^2]$$
2-11

60

On the other hand, the assumption that the plastic hinge can work as a nonlinear spring is only valid before the plastic hinge jams, so it is necessary to determine the angle of jamming θ_J for this assumption. D. Kecman [30] illustrated that the jamming happened when the two buckled halves of the compression flange contact each other. The appropriate angle of jamming is

$$\theta_J = 2\arcsin\left(\frac{h - 0.5t}{b}\right)$$

2-12

where h = min$\{a/2, b/2\}$ and t is the wall thickness.

After substituting all the given parameters into above equations, the M_p and the related θ_p are then calculated in addition to the jamming angle θ_J. Therefore, the spring's moment-rotation characteristics are entirely displayed by an $M(\theta) - \theta$ plot, which is composed of a straight line for the initial θ and a curve defined by equation 2-5 (as shown in Figure 36).
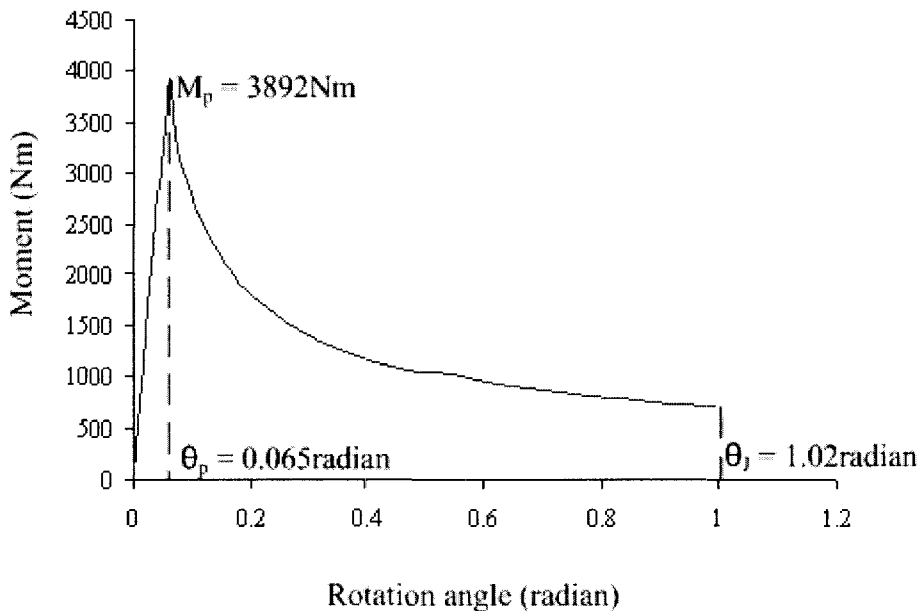
Figure 36. $M(\theta) - \theta$ curve of nonlinear spring element for "Z" shaped box section beam

2.3.4 Development of Simplified Model

To develop the simplified model for the "Z" shaped beam, the entire beam is assumed to be composed of three straight beam segments which are connected by three plastic hinges. Then in the simplified model, the straight beam segments are modeled using the Hughes – Liu beam elements with the appropriate cross sectional information. The nonlinear rotational spring elements developed in 2.3.3 are used for modeling the local plastic hinges. Similarly, a rotational angle – moment table is created in LS-DYNA to generate the nonlinear rotational spring element. As shown in Figure 36, (0, 0) and (0.065, 3892) are input to describe the linear portion of the spring's bending resistance. Next, a series of moment $M(\theta)$ is calculated using Microsoft Excel in terms of varying θ from 0.065radian to 1.02radian with an equal spacing of 0.05radian. Then, these angles and moments are entered into the table to completely define the nonlinear spring element. This method is used to create the other rotational nonlinear spring elements involved in this project. Figure37 shows the model in which each straight segment is modeled using 32 beam elements. The effects of the mesh density are studied later.
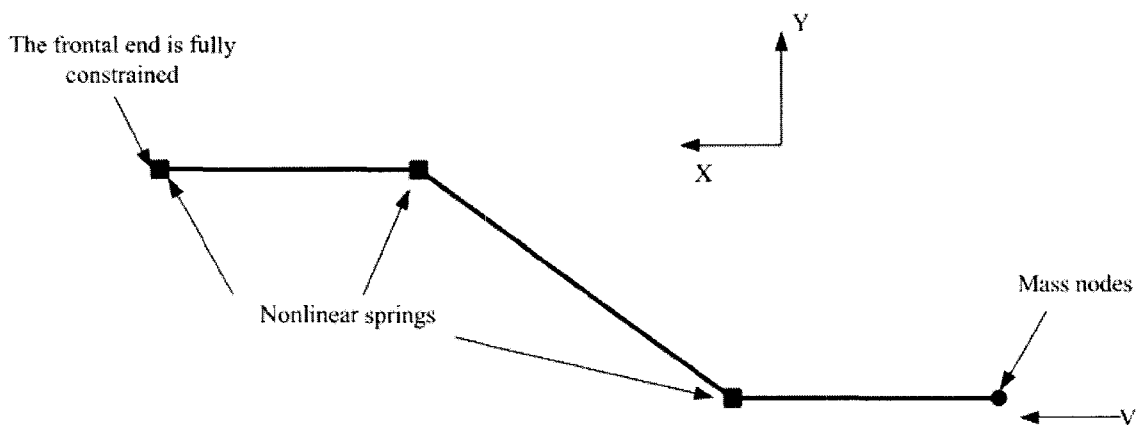
Figure 37. Simplified model for thin-walled "Z" shaped box section beam

In deciding the simplified model's boundary conditions, the boundary conditions of the previous detailed model are referenced. In the simplified model, the impact-end node of the "Z" beam is fully constrained by fixing all of its six degrees of freedom. Only the translational degree of freedom along the length is set free for the rear end node, where the initial velocity is imposed. Additionally, since the "Z" beam is defined along a 2D plane, certain constraints are applied on all its nodes to prevent out-of-plane motion. Meanwhile, the coincident nodes where the spring elements are defined are set to move together during the crash to ensure correct connectivity.

2.3.5 Dynamic Results and Comparisons

After finishing the modeling, both the detailed and the simplified models are used in the crash analysis. Their results are compared to each other to determine the correlations. To thoroughly investigate the motion of the "Z" shaped beam and to verify the efficiency of the simplified model, the deformations at hinge 1 and 2 are compared in addition to the hinge at the rear end. The following table and Figures display all the results.
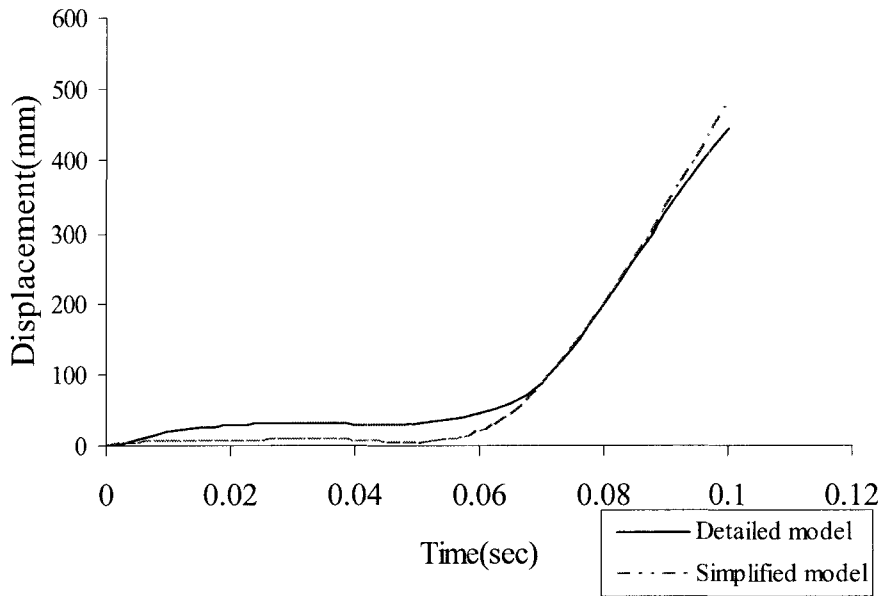
Figure 38. Displacement at hinge1 of "Z" shaped square section beam models
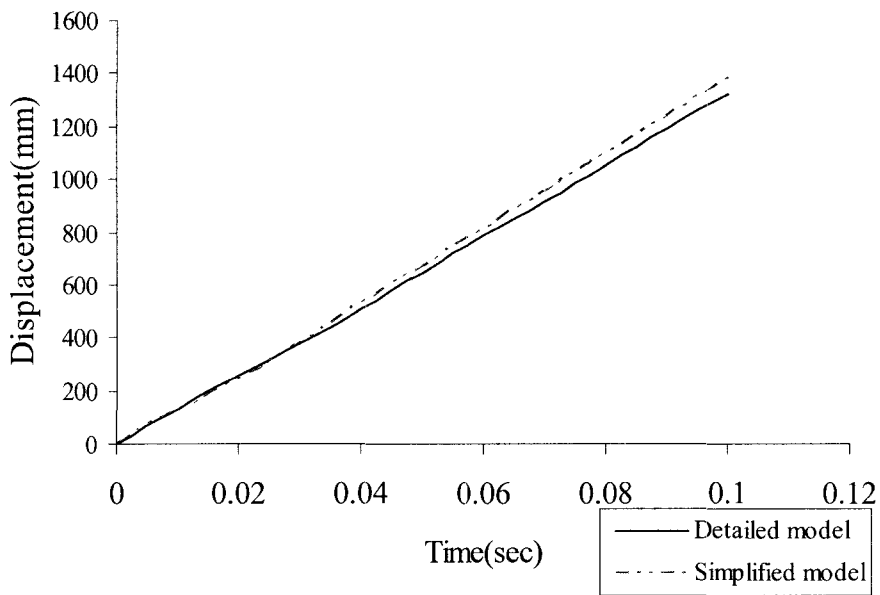
Figure 39. Displacement at hinge2 of "Z" shaped square section beam models
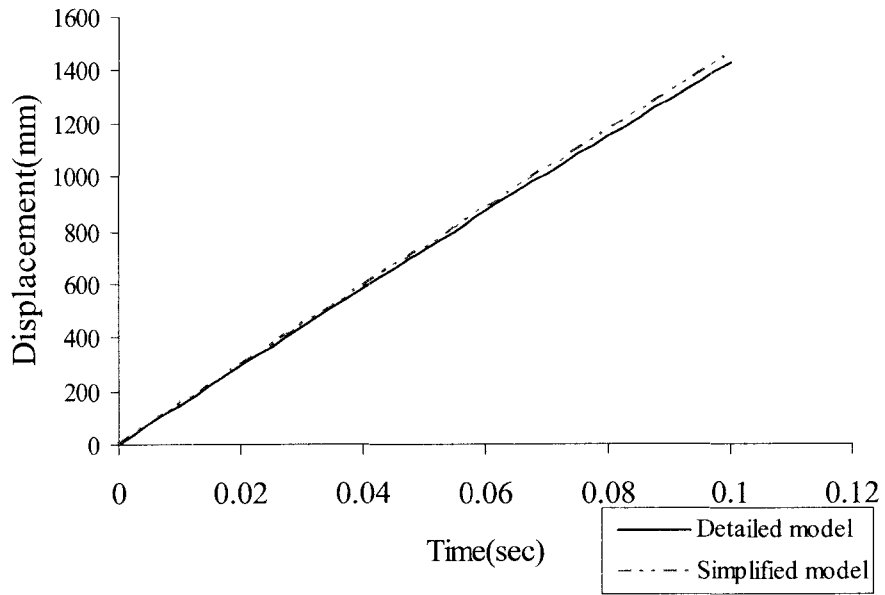
Figure 40. Displacement at end of "Z" shaped square section beam models
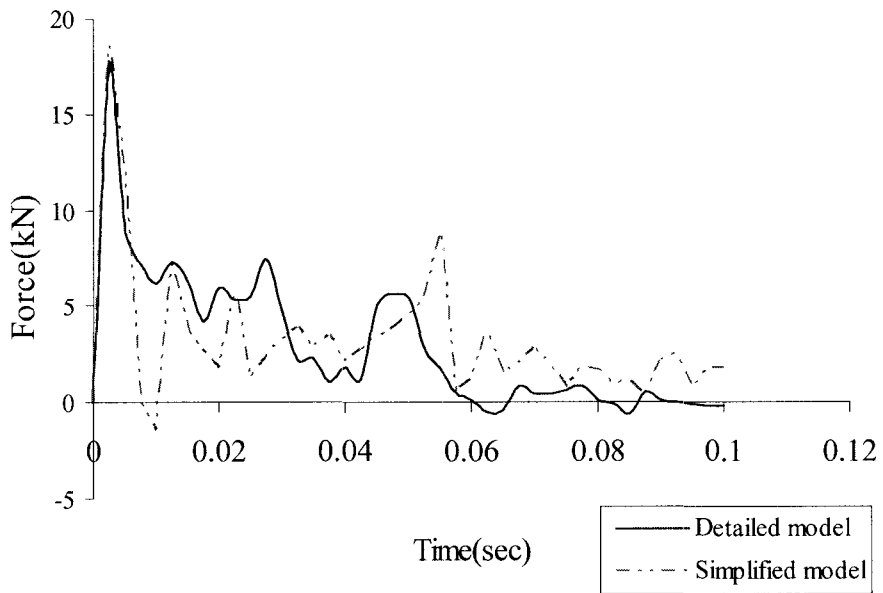
Figure 41. Crushing forces for "Z" shaped square section beam models

65
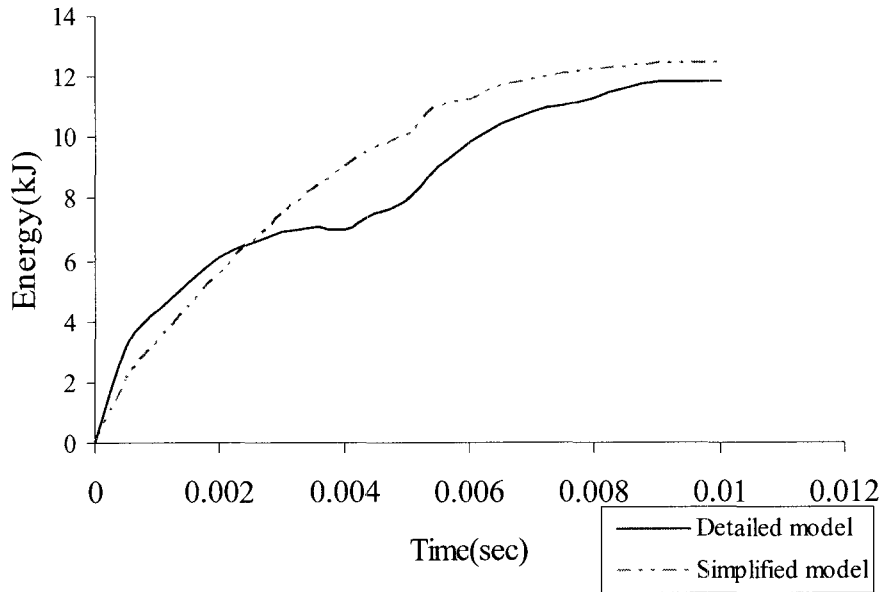
Figure 42. Absorbed energies for "Z" shaped box section beam models

Table 9. Comparison of Dynamic Results from Detailed and Simplified "Z" Shaped
Square Section Beam Models

	Detailed model	Simplified model	Difference (%)
Displacement at hinge1 (mm)	444	482	8.6
Displacement at hinge2 (mm)	1318	1379	4.6
Global displacement (mm)	1429	1464	2.4
Peak crushing force (kN)	17.6	18.7	6.3
Absorbed energy (kJ)	11.9	12.4	4.2
Computer time (sec)	4277	358	-91.6

From comparison of the results, it is shown that the developed simplified "Z" shaped model is qualified for replacing the detailed model to be used for crash analyses. Table 9 shows that the dynamic results yielded from the 32-element simplified model correlated to those from the detailed model very well. All the errors are below 10%, and the simplified model only takes about 8% of the computer time of the detailed model.

From the output of the global displacements, it is found that the detailed model's global displacement at time 50msec is 733. 7mm, which correlates very well to 735.4mm, the value previously estimated from Figure 32. Also, in comparing the displacements at hinges1 and 2, it is seen that both the simplified and the detailed model simulated the crash behavior of the plastic hinges similarly.

2.3.6 Effects of Mesh Density

In the developed simplified model, each straight segment is meshed by 32 beam elements. Since this mesh is fine enough to accurately simulate the crash behavior of the detailed model, is it possible to use less beam elements to further simplify this model and still yield good dynamic results? How would the dynamic results be if different numbers of beam elements were used? To answer these questions, the segments of the simplified "Z" shaped model are re-meshed by 16, 8, 4, 2, and 1 element to obtain a series of simplified models with different numbers of beam elements. These models are used in the same crash analyses, and the dynamic results are compared to investigate the effects of the mesh density on the model's crash response. Table10 lists the results of the comparisons, and all the resulting plots are listed in appendix B.

Table 10. Comparison of Dynamic Results from Simplified "Z" Shaped Beam Models with Different Numbers of Elements

# of elements for each segment	Detailed model	1	2	4	8	16	32
Displacement at hinge1 (mm)	444	516	504	505	510	502	482
Difference (%)		16.2	13.5	13.7	14.9	13.1	8.9
Displacement at hinge2 (mm)	1318	1344	1404	1408	1415	1404	1379
Difference (%)		2.0	6.5	6.8	7.4	6.5	4.6
Global displacement (mm)	1429	1473	1460	1465	1462	1468	1464
Difference (%)		3.1	2.2	2.5	2.3	2.7	2.4
Peak force (kN)	17.6	27.1	26.7	26.4	23.3	22.2	20.1
Difference (%)		54.0	51.7	50.0	32.4	26.1	14.2
Absorbed energy (kJ)	11.9	16.6	9.7	9.7	9.4	10.3	12.4
Difference (%)		39.5	-18.5	-18.5	-21.0	-13.4	4.2
Computer time (sec)	4277	7	8	14	34	104	358
Difference (%)		-99.9	-99.8	-99.7	-99.2	-97.6	-91.6

From Table 10 it is concluded that the mesh density obviously affects the peak crushing force value and the absorbed energy. As shown in this table, the finer the model is meshed, the lower error is and the more computer time it takes. The 32-element model is an appropriate choice that uses the least number of elements to give qualified errors (<15%) and that is fine enough to avoid a significant element-size effect.

2.3.7 Conclusions

In the end of this section, the simplified modeling method for the "Z" shaped thin-walled beams with box sections is described. Briefly, it is to use beam elements to construct the body of the beam and to use nonlinear rotational springs to model the plastic hinges that connect the elements together. Those plastic hinges are located at the intersections of the straight beam segments. In determining the bending resistance of the

nonlinear rotational springs, the full plastic moment M_P and the angle of jamming θ_J are decided first. Then, the previously published equations 2-5 through 2-10 are applied to create the $M(\theta) - \theta$ curve which starts from (θ_P, M_P) and ends at $(\theta_J, M(\theta_J))$. Also, the moment – angle relationship between $(0, 0)$ and (θ_P, M_P) is assumed to be linear. Therefore, an entire $M(\theta) - \theta$ curve is created, and the spring's deflection limit is defined as θ_J.

2.4 Simplified Modeling of "S" Shaped Beams

In the previous section, simplified models are created for straight and "Z" shaped beams, which only have straight segments. In this part, an "S" shaped thin-walled beam is used for developing a corresponding simplified model, which contains arc segments as well as straight segments. During the modeling process, the simplified modeling method developed in section 2.3 is applied. Several simplified models are created to find the best way to represent the crash behavior of the arc segments.

2.4.1 Detailed Model

The "S" shaped model is derived from P. Drazetic's paper [24]; Figure 43 shows its geometries, and Figure 44 presents the detailed model. All the other information and crash conditions about the model are plotted and listed in Figure 44 and Table 11.
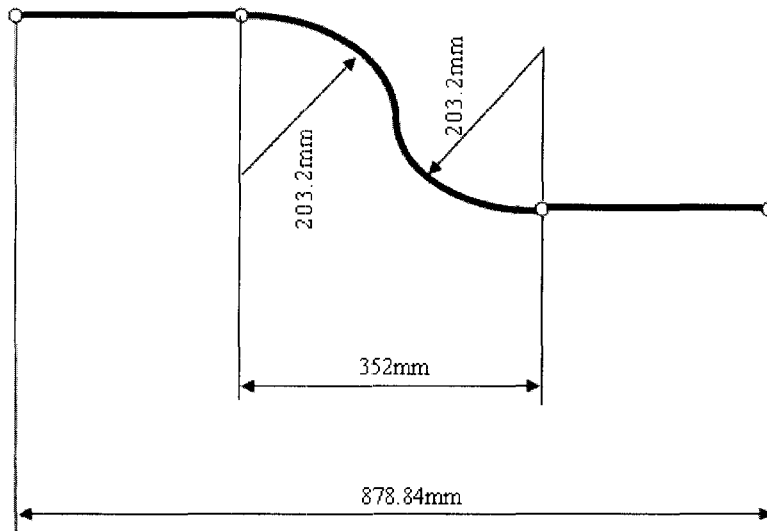
Figure 43. Geometries of detailed thin-walled "S" shaped beam model
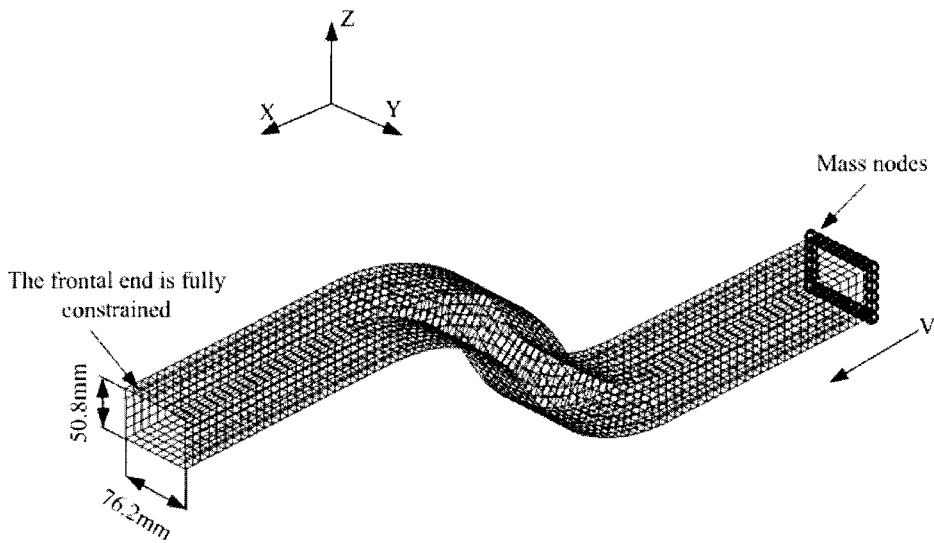
Figure 44. Detailed model for thin-walled "S" shaped beam with rectangular section

Table 11. Thin-Walled "S" Shaped Beam Input Data

Material Properties	
Young's modulus (E)	2.07E5MPa
Density (ρ)	7902.4kg/m^3
Yield Stress (σ_y)	248.3MPa
Ultimate Stress (σ_u)	448MPa
Hardening modulus (E_{sn})	0
Poisson's ratio (ν)	0.3

Geometries	
Total length (L)	878.84mm
Cross section (a,b)	76.2mm×50.8mm
Wall thickness (t)	3.175mm

Crash conditions	
Added mass (m)	965kg
Initial velocity (v_0)	4.5m/s
Crash time (t_c)	0.007sec

2.4.2 Development of the Simplified Model

In developing the simplified model for the "S" shaped beam model, the modeling method presented in section 2.3 is used. Equations 2-5 through 2-12 are applied to calculate the bending resistance of the equivalent rotational spring. Since this model has a rectangular cross section, the cross sectional width, a, and its depth, b, have to be correctly distinguished, which set to 76.2mm and 50.8mm respectively. Performing the calculations, M_P is found to be 3639 ($N \cdot m$), and the θ_J and $M(\theta_J)$ are calculated as 0.97(radians) and 712($N \cdot m$). Then, the $M(\theta) - \theta$ curve as shown in Figure 45 is obtained.
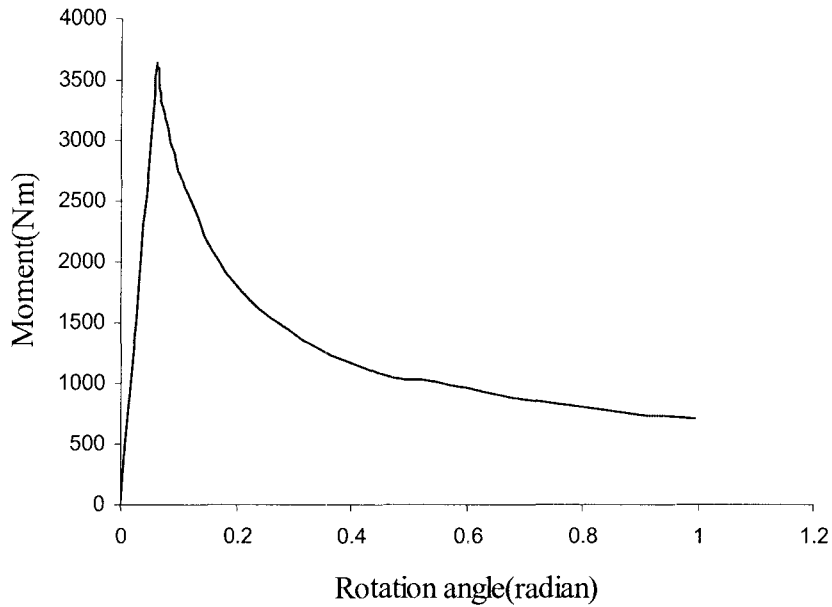
Figure 45. M(θ) $-$ θ curve of nonlinear spring element for "S" shaped box section beam

Another problem in simplifying the "S" shaped mode is how to determine the

locations of the nonlinear springs. In the "Z" shaped model, the springs can be easily set

at the intersections of two neighboring segments and at the impact end, while for the "S"

shaped model, it is hard to predict the spring's locations because of the arc segment. To

remove this problem, the arc segments are equally divided into several parts, and the

nonlinear spring elements will be used to connect them together. Three simplified

models are created by applying this method. Depending on the number of the bodies the

entire model is divided into and the number of spring elements that are used, these three

models are called: 3-beams-3-springs model, 6-beams-6-springs model, and 8-beams-8-

springs model, as shown in Figures 46 through 48.
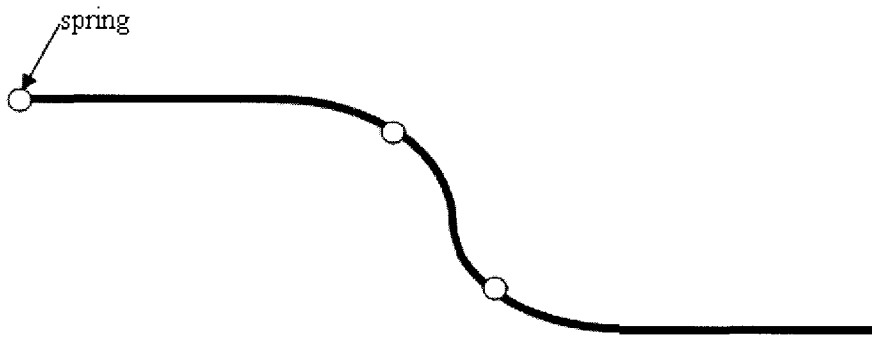
Figure 46. 3-beams-3-springs "S" shaped model
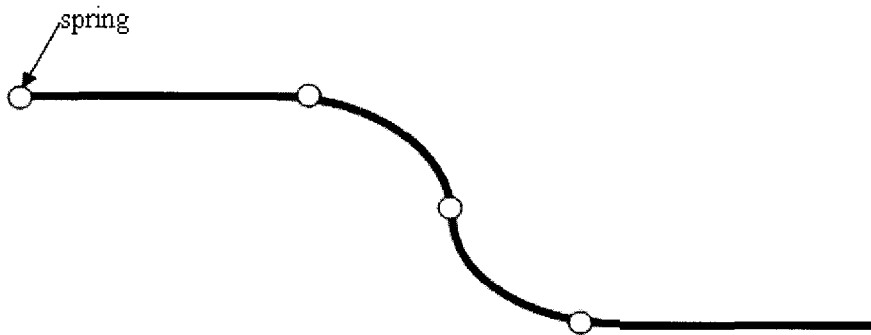
Figure 47. 6-beams-6-springs "S" shaped model
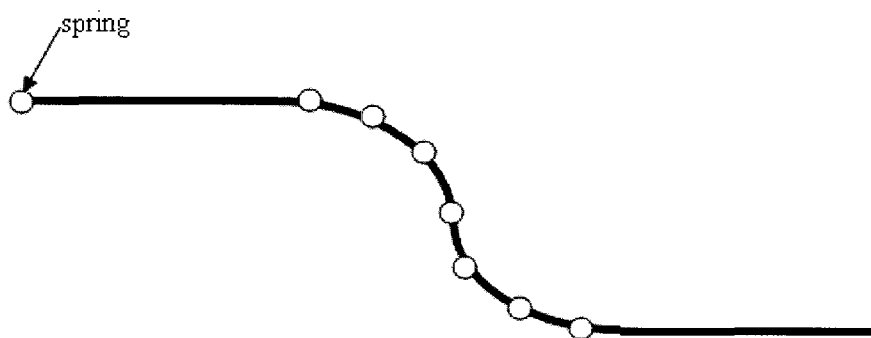
Figure 48. 8-Beams-8-Springs "S" Shaped Model

2.4.3 Dynamic Results and Comparisons

After finishing the simplified models, the same crash analysis is performed on these simplified models as well as the detailed model. Figures 49 through 51 display the forces, displacements, and absorbed energies from the 8-beams-8-springs model and the detailed model. The results from the other two simplified models are also presented in appendix C. Figures 52 through 55 plot the deformed geometries of these models. Table 12 lists all the values and the results of comparisons.
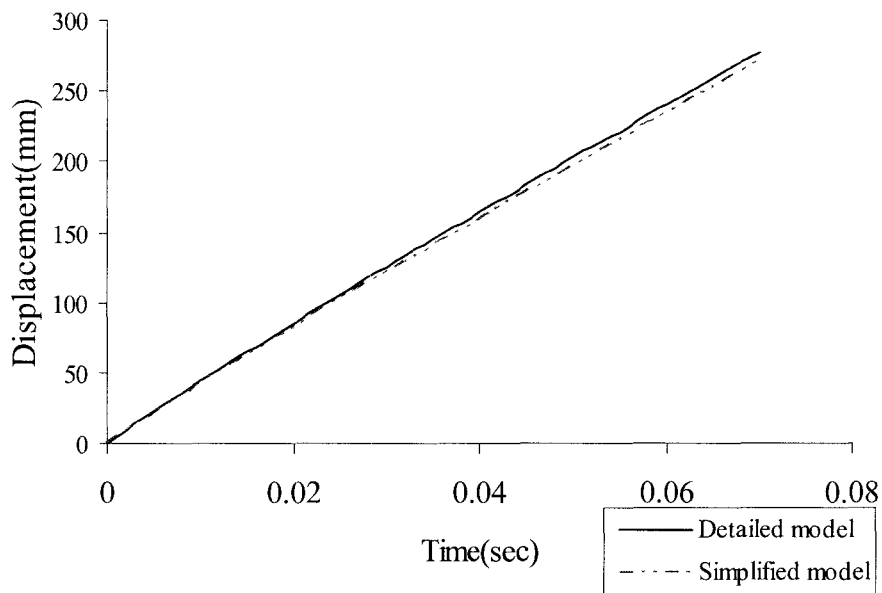
Figure 49. Displacements for "S" shaped beam models with rectangular section
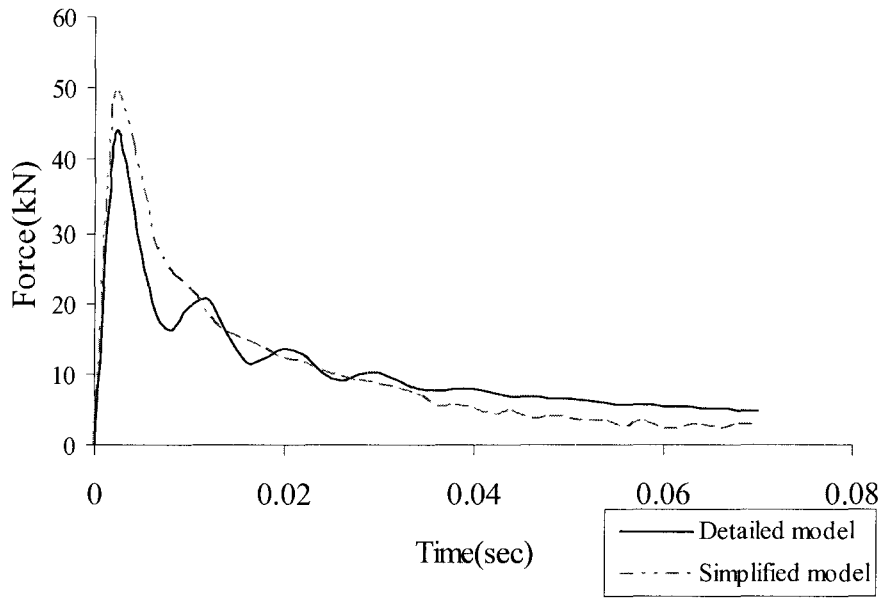
Figure 50. Crushing forces for "S" shaped beam models with rectangular section
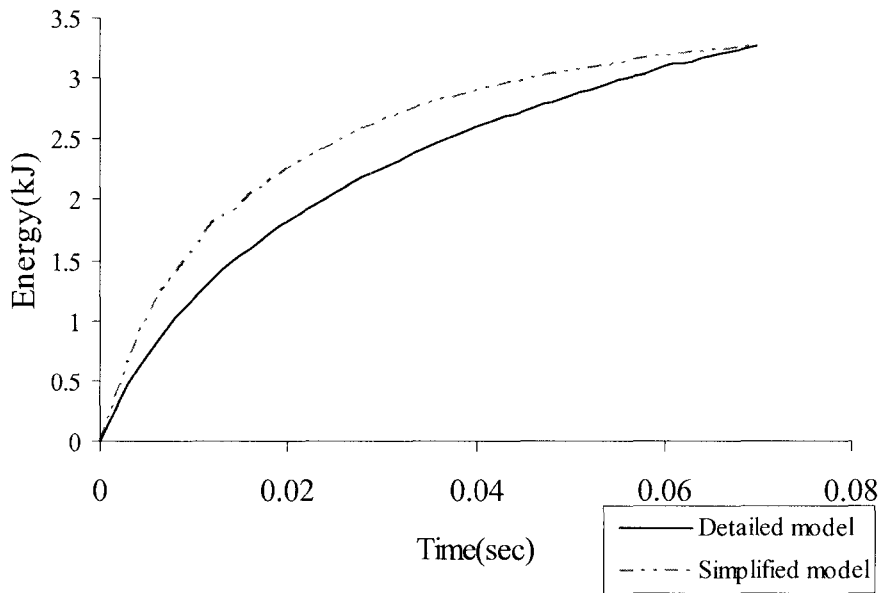
Figure 51. Absorbed energies for "S" shaped beam models with rectangular section
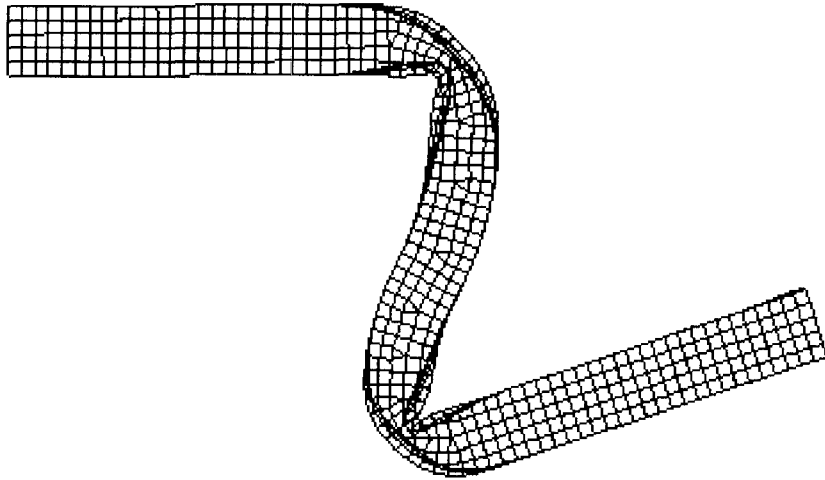
Figure 52. Deformed shape of detailed thin-walled "S" shaped beam model, t = 70msec
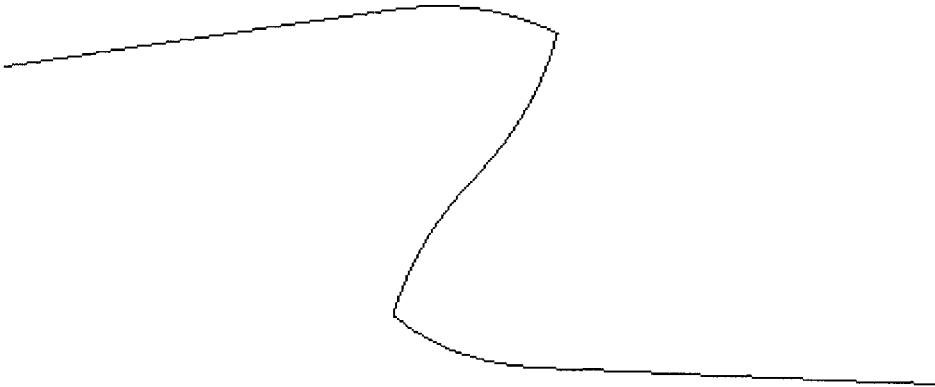
Figure 53. Deformed shape of 3-beams-3-springs "S" shaped model, t = 70msec
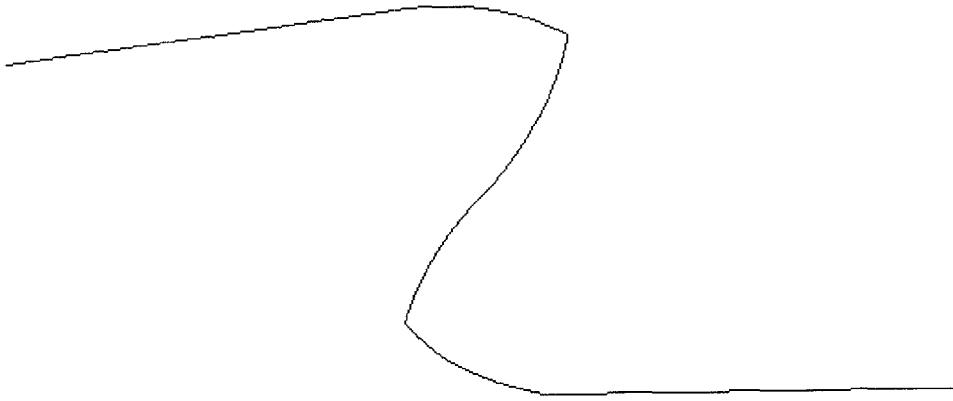
Figure 54. Deformed shape of 6-beams-6-springs "S" shaped model, t = 70msec
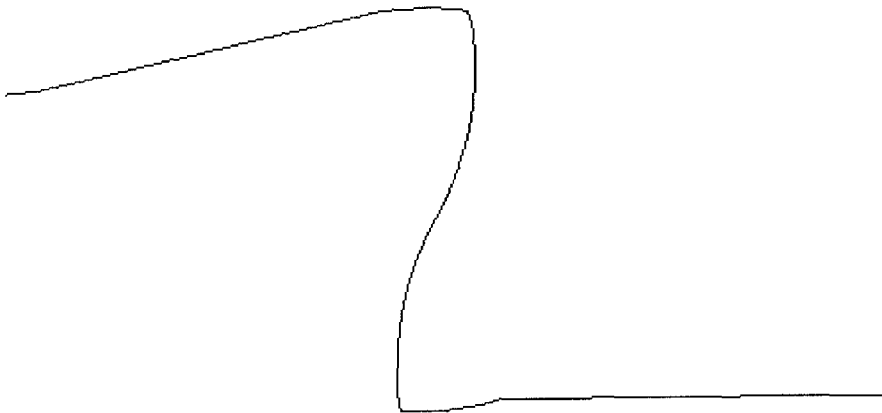
Figure 55. Deformed Shape of 8-Beams-8-Springs "S" Shaped Model, t = 70msec

Table 12. Comparison of Dynamic Results from Simplified "S" Shaped Beam Models with Different Numbers of Spring Elements and Detailed Model

Models	Detailed model	3beams 3springs	6beams 6springs	8beams 8springs
Global displacement (mm)	277	267	267	271
Difference (%)		-3.6	-3.6	-2.2
Peak force (kN)	43.0	58.0	57.9	48.6
Difference (%)		34.9	34.7	13.0
Absorbed energy (kJ)	3.27	3.76	3.59	3.27
Difference (%)		15.0	8.6	0
Computer time (sec)	1589	223	199	233
Difference (%)		-86	-87.5	-85.4

From Table 12, it is found that the 8-beams-8-springs simplified model and the detailed model show the best correlation in representing the "S" shaped beam's crash behavior; all the errors are below 15%. When compared among the simplified models, it is found that the 8-beams-8-springs model is much better than the other two models in simulating the crash behavior of the detailed model. One possible reason is by comparing Figures 45 through 47. From the figures, it can be inferred that since the 3-beams-3-springs and 6-beams-6-springs model divide one arc segment into two parts; then, each arc segment rotates around its midpoint, and only the spring elements at those midpoints work during the crash. The 8-beams-8-springs model divides one arc segment into three parts; thus, two of the spring elements along the arc segment will operate during crash analysis. This phenomenon also verifies that in the "S" shaped model, most of the bending collapse appears in the arc segments. In simplified modeling, the more bodies into which the arc segment is divided, the better the results the simplified model

can provide. Table 12 shows that the models with more beams and more springs do not take more computer time, but only require more labor during the modeling stages.

2.4.4 Conclusions

As described in earlier sections, the results of the comparisons verify that the developed simplified model can simulate the crash behavior of the "S" shaped beam very well. Similar to the simplified "Z" shaped model, in creating the simplified model for the "S" shaped beam, the rotational spring's characteristics need to be decided first. Then the beam elements are used to form the body and to simulate the behavior of the plastic hinges. The only difference in the simplified "S" shaped model is brought by the arc segments. During modeling, the arc segments of the "S" shaped model must be divided into several parts (at least three). Also, the number of rotational spring elements are arranged to connect those parts together to correctly simulate the bending behavior of the arc segments during the crash. In contrast, the "Z" shaped model is easier because the springs can be defined at the "corner nodes".

2.5 Conclusions

In this chapter, the crash behaviors of thin-walled box section beams are investigated, including the straight beam, the "Z" shaped beam, and the "S" shaped beam. Based on current collapse theories, the simplified models for such beams are developed. Respective modeling methods are also summarized and presented. In these simplified models, beam elements and nonlinear spring elements are used to simplify the existing

detailed models by replacing the shell elements. The validity of these simplified models is verified via a series of crash analyses and comparisons.

As an extensional work, the next chapter discusses the thin-walled beams with channel section ("C" cross section) and develops the simplified models for such beams. Similarly, these simplified models use beam elements and nonlinear spring elements. The next chapter begins with the derivation of the bending resistance of the channel section beam based on current theories about the box section beams.

CHAPTER III

DERIVATION OF THE BENDING RESISTANCE OF THE THIN-WALLED

CHANNEL SECTION BEAM

3.1 Introduction

In chapter 2, the simplified crash models for the thin-walled box section beam are

created. In this chapter, the thin-walled beam with channel cross section is studied, and a

reliable simplified model is developed. Unlike the box section beam, there is a very

limited amount of literature about the bending resistance of the channel section beam.

Therefore, this chapter initially derives the mathematic equations necessary to accurately

predict the bending behavior of the channel section beam. Then, as in chapter 2, the

derived bending resistance of the channel section beam is used to define new spring

elements. The same simplified modeling method illustrated in chapter 2 is then applied

to the development of the simplified model for the channel section beam. Three

simplified models are developed with respect to three channel section beams whose cross

sections have different geometries. These simplified models are then used in crash

analyses. The dynamic results are compared with those from the corresponding detailed

models to validate the developed nonlinear spring elements and the derived bending

resistance. The effects of the mesh density are studied in evaluating the simplified

models. The developed nonlinear spring elements are presented and evaluated.

3.2 Background

The relationship between the applied moment and the rotation angle of the thin-walled beam arouses a lot of interest. Previous researchers have developed various mathematical equations to describe or predict the relationship. These equations are very helpful for understanding the crash behavior of the bending thin-walled beams. As introduced in chapter 2, these equations are used to determine the bending resistance of the plastic hinges, which is significant in the development the simplified crash models. W. Abramowicz [29, 31, 32, 33, 34], D. Kecman [30], and T. Wierzbicki [31, 32, 33, 34] apply different ways of deriving the mathematical equations that accurately predict the bending resistance of the box section beams. In some of the simplified crash models developed previously in the literatures [24, 27] and in chapter 2, these equations define the nonlinear spring elements, which simulate the crash behavior of the plastic hinges during a crash. In addition to the box section beam, the channel section beam is another important member widely used in engineering as part of architectural structures, vehicles, and etc. Nevertheless, little research concentrates on the derivation of the bending resistance. Thus, in this chapter, the bending behavior of the thin-walled channel section beam is studied, and its bending resistance is derived.

3.3 Mathematical Derivation

3.3.1 Kinematics of Collapse Model

Figure 56 shows one segment of a regular channel section beam, whose width is a (web), depth is b (flange), and thickness is t. A hard-paper model is made for the

channel section beam. The beam's collapse mode is then observed from the bending behavior of the hard-paper model (as shown in Figure 56). Also, this collapse mode is viewable from a deformed computer model for such a beam after the crash analysis as shown in Figure 57. In this section, the theoretical prediction for the bending resistance of the channel section beam is derived based on this collapse mode.
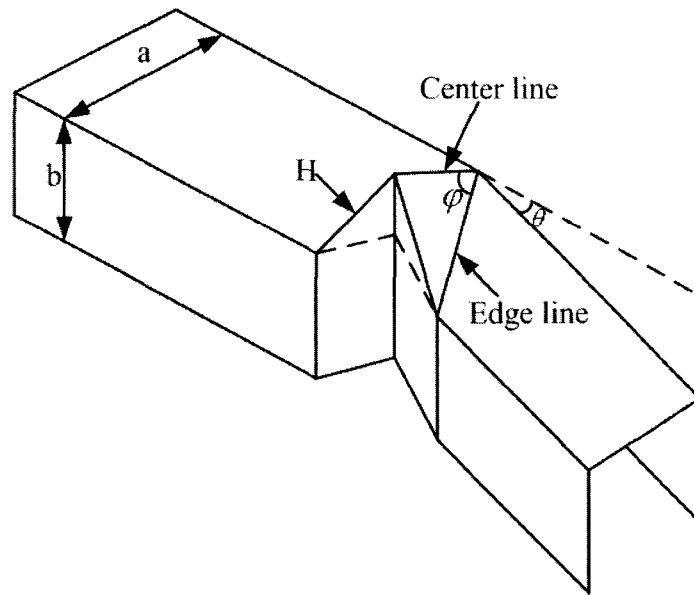
Figure 56. Collapse mode of thin-walled channel section beam
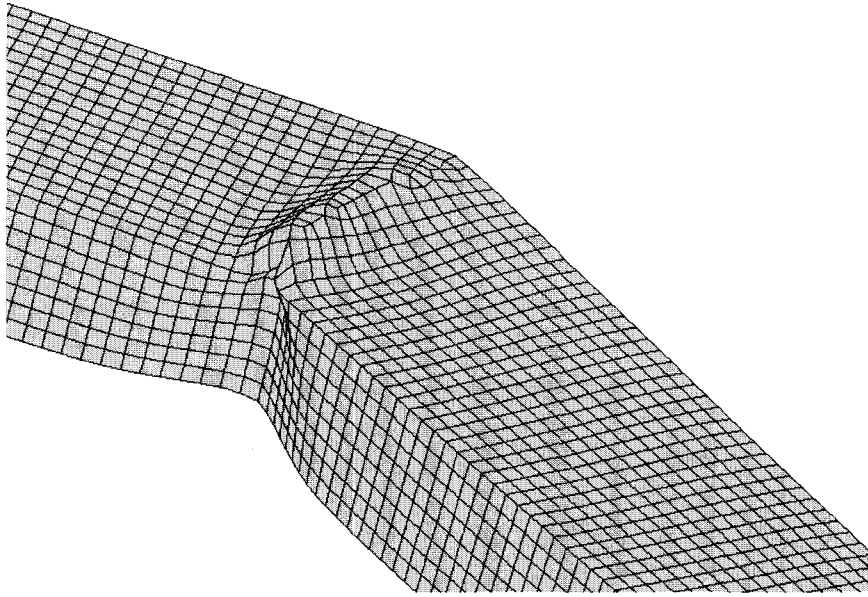
Figure 57. Plastic bending of a computer model

Figure 58 shows a conceptual configuration when a plastic fold is formed. A basic geometric relationship found from that Figure is

$$\delta = 2H(1 - \cos\alpha)$$

3-1

where δ is the axial shortening of the plastic fold, H is its half length, and α is the folding angle (as shown in Figure 58).
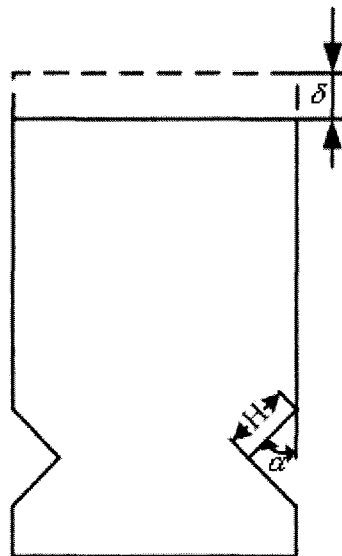
Figure 58. Bending of channel section beams

3.3.2 Global Equilibrium in Energy

According to the equilibrium of the energy during the crash, the rate of the internal energy absorbed by the collapsed mechanism should equal the rate of work of the external forces. Therefore,

$$E_{ext} = E_{int}, \text{ and } \dot{E}_{ext} = \dot{E}_{int}. \qquad 3\text{-}2$$

In equation 3-2, the rate of work of the external force $\dot{E}_{ext}$ is expressed as $P\dot{\delta}$ according to the principle of virtual velocities [55]. The P is the instantaneous crushing force, and $\dot{\delta}$ stands for the generalized relative velocity of the shortened folding mechanism.

Applying equation 3-1 here, the $\dot{E}_{ext}$ is re-expressed in terms of H and α, which is

$$\dot{E}_{ext} = P\dot{\delta} = P\left(2H\left(\frac{d(1-\cos\alpha)}{dt}\right)\right) = 2PH\sin\alpha\frac{d\alpha}{dt} = 2PH\sin\alpha\,\dot{\alpha} \qquad 3\text{-}3$$

3.3.3 Total Internal Energy

During the crash, the internal energy E_{int} is dissipated in the beam's compressive flange, tensile flange, and its web. Thus, the rate of the internal energy $\dot{E}_{int}$ is represented as the summation of the rate of the energy absorbed in those three energy absorbing mechanisms, which is $\dot{E}_{comp} + \dot{E}_{web} + \dot{E}_{ten}$. The $\dot{E}_{comp}$, $\dot{E}_{web}$, and $\dot{E}_{ten}$ are derived separately.

85

3.3.3.1 Energy Dissipating through the Compressive Flange

When comparing the bending mechanisms (Figure 59) of the channel section beam and the box section beam, it is found that both of the collapsed beams show similar bending mechanisms in their compressive flanges. Therefore, for the energy dissipated along the compressive flange $\dot{E}_{comp}$, the equations derived in [33], [34] are adjusted while considering the geometric differences between box and channel cross sections. It is applied here as

$$\dot{E}_{comp} = \dot{E}_{cor} + \dot{E}_{diag} + \dot{E}_{b} = 8M_0 \frac{r}{t} HI_1(\alpha)\dot{\alpha} + 2M_0 \frac{H^2}{r} I_2(\alpha)\dot{\alpha} + 2M_0 b \dot{\alpha} \qquad 3\text{-}4$$

where, $\dot{E}_{cor}, \dot{E}_{diag}, \dot{E}_{b}$ denote rate of energy dissipation by the corner deformations, diagonal hinge lines, and vertical hinge lines, respectively (see Figure 59). According to [33]

$$I_1(\alpha) = \cos\alpha \int_0^{\frac{\sqrt{2}\alpha}{2}} \frac{d\phi}{\sqrt{1 + \cos^2\phi}} \qquad 3\text{-}5$$

$$I_2(\alpha) = \cos\alpha \sqrt{1 + \sin^2\alpha} \qquad 3\text{-}6$$

r is the rolling radius of the plastic folds (as shown in Figure 60), H is the half length of plastic fold, and M_0 is the fully plastic bending moment per unit width. Applying equation 2-6 it becomes

$$M_0 = \frac{1}{4}\sigma_0 t^2 \qquad 3\text{-}7$$
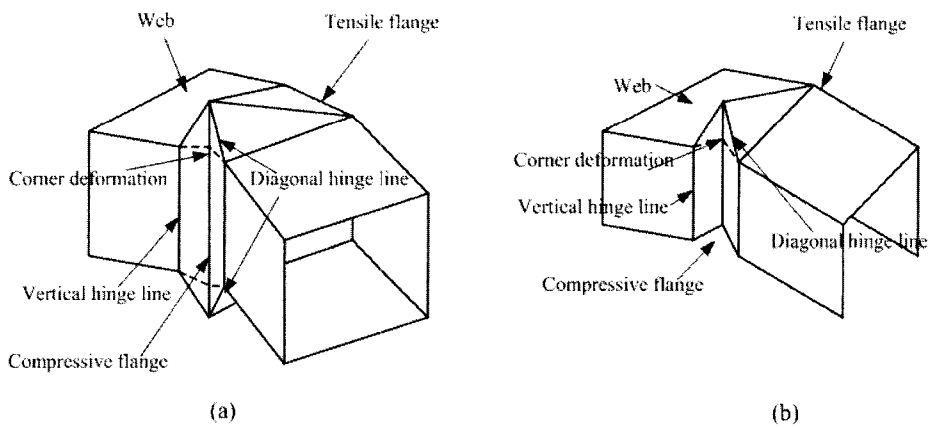
Figure 59. Collapse mechanisms of (a) box section beam and (b) channel section beam
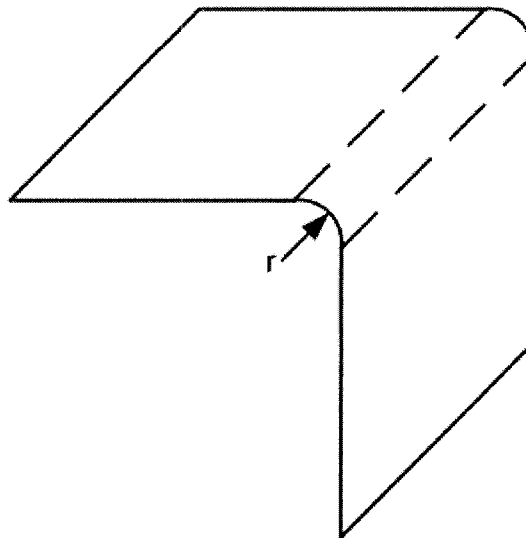
Figure 60. Rolling radius of plastic fold

3.3.3.2 Energy Dissipating through the Web

As shown in Figures 56 and 59, during the crash, the web buckles and different

parts buckle experiencing relative rotations around the hinge lines. The folding

mechanism of the web is viewed as symmetric in which each half includes one center

hinge line and one edge hinge line (as shown in Figure 56). Thus, the energy dissipating

across the web $\dot{E}_{web}$ equals the limit bending moment per unit length M_0 multiplied by

the rate of relative rotations $\dot{\psi}_i$ which is multiplied by the length of hinge lines ℓ_i.

$$\dot{E}_{web} = 2\sum_i \dot{\psi}_i \ell_i M_0 \qquad\qquad 3\text{-}8$$

The coefficient 2 reflects the symmetry of the web's folding mechanism. Figure 61

illustrates its geometric relationships:
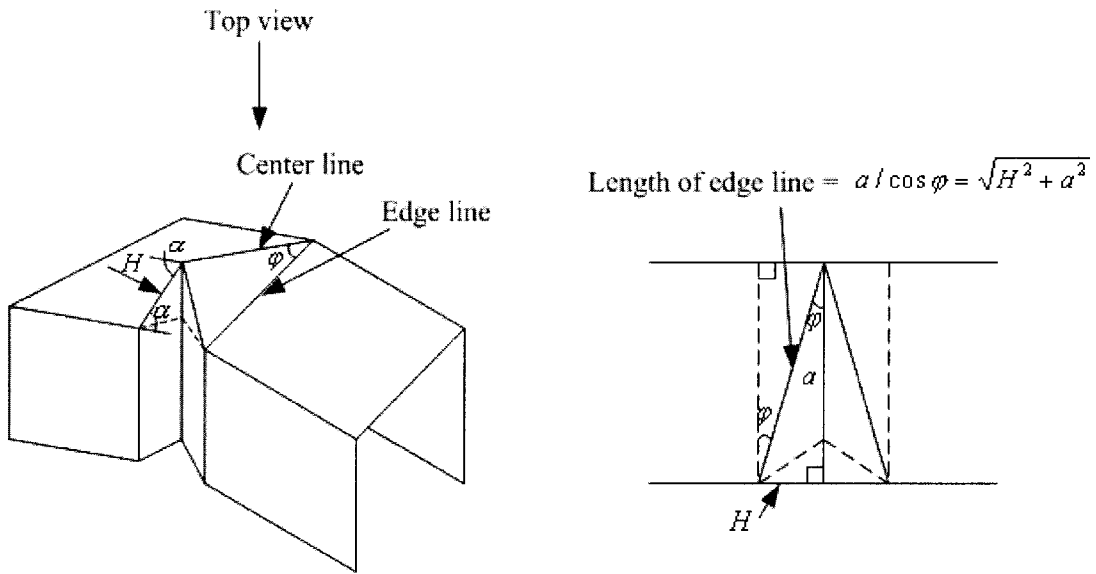
Figure 61. Bending mechanism of web

From Figure 61, it is concluded that in the bending mechanism of the web, the

center line, edge line, and the plastic fold, H compose a right triangle and follow the

Pythagorean Theorem. Also, from the same figure, it is seen that the bending of H leads

to the rotation of the center line. Therefore, the rate of rotation of the center line equals

the rate of the bending of H, which is $\dot{\alpha}$. Furthermore, since the center line, edge line,

and H remain in one plane during the folding, the rate of the rotations of the edge line and

of the center lines follow the same right triangle rule as their lengths. All the values of $\dot{\psi}_i$ and ℓ_i that are shown in equation 3-8 are listed in Table 13.

Table 13. Rotational Rates and Corresponding Hinge Lengths in Collapse Channel Section Beam Model

	I	$\dot{\psi}_i$	ℓ_i
Center line	1	$\dot{\alpha}$	a
Edge line	2	$\dot{\alpha}/\cos\varphi$	$a/\cos\varphi$

Still from Figure 61, the equation is

$$a/\cos\varphi = \sqrt{H^2 + a^2} \Rightarrow \cos^2\varphi = \frac{a^2}{H^2 + a^2}$$ 3-9

Then, substituting this equation into 3-8 and expanding it yields the formula to calculate the $\dot{E}_{web}$ as

$$\dot{E}_{web} = 2\sum_i \dot{\psi}_i \ell_i M_0 = 2\left(\dot{\psi}_1 \ell_1 + \dot{\psi}_2 \ell_2\right) M_0 = 2M_0\left(a\dot{\alpha} + \frac{a\dot{\alpha}}{\cos^2\varphi}\right) = 2M_0\left(a\dot{\alpha} + \frac{H^2 + a^2}{a}\dot{\alpha}\right)$$ 3-10

3.3.3.3 Energy Dissipating through the Tensile Flange

The energy dissipating through the tensile flange $\dot{E}_{ten}$ is also calculated. From Figure 62, it is deduced that the $\dot{E}_{ten}$ equals the limit bending moment per unit length M_0 multiplied by the rate of the relative rotations $\dot{\theta}$ multiplied by the length of hinge lines b.

$$\dot{E}_{ten} = M_0 b \dot{\theta}$$ 3-11
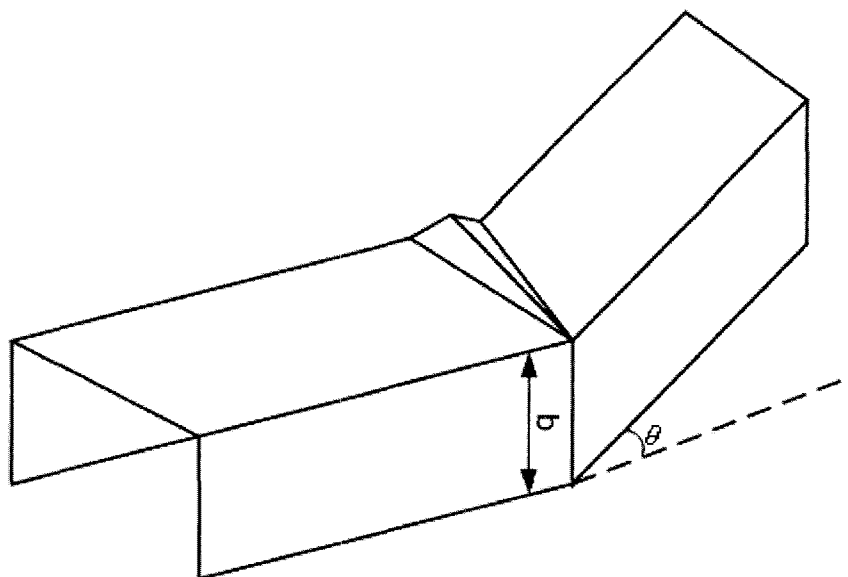
Figure 62. Bending along the tensile flange

The relationship between α and the beam's rotation angle θ is deducible from Figure 63.
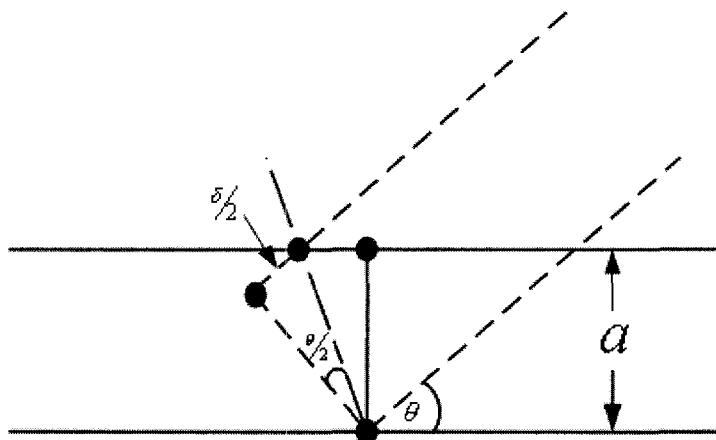
Figure 63. Relationship between α and θ

From Figure 62, it is inferred that

$$tg\left(\frac{\theta}{2}\right) = \frac{\delta/2}{a} = \frac{H(1-\cos\alpha)}{a} \qquad 3\text{-}12$$

For small α and θ, 3-12 can be rewritten as

$$\theta\!\!\!/_2 = \frac{H\left(1-\left(1-\frac{\alpha^2}{2}\right)\right)}{a} \Rightarrow \theta = \frac{H}{a}\alpha^2 \Rightarrow \alpha = \left(\frac{a\theta}{H}\right)^{1/2} \qquad \text{3-13}$$

Thus, $\dot{E}_{ten}$ can be expressed in terms of α, which is

$$\dot{E}_{ten} = M_0 b\dot{\theta} = 2M_0 b\frac{H}{a}\alpha\dot{\alpha} \qquad \text{3-14}$$

At last, all the three items combine to form the expression for the rate of internal energy dissipation $\dot{E}_{int}$.

$$\dot{E}_{int} = \dot{E}_{comp} + \dot{E}_{web} + \dot{E}_{ten} = 8M_0\frac{r}{t}HI_1(\alpha)\dot{\alpha} + 2M_0\frac{H^2}{r}I_2(\alpha)\dot{\alpha} + 2M_0 b\dot{\alpha} + 2M_0 a\dot{\alpha}$$

$$+ 2M_0\frac{H^2+a^2}{a}\dot{\alpha} + 2M_0 b\frac{H}{a}\alpha\dot{\alpha}$$

$$\text{3-15}$$

The total internal energy E_{int} is

$$E_{int} = \int \dot{E}_{int}\,dt \qquad \text{3-16}$$

Substitute 3-16 into 3-15 and expand it to obtain

$$E_{int} = \int\left(8M_0\frac{r}{t}HI_1(\alpha) + 2M_0\frac{H^2}{r}I_2(\alpha) + 2M_0 b + 2M_0 a + 2M_0\frac{H^2+a^2}{a} + 2M_0 b\frac{H}{a}\alpha\right)\dot{\alpha}\,dt$$

$$= M_0\int_0^{\pi/2}\left(8\frac{r}{t}HI_1(\alpha) + 2\frac{H^2}{r}I_2(\alpha) + 2b + 2a + 2\frac{H^2+a^2}{a} + 2b\frac{H}{a}\alpha\right)d\alpha \qquad \text{3-17}$$

3.3.4 Mean Crushing Force P_m and Bending Wavelength H

The folding mechanism of the thin-walled channel section beam shows that during bending the total crush distance of the compressive flange is $2H$. Here an equivalent mean crushing force is applied and is defined as $P_m(2H) = \int_0^{2H} Pd\delta$ (as shown in Figure 64). Then, the total external energy equal the total plastic work required to crush the compressive flange through the distance $2H$

$$E_{ext} = \int \dot{E}_{ext} dt = P_m \cdot 2H \qquad\qquad 3\text{-}18$$
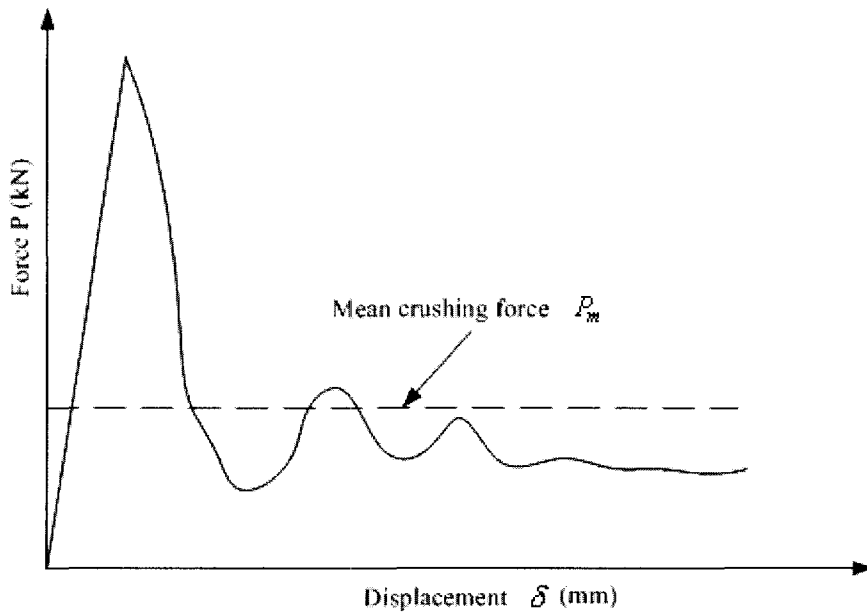
Figure 64. Mean crushing force P_m

Substituting 3-17 and 3-18 into 3-2 obtains

$$P_m(2H) = M_0 \int_0^{\pi/2} \left(8\frac{r}{t}HI_1(\alpha) + 2\frac{H^2}{r}I_2(\alpha) + 2b + 2a + 2\frac{H^2+a^2}{a} + 2b\frac{H}{a}\alpha \right) d\alpha \quad 3\text{-}19$$

After substituting $I_1(\alpha)$ and $I_2(\alpha)$ and integrating this equation, the P_m is calculated as

$$P_m = M_0(2.32\frac{r}{t} + 1.15\frac{H}{r} + \frac{\pi(2a+b)}{2H} + \frac{\pi H}{2a} + \frac{b\pi^2}{8a}) \qquad 3\text{-}20$$

92

From 3-20, it is found that the mean crushing force P_m is related to two unknown

parameters: H and r. According to Martin and Hill's theory [56, 57], H and r always

lead to the minimum crushing force P_m. Thus, the values of H and r are obtained by

minimizing the mean crushing force

$$\frac{\partial P_m}{\partial H} = 0 \qquad\qquad 3\text{-}22$$

and

$$\frac{\partial P_m}{\partial r} = 0 \qquad\qquad 3\text{-}23$$

Substitute 3-20 into 3-22 and 3-23 to derive the following equations:

$$\frac{\partial P_m}{\partial H} = 0 \Rightarrow \frac{1.15}{r} - \frac{\pi(2a+b)}{2H^2} + \frac{\pi}{2a} = 0 \qquad\qquad 3\text{-}24$$

$$\frac{\partial P_m}{\partial r} = 0 \Rightarrow \frac{2.32}{t} - \frac{1.15H}{r^2} = 0 \qquad\qquad 3\text{-}25$$

From 3-25, r is solvable as

$$H = \frac{2.32r^2}{1.15t} \qquad\qquad 3\text{-}26$$

Substitute it into 3-24 to obtain a polynomial of the fourth degree, which is

$$\frac{8.2\pi}{t^2}r^4 + \frac{18.7a}{t^2}r^3 - 2a\pi(2a+b) = 0 \qquad\qquad 3\text{-}27$$

Since equation 3-27 is a high-order polynomial and a closed-form solution cannot be

determined from that equation, the original equation 3-20 is simplified to

generate H and r with a simple closed form.

Reviewing 3-20 reveals that the term $\frac{\pi H}{2a}$ contributes less to the mean crushing

force compared to other terms. This is because the plastic bending of the thin-walled

93

beams is always localized in a narrow zone [36]. Thus, the value of $\frac{\pi H}{2a}$ should be very small compared to the other terms in that equation. Therefore, this item is removed from 3-20 to simplify the equation. This assertion is verified later by reviewing the results of calculations.

In order to eliminate another parameter, the ratio between a and b is set to be a real number enabling a to be expressed in terms of b. Here, the ratio λ is first assumed to be 2 to derive the corresponding bending resistance. The influences of various ratios are discussed later.

Using all of the assumptions and approximations, equation 3-20 is rewritten as

$$P_m = M_0(2.32\frac{r}{t} + 1.15\frac{H}{r} + \frac{5\pi b}{2H} + \frac{\pi^2}{16}) \qquad \text{3-28}$$

Equation 3-24 changes to

$$\frac{\partial P_m}{\partial H} = 0 \Rightarrow \frac{1.15}{r} - \frac{5\pi b}{2H^2} = 0 \qquad \text{3-29}$$

Substitute 3-26 into 3-29 and solve for H and r to obtain

$$H = 2.85b^{\frac{2}{3}}t^{\frac{1}{3}} \qquad \text{3-30}$$

and

$$r = 1.19b^{\frac{1}{3}}t^{\frac{2}{3}} \qquad \text{3-31}$$

After that, substitute 3-30 and 3-31 back into equation 3-28 and derive the mean crushing force using

$$P_m = 8.27M_0\left(\frac{b}{t}\right)^{\frac{1}{3}} + 0.62M_0 \qquad \text{3-32}$$

94

For a thin-walled beam, $\dfrac{b}{t}$ is no less than 10, and the term $0.62M_0$ contributes no more

than 3% to the mean crushing force. Thus, equation 3-32 is simplified to

$$P_m = 8.27 M_0 \left(\frac{b}{t}\right)^{\frac{1}{3}}$$

3-33

3.3.5 Derivation of Approximate Moment – Rotation Characteristic

Based on the derived mean crushing force P_m, the instantaneous crushing force is

determined. Equations 3-2, 3-3, and 3-15 establish this:

$$2PH \sin\alpha\,\dot{\alpha} = 8M_0\frac{r}{t}HI_1(\alpha)\dot{\alpha} + 2M_0\frac{H^2}{r}I_2(\alpha)\dot{\alpha} + 2M_0 b\,\dot{\alpha} + 2M_0 a\,\dot{\alpha} + 2M_0\frac{H^2+a^2}{a}\dot{\alpha} + 2M_0 b\frac{H}{a}\alpha\,\dot{\alpha}$$

$$\Rightarrow P\sin\alpha = M_0\left(\frac{4r}{t}I_1(\alpha) + \frac{H}{r}I_2(\alpha) + \frac{2a+b}{H} + \frac{H}{a} + \frac{b}{a}\alpha\right)$$

3-34

Similarly, in 3-34, the term $\dfrac{H}{a}$ is neglected because of its small value, assuming

$a = 2b$ gives:

$$P\sin\alpha = M_0\left(\frac{4r}{t}I_1(\alpha) + \frac{H}{r}I_2(\alpha) + \frac{5b}{H} + \frac{\alpha}{2}\right)$$

3-35

Substitute H and r into 3-35 and compare to 3-33 to obtain:

$$P = \frac{M_0}{\sin\alpha}\left((4.75I_1(\alpha) + 2.40I_2(\alpha) + 1.76\left(\frac{b}{t}\right)^{\frac{1}{3}} + \frac{\alpha}{2}\right) = P_m\left(\frac{0.58I_1(\alpha)}{\sin\alpha} + \frac{0.29I_2(\alpha)}{\sin\alpha} + \frac{0.21}{\sin\alpha}\right) + \frac{M_0\alpha}{2\sin\alpha}$$

3-36

Substitute $I_1(\alpha)$ and $I_2(\alpha)$ into the above equation; for a small angle α, the instantaneous

force $P(\alpha)$ can be simplified to

$$P = P_m\left[0.58 + \frac{1}{2\alpha}\right] + \frac{M_0}{2}$$

3-37

Finally, the bending resistance M – θ is developed. From Figure 65, this relationship becomes clear:

$$M(\theta) = P \cdot a = \left(P_m \left[0.58 + \frac{1}{2\alpha} \right] + \frac{M_0}{2} \right) a \qquad 3\text{-}38$$
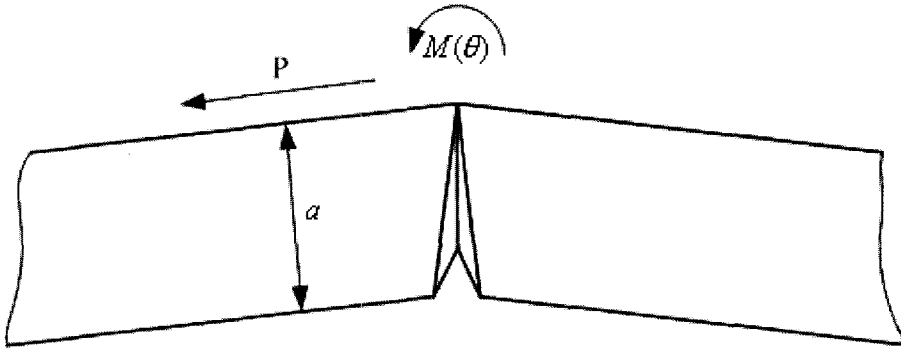
Figure 65. Relationship between $M(\theta)$ and P

Substitute 3-13 into 3-38 and assume that $a = 2b$, the moment – rotation characteristic is obtained by

$$M(\theta) = a \cdot P_m \left[0.58 + \frac{1}{2\sqrt{\theta}} \sqrt{\frac{H}{a}} \right] + \frac{M_0 a}{2} = 8.27(2b) M_0 \left(\frac{b}{t} \right)^{1/3} \left[0.58 + \frac{1}{2\sqrt{\theta}} \sqrt{\frac{2.85 b^{\frac{2}{3}} t^{\frac{1}{3}}}{2b}} \right] + M_0 b$$

$$= 16.54 b M_0 \left(\frac{b}{t} \right)^{1/3} \left[0.58 + 0.6 \left(\frac{t}{b} \right)^{1/6} \frac{1}{\sqrt{\theta}} \right] + M_0 b$$

$$3\text{-}39$$

3.3.6 M(θ) – θ Relationship with Different λ

In the previous section, the M(θ) – θ relationship is developed for the ratio λ = a/b = 2. Nevertheless, practical channel beams have different λ, and the ratios usually vary from 1.9 to 4.43 [54]. Therefore, in this section, two other ratios, 3 and 4, are applied to the above equations to derive the corresponding moment – rotation

characteristics. This covers most of the range within which a real λ varies. Moreover, the influences of different ratios on the channel beam's bending resistance are discussed.

The moment – rotation characteristic for the ratios 3 and 4 are developed following steps similar to those used to derive the bending resistance for the ratio $\lambda = 2$. Here, the two ratios, 3 and 4, are substituted into 3-20 and are following the same routines from 3-28 through 3-39. The half wavelength H, the small rolling radius r and the bending resistances for the two ratios are then calculable.

For $a/b = 3$:

$$H = 3.76b^{\frac{2}{3}}t^{\frac{1}{3}} \qquad\qquad 3\text{-}40$$

$$r = 1.36b^{\frac{1}{3}}t^{\frac{2}{3}} \qquad\qquad 3\text{-}41$$

$$P_m = 9.26M_0\left(\frac{b}{t}\right)^{\frac{1}{3}} \qquad\qquad 3\text{-}42$$

$$M(\theta) = 27.78bM_0\left(\frac{b}{t}\right)^{\frac{1}{3}}\left[0.58 + 0.56\left(\frac{t}{b}\right)^{\frac{1}{6}}\frac{1}{\sqrt{\theta}}\right] + M_0 b \qquad\qquad 3\text{-}43$$

For $a/b = 4$:

$$H = 4.22b^{\frac{2}{3}}t^{\frac{1}{3}} \qquad\qquad 3\text{-}44$$

$$r = 1.45b^{\frac{1}{3}}t^{\frac{2}{3}} \qquad\qquad 3\text{-}45$$

$$P_m = 10.06M_0\left(\frac{b}{t}\right)^{\frac{1}{3}} \qquad\qquad 3\text{-}46$$

$$M(\theta) = 40.24bM_0\left(\frac{b}{t}\right)^{\frac{1}{3}}\left[0.58 + 0.51\left(\frac{t}{b}\right)^{\frac{1}{6}}\frac{1}{\sqrt{\theta}}\right] + M_0 b \qquad\qquad 3\text{-}47$$

Results 3-40 through 3-47 show that the bending characteristics generated from

different λ have similar forms; the ratio only affects the coefficients. To visually

demonstrate the effects of the ratio on the bending characteristics, $\left(\dfrac{b}{t}\right)$ is assumed to be

10, and equations 3-39, 43, 47 are used to plot the $\dfrac{M(\theta)}{M_0 b}$ - θ curves with respect to ratios:

2, 3 and 4.
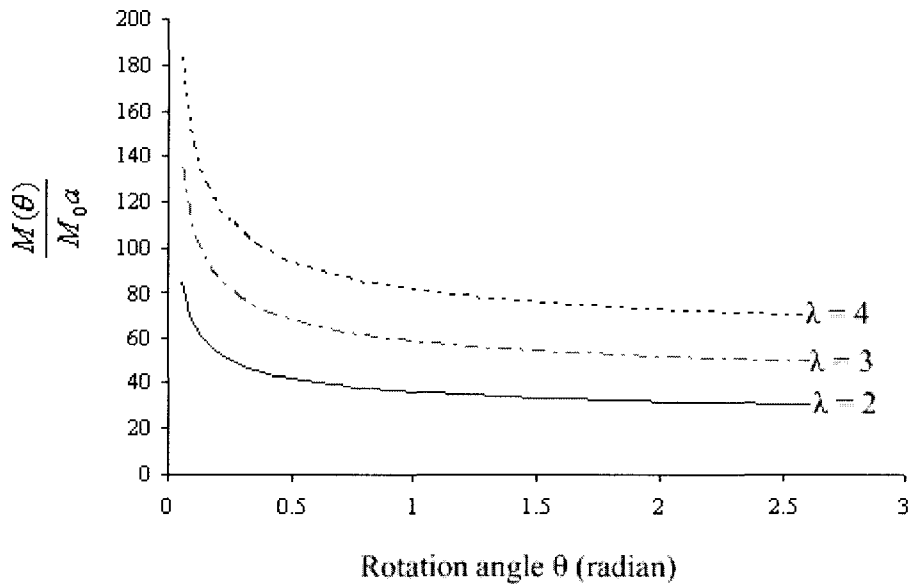
Figure 66. $\dfrac{M(\theta)}{M_0 b}$ Vs. θ for various λ, channel section beam

From Figure 66, it becomes clear that the three $\dfrac{M(\theta)}{M_0 b}$ - θ curves show similar

features in spite of different ratios they are associated with. Meanwhile, Figure 66 also

shows that the higher ratio correlates to the higher moment value, which means that a

thin-walled channel section beam's bending resistance about X-axis increases with higher

ratios, $\lambda = \dfrac{a}{b}$ (as shown in Figure 67).
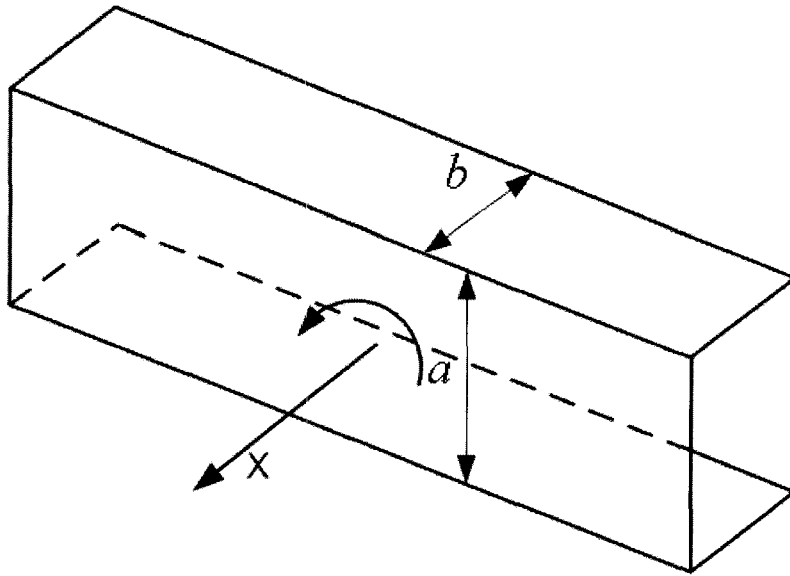
Figure 67. Bending resistance about X-axis

3.3.7 Drawing the Entire $M(\theta) - \theta$ Curve

Similar to the box section beam illustrated in chapter 2, the bending moment $M(\theta)$ of the channel section beam also increases linearly from 0 to its fully plastic bending moment M_p, then decreases following the curve defined by equation 3-39. Meanwhile, in the real crash test, the channel section beam stops bending because of jamming. Correspondingly, its $M(\theta) - \theta$ curve stops when the rotation angle θ reaches θ_J, where the θ_J is the angle of jamming. In this section, the M_p and θ_J of the channel cross section are derived respectively.

For a channel cross section beam, when it suffers its fully plastic bending moment M_p, the flow stress along its cross section area is distributed as shown in Figures 68a, b, and c, where the σ_0 is the material's yield stress. In Figure 68a, the entire cross section area is divided into zones I and II. From Figure 68b, the fully plastic bending moment of

zone I is written as: $\sigma_0 bt(a-t)$, and from Figure 68c, the moment of zone II is:

$0.25\sigma_0 t(a-2t)^2$. Thus, the total fully plastic bending moment M_p is expressed as:

$$M_P = \sigma_0 t\left(b(a-t)+0.25(a-2t)^2\right).$$

3-48
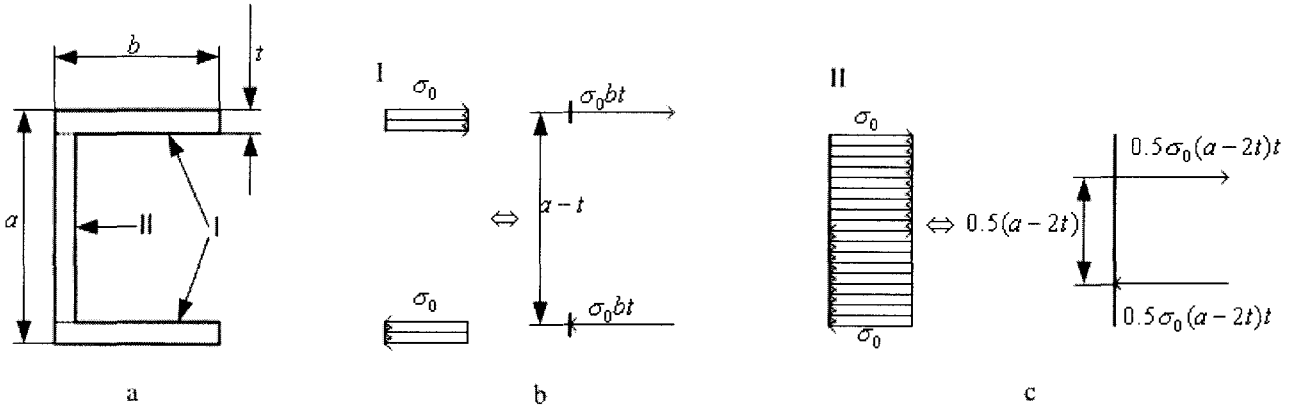
Figure 68. Flow Stress Distribution along the Cross Section

The angle of jamming θ_J is found easily from Figure 69 to be:

$$\theta_J = 2arctg\left(\frac{H}{a}\right).$$

3-49
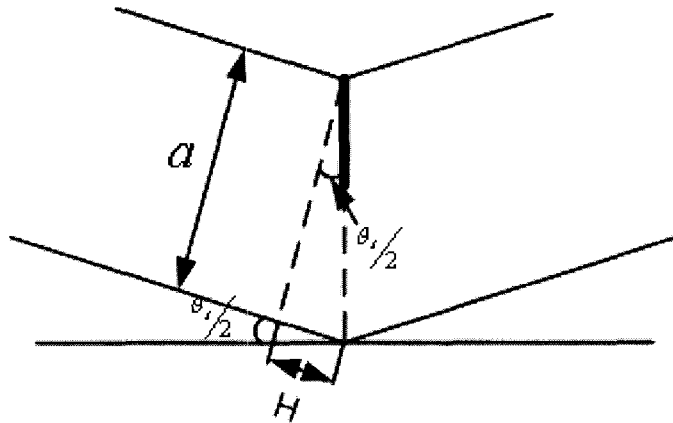
Figure 69. Calculation of jamming angle θ_J

100

3.4 Application of the Newly Derived Bending Resistance

Section 3.3 shows the derivation of the moment – rotation characteristics of the channel section beam with ratios $\lambda = 2$, 3, and 4. In this section, the derived bending resistance is applied to the creation of simplified models for such channel section beams. First, the development of the simplified channel section beam with ratio $\lambda = 2$ is thoroughly illustrated, and next, the same modeling method is applied to the creation of the other two simplified channel section beam models whose ratios are 3 and 4.

3.4.1 Detailed Model

At first, a detailed channel section beam model with $a / b = 2$ is created and used for the crashworthiness analysis. The curved channel section beam has the same outline as the "Z" shaped beam model chapter 2, except that it has "C" cross sections instead of the box cross sections. Figure 70 shows the detailed model, and Table 14 lists all its related conditions and information.
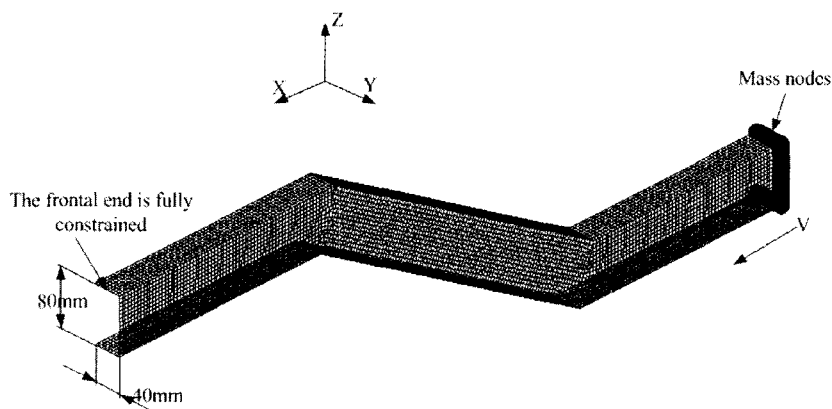
Figure 70. Detailed model for thin-walled "Z" shaped beam with channel section

Table 14 Thin-Walled Straight Beam Input Data

Material Properties	
Young's modulus (E)	2.07E5MPa
Density (ρ)	7830kg/m^3
Yield Stress (σ_y)	200MPa
Ultimate Stress (σ_u)	448MPa
Hardening modulus (E_{sn})	0
Poisson's ratio (ν)	0.3

Geometries	
Total length (L)	300mm
Cross section (a, b)	40mm×80mm
Wall thickness (t)	1.6mm

Crash conditions	
Added mass (m)	330kg
Initial velocity (v_0)	15m/s
Crash time (t_c)	0.006sec

In crash analysis, the crash time is set to 6msec to avoid the occurrence of the undesired contact between the outside of the two adjacent segments when the model totally collapses. Thus, the computer results will only display the model's response within a short time after it impacts a rigid wall.

After finishing the analysis, the entire crash process is animated, and the animation verifies that the "Z" shaped channel section beam shows similar collapse mechanisms as those beams with box sections. The only difference is that the channel section beam twists along its body, which is due to the instability of the open cross section. This research mainly concentrates on the global deformation, and the local twisting is verified later by comparing the detailed model's maximum twisting angle and the final rotational displacement of the simplified model. Figure 71 shows the deformed

shape of this model with local twisting while, Figure 72 displays the maximum twisting

of the channel cross section.

Top view

Side view

Isometric view
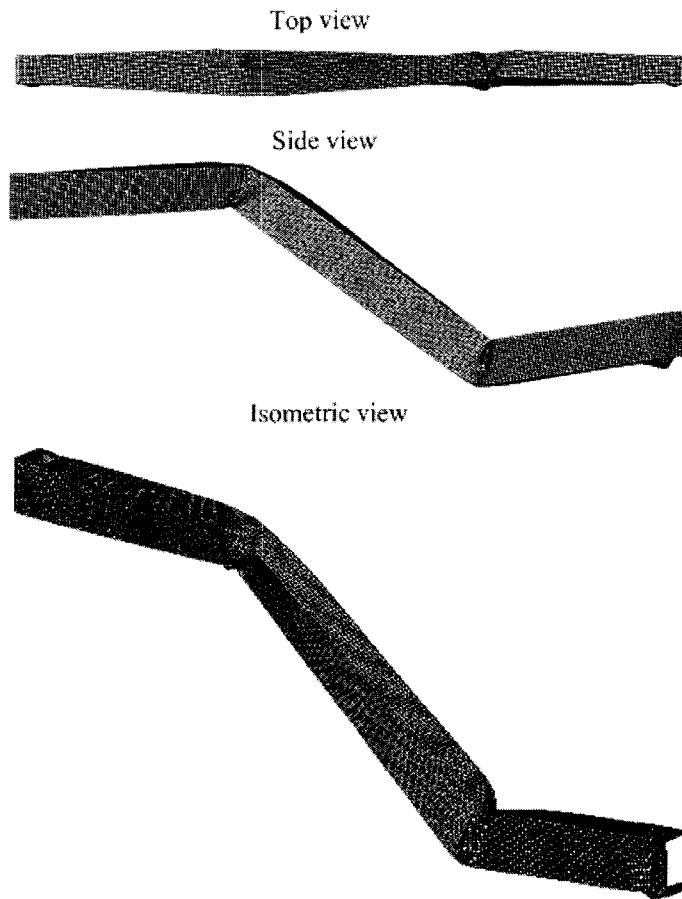
Figure 71. Deformed shape of detailed "Z" shaped channel section beam model

18°
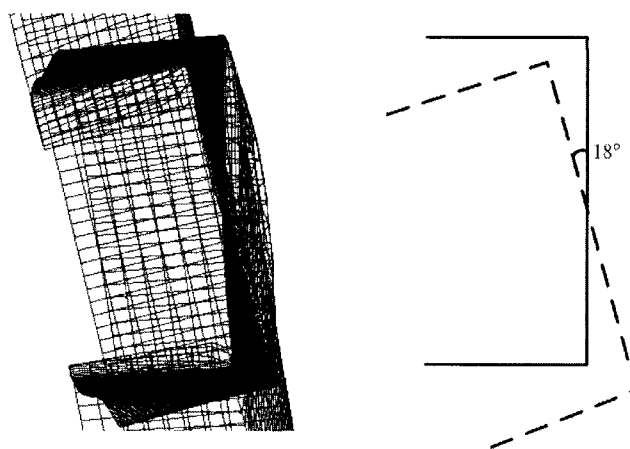
Figure 72. Twisting of channel section beam model

103

3.4.2 Simplified Modeling Applying the New-derived Bending Resistance

The simplified model is then developed based on the collapse mechanisms of the detailed channel section beam model and the application of the derived moment – rotation characteristic. In developing the simplified model, the modeling methodology summarized in chapter 2 is applied, and the characteristics of the nonlinear rotational spring element are determined by the derived bending resistance of the channel section beam. In this model, the ratio $a/b = 2$, so equations 3-39, 48, and 49 are used directly to generate the $M(\theta) - \theta$ curve of the spring elements. Figure 73 shows the $M(\theta) - \theta$ relationship, where the fully plastic bending moment M_p is calculated as 3040Nm, the jamming angle θ_J is found to be 0.91rad, and its corresponding bending moment M_J is 491Nm.

Furthermore, since in this model, all the parameters such as H and r are fully determined, it is possible to use equation 3-20 to verify the initial assumptions involved in the mathematical derivations. Given $a = 80mm$, $b = 40mm$, and $t = 1.6mm$, H and r are calculated to be 39mm and 5.6mm respectively. Thus, the values of the different terms in equation 3-20 are determined, and their contributions to the mean crushing force are then evaluated. Table 15 lists the related results and evaluations.
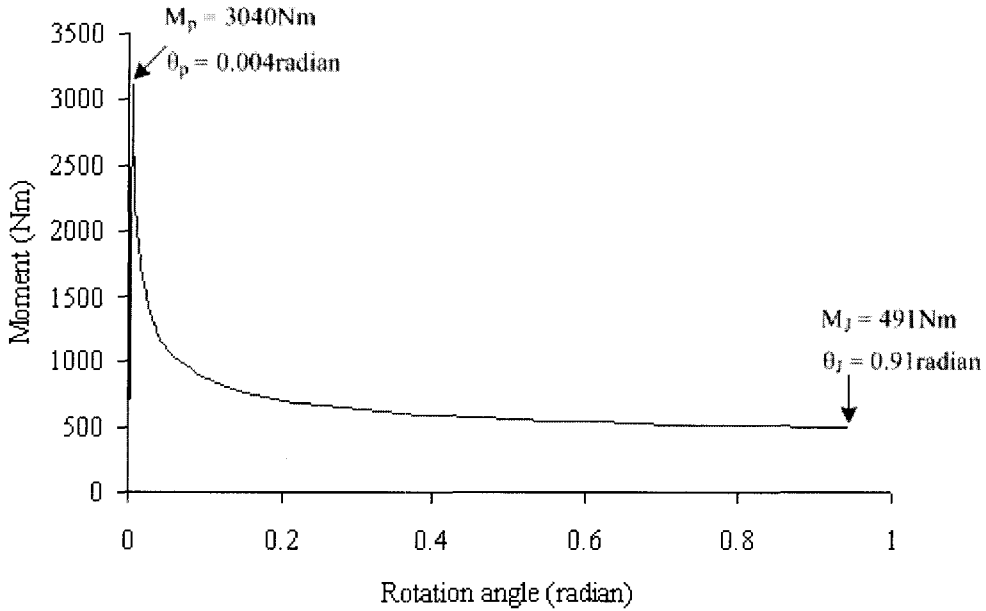
Figure 73. M(θ) – θ curve of nonlinear spring element for "Z" shaped channel section beam

Table 15. Contribution of Different Terms to Mean Crushing Force

Different terms in 3-20	Values	Contributions to mean crushing force
$2.32\dfrac{r}{t}$	8.12	31.7%
$1.15\dfrac{H}{r}$	8.01	31.3%
$\dfrac{\pi(2a+b)}{2H}$	8.06	31.5%
$\dfrac{\pi H}{2a}$	0.77	3%
$\dfrac{b\pi^2}{8a}$	0.62	2.4%

From Table 15, it is found that the sum of the last two terms only contributes 5.4% to the mean crushing force. Thus, it is reasonable to neglect the influences of these two terms in order to simplify the overall routine of the derivation. Moreover, the mean crushing

force P_m is calculated to be 6.7KN using equation 3-20 while, equation 3-33 gives the value as 6.4KN—an error of only about 4%.

After creating the rotational spring element, the simplified model is created using the Hughes – Liu beam element with the given cross sectional information. Like the simplified models for the box section beams, the spring elements are defined at the intersections of two neighboring segments and the fixed end to model the local plastic hinges. Figure 74 plots the simplified model.
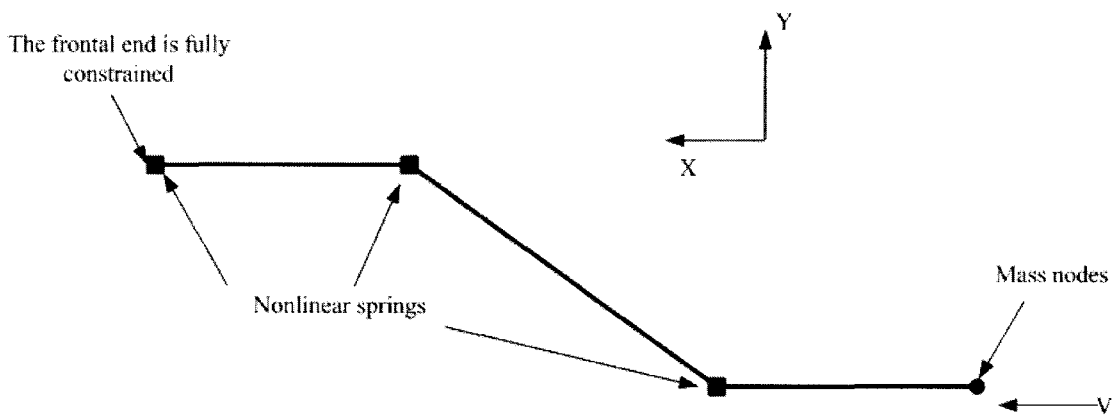
Figure 74. Simplified model for thin-walled "Z" shaped beam with channel section

3.4.3 Dynamic Results and Comparisons

After finishing modeling, the simplified model is used for the same crash analysis, and the dynamic results are compared with those of the detailed model to verify the validity of the simplified model. Table 16 lists the results of the comparisons, and Figures 75 through 78 plot these results and the deformed shape as well.
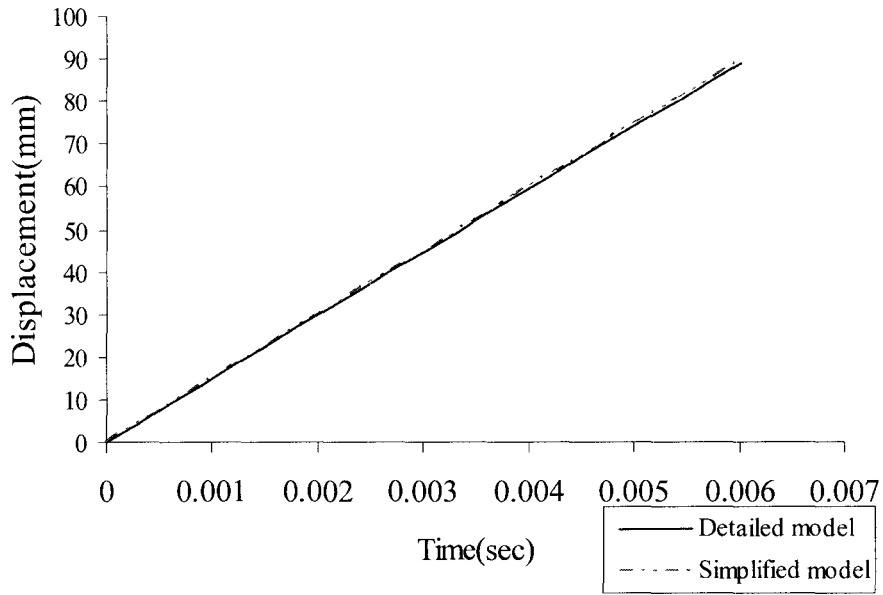
Figure 75. Displacements for "Z" shaped channel section beam models, $a/b = 2$
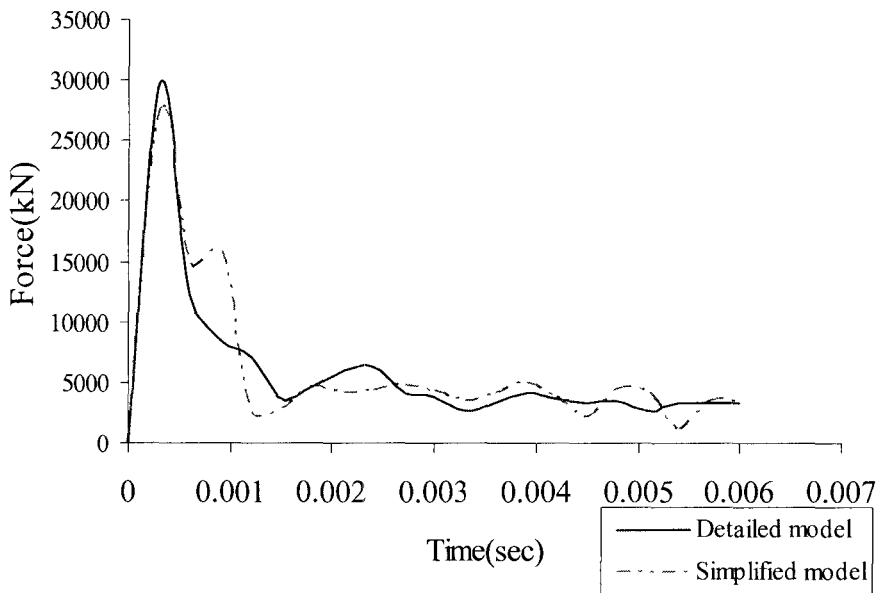
Figure 76. Crushing forces for "Z" shaped channel section beam models, $a/b = 2$

107
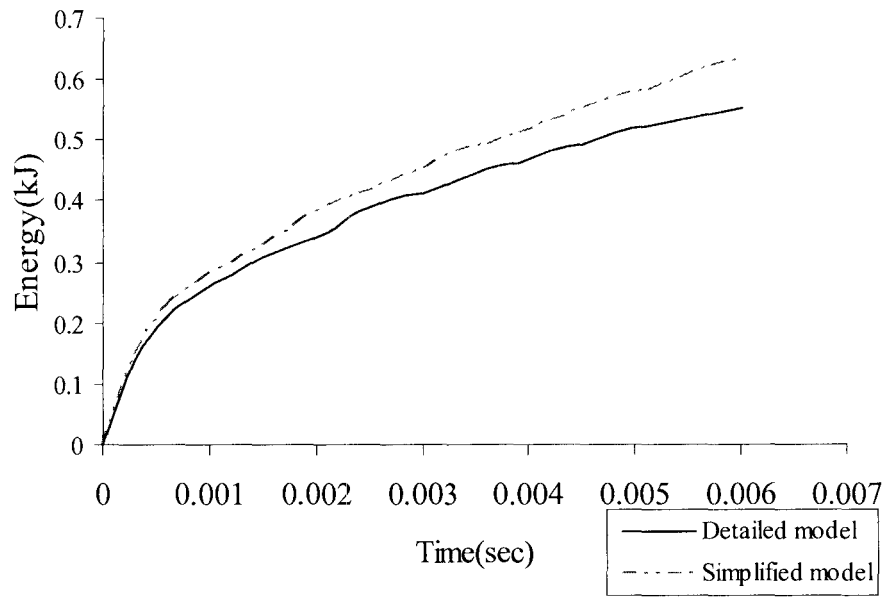
Figure 77. Absorbed energies for "Z" shaped channel section beam models, $a / b = 2$
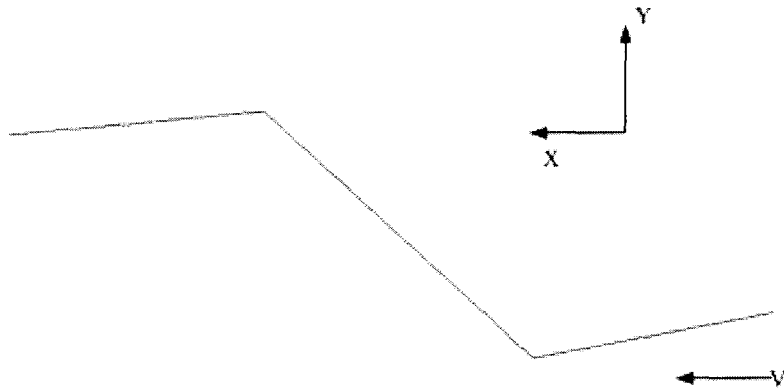
Figure 78. Deformed shape of simplified "Z" shaped channel section beam model, $a / b = 2$

Table 16. Comparison of Dynamic Results from Detailed and Simplified "Z" Shaped Square Section Beam Models, $a / b = 2$

	Detailed model	Simplified model	Difference (%)
Global displacement (mm)	88.7	89.3	0.7
Peak crushing force (kN)	29.9	27.5	-8
Absorbed energy (kJ)	0.55	0.63	14.5
Computer time (sec)	1378	62	-95.5

As Table 16 shows, the errors of the important dynamic results are below 15%, and the simplified model only requires about 5% of computer time of the detailed model. From the results of comparisons, it is concluded that the developed simplified model can accurately represent the crash behavior of the detailed model during a crash analysis. The rotational displacements of the beam nodes are given as output, and the maximum rotational displacement is found to be 17.2°, which agrees with the twisting angle value that was measured as18° from the detailed channel beam model (see Figure 72). Therefore, it is preliminarily verified that the equation 3-39 can correctly predict the bending behavior of the channel section beam even if it is derived by taking small angle approximations. Undoubtedly, it is applicable to determining the nonlinear spring elements, which are used in simplified modeling.

3.4.4 Effects of Mesh Density

In this simplified model, each straight segment is meshed using 32 beam elements. During simplified modeling, a simpler model with coarser meshes is always sought. Therefore, based on the existing simplified model, three other models are created here

with each of their straight segments being meshed by 16, 8, or 4 elements respectively. The same crash analysis is performed on these models. The dynamic results are compared to the existing simplified model to investigate the effects of the mesh density on the model's crash response and to find the optimum mesh density that can achieve similar results to those from the detailed model while fully minimizing the simplified model's size. Table 17 lists the results of the comparisons, and all of the related plots are listed in appendix D.

Table 17. Comparison of Dynamic Results from Simplified "Z" Shaped Channel Section Beam Models with Differing Numbers of Elements

# of elements for each segment	Detailed model	4	8	16	32
Global displacement (mm)	88.7	89.2	89.3	89.3	89.3
Difference (%)		0.6	0.7	0.7	0.7
Peak force (kN)	29.9	49	34.3	27.1	27.5
Difference (%)		63.9	14.7	-9.4	-8
Absorbed energy (kJ)	0.55	0.73	0.68	0.65	0.63
Difference (%)		32.7	32.6	18.2	14.5
Computer time (sec)	1378	5	5	10	62
Difference (%)		-99.6	-99.6	-99.3	-95.5

From Table 17, it is found that models with different mesh densities generate similar results for the global displacements, but for the peak crushing force and the absorbed energy, the coarse-mesh models cause higher errors. Comparing all the data, it is seen that only the 32-element model can keep all the errors below 15%. Therefore, it is verified that the current simplified model of 32 beam elements in each of its straight

segments is an optimum option for maintaining the balance between simplification and efficiency.

3.4.5 Validation of the Newly Derived Bending Resistance through More Examples

In addition to equation 3-39, equations 3-43 and 3-47 are also derived to predict the bending resistance of the channel section beam with $\lambda = 3$ and 4. In this section, two more "Z" shaped thin-walled channel section beams are studied, and corresponding simplified models are developed for each of them. These two models have the same dimensions and properties as the previous one, except for their cross sections, which are $30mm \times 90mm(\lambda = 3)$ and $25mm \times 100mm(\lambda = 4)$. In developing the simplified models, the same modeling steps are followed, and equations 3-40 through 3-49 are applied to determine their moment-rotation characteristics. Table18 lists some of the intermediate results, which are calculated along with the derivation of their bending resistances.

Table 18. Moment-Rotation Characteristics of Channel Section Models with $\lambda = 3$ and 4

Model	$30mm \times 90mm$	$25mm \times 100mm$
Cross section	$\lambda = 3$	$\lambda = 4$
Half length of plastic fold H (mm)	32.2	28.5
Rolling radius r (mm)	5.1	4.8
Fully plastic moment M_p (Nm)	2991	3167
Angle of fully plastic bending θ_p (radian)	0.006	0.006
Angle of jamming θ_J (radian)	0.69	0.56

With all the intermediate results listed in Table 18, both spring elements' bending resistance is obtained, and the general moment – rotation relationship for such beam models is shown in Figure 79. Then, the simplified models are developed following the same steps illustrated above.

111
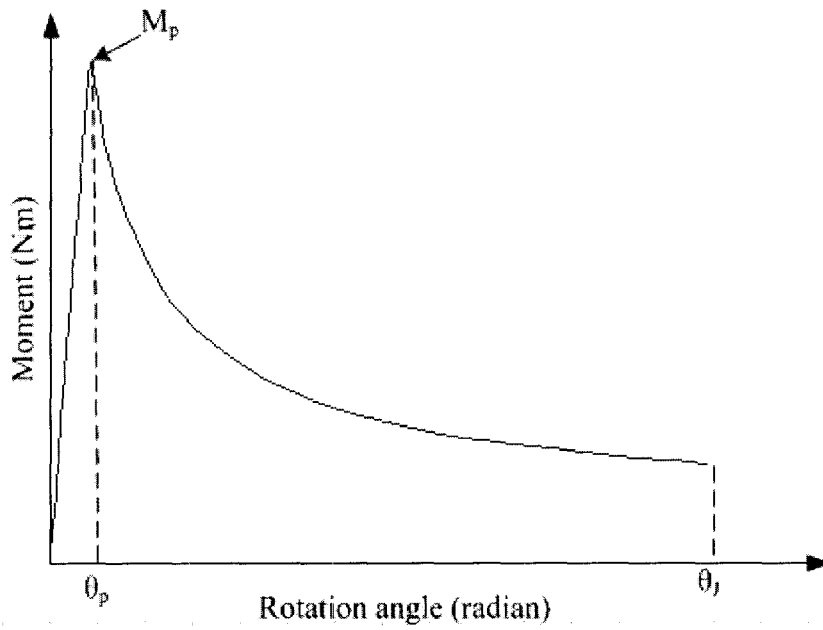
Figure 79. Moment – rotation relationship for arbitrary "Z" shaped channel section beam

After creating the simplified models, the same crash analyses are performed on the two models. The following Figures and tables display the related dynamic results and comparisons.
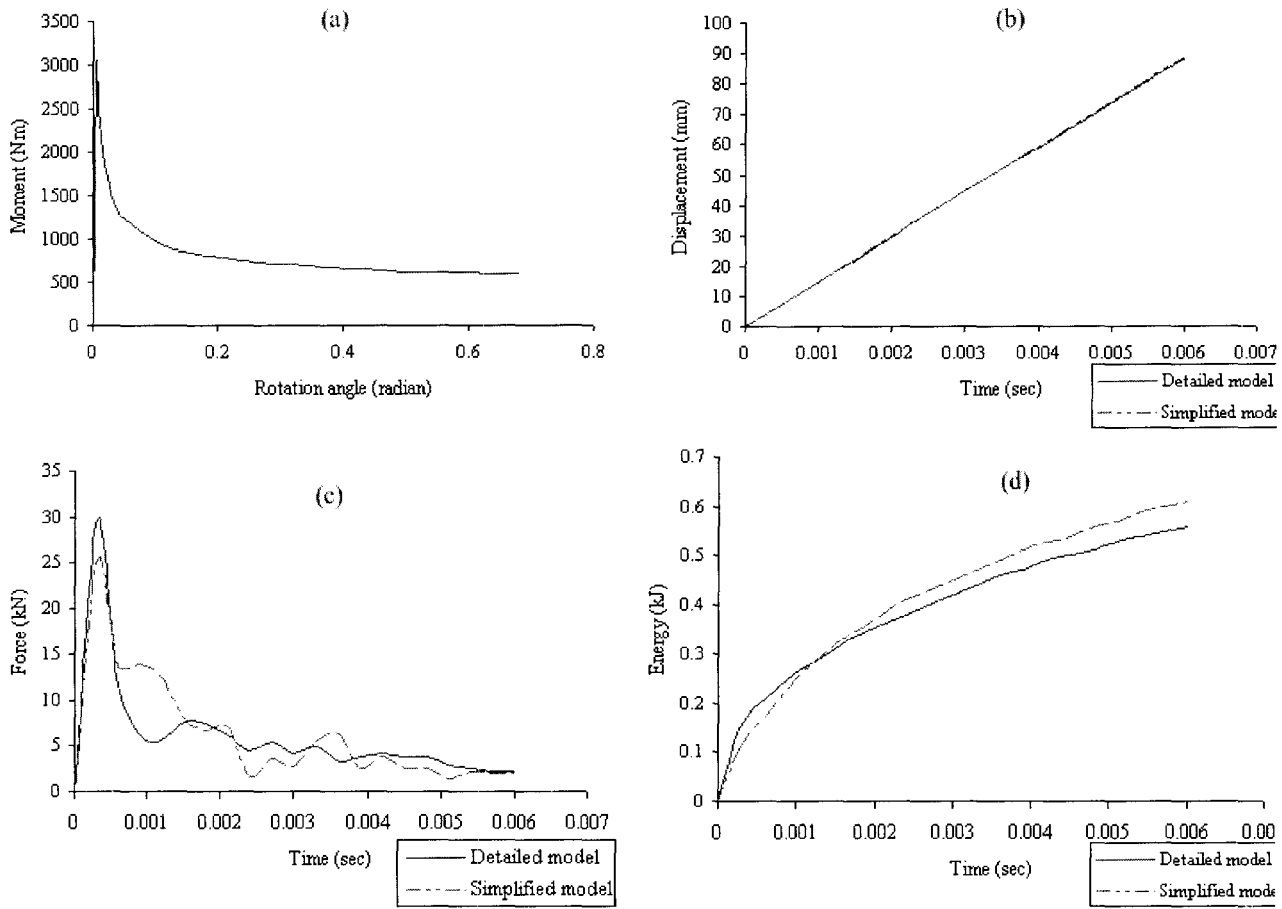
Figure 80. Dynamic results of "Z" shaped channel section beam models, $a / b = 3$, a) bending resistance, b) global displacement, c) crushing force, d) absorbed energy
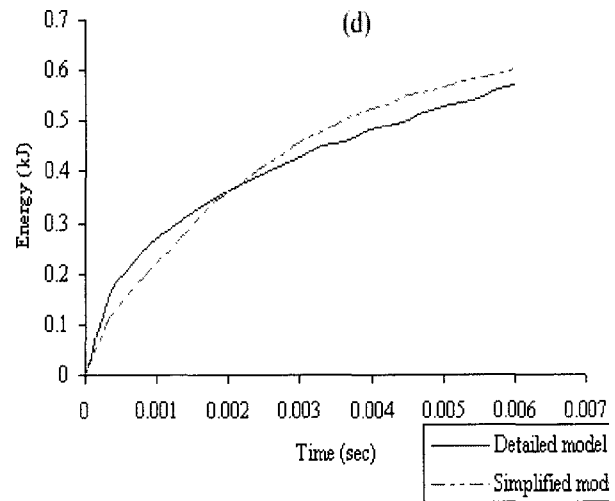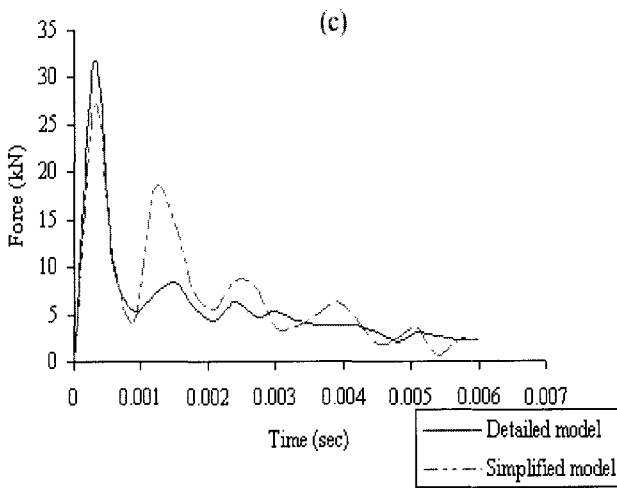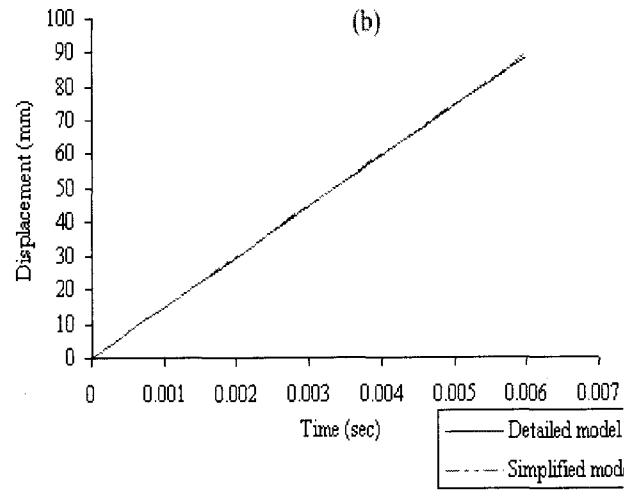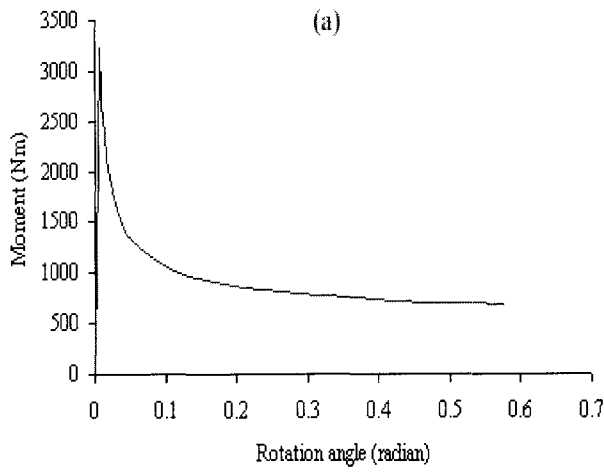
Figure 81. Dynamic results of "Z" shaped channel section beam models, $a / b = 4$, a) bending resistance, b) global displacement, c) crushing force, d) absorbed energy

114

Table 19. Comparison of Dynamic Results from Detailed and Simplified "Z" Shaped Channel Section Beam Models, $a/b = 3$

	Detailed model	Simplified model	Difference (%)
Global displacement (mm)	88.6	89.2	0.7
Peak crushing force (kN)	29.8	25.5	-14.4
Absorbed energy (kJ)	0.56	0.61	8.9
Computer time (sec)	844	48	-94.3

Table 20. Comparison of Dynamic Results from Detailed and Simplified "Z" Shaped Channel Section Beam Models, $a/b = 4$

	Detailed model	Simplified model	Difference (%)
Global displacement (mm)	88.7	89.3	0.7
Peak crushing force (kN)	31.7	27.1	-14.5
Absorbed energy (kJ)	0.57	0.6	5.3
Computer time (sec)	1513	103	-93.2

The results of the comparisons demonstrate that the developed simplified models correlate very well with the detailed ones. From both tables it is found that all of the errors are fewer than 15%. Meanwhile, the simplified models save much more computer time than the detailed ones.

3.4.6 Discussion

In this section, three simplified models are created for the three channel section beams with different aspect ratios, λ. From the results of comparisons, it is verified that the developed simplified models are qualified to replace the detailed model in crash

analyses while, saving computer time. The modeling method of chapter 2 is applied to the creation of these models, and the bending resistance of the channel section beam that was derived in section 3.3 is used to determine the characteristics of the nonlinear spring elements. A high correlation is acquired from the comparison of the dynamic results of the detailed and the simplified models, which also prove the accuracy of the mathematical derivation described in section 3.3.

3.5 Conclusions

This chapter studies the bending collapse of the thin-walled channel section beams and derives their approximate moment – rotation characteristics. The derived bending resistance is then used to develop the simplified models for channel section beams. Through a series of crash analyses and results comparisons, it is verified that the derived bending resistance is valid for predicting the channel section beam's crash behavior and is useable for determining the nonlinear rotational spring elements during the simplified modeling. As shown in section 3.3, the channel section beam's bending resistance is appropriately expressed as an equation with a simple closed solution form. The only limitation of the solution is that for the beams with different aspect ratios, the ratio, λ, must be substituted each time and certain steps must be followed to obtain the corresponding $M(\theta) - \theta$ relationships.

After developing qualified simplified models for the detailed channel section beam models, the modeling method is then applied to the development of the simplified crash model for a detailed truck chassis model, whose two side-rails are composed of channel section beams that absorb most of the crash energy and bear the most impact

loads during the crashes. The next chapter thoroughly illustrates how to develop the

simplified truck chassis model that is useable for crashworthiness analysis.

CHAPTER IV

DEVELOPMENT OF A SIMPLIFIED MODEL FOR THE TRUCK CHASSIS

4.1 Introduction

Based on the modeling methodology of simplifying the channel section beam that was developed in chapter 3, this chapter continues to apply this method in the development of the simplified truck chassis model and to validate this simplified model for crashworthiness analysis. Before creating the simplified model, the crashworthiness analysis is first performed on the existing detailed chassis model; the detailed model's crash response is presented. Next, the entire chassis model is divided into two parts; first, two side-rails that are composed of channel section beams and second, six plate-like cross members (as shown in Figure 82). Different modeling techniques are applied to simplify these two parts: the modeling method of the earlier chapters models the side-rails and the superelement method along with the equivalent beam method models the cross members. These two simplified parts are combined to accomplish the final simplified model; the efficiencies of both superelement method and equivalent beam method are compared, and the best modeling method is summarized and recommended. To validate the simplified models, the same crashworthiness analysis is performed, and the crash results are compared with those from the detailed model to validate the simplified model and the modeling method as well. Additionally, a series of transitional models are created and

used for the same crashworthiness analysis. The results fully reveal the efficiency and

the advantages of the developed simplified model and the simplified modeling method.

4.2 Crash Behavior of the Detailed Truck Chassis Model

4.2.1 Finite Element Model

Figure 82 shows the detailed truck chassis model (provided by the Ford Company,

including the material properties and geometries), and the input data is listed in Table 21.

4.2.2 Crash Results and Discussion

The detailed model is used for the crashworthiness analysis; Figures 83 through

85 display the important crash results including the crushing force, the global

displacement, and the absorbed energy. Figure 81 shows that during the crash, the

impact force reaches its peak value instantly then, drops quickly, and finally, tends

towards zero. This phenomenon shows that in this test 100msec is an appropriate time

interval for displaying the entire crash history. From the displacement plot, it is inferred

that after the model impacts the rigid wall, the rest of the model continues its forward

motion; at about 20msec, it stops moving, experiences a small rebound, and then,

oscillates around its position of equilibrium. Accordingly, this characteristic is also

reflected in the absorbed energy plot, where the absorbed energy reaches a steady-state

value at the end of the analysis.

Top view
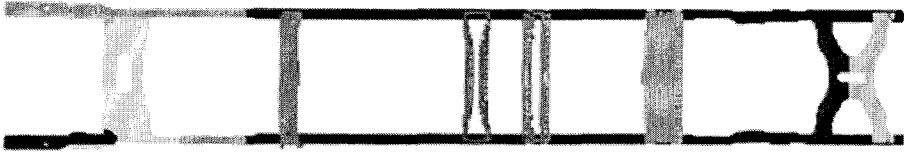
Side view

Isometric view
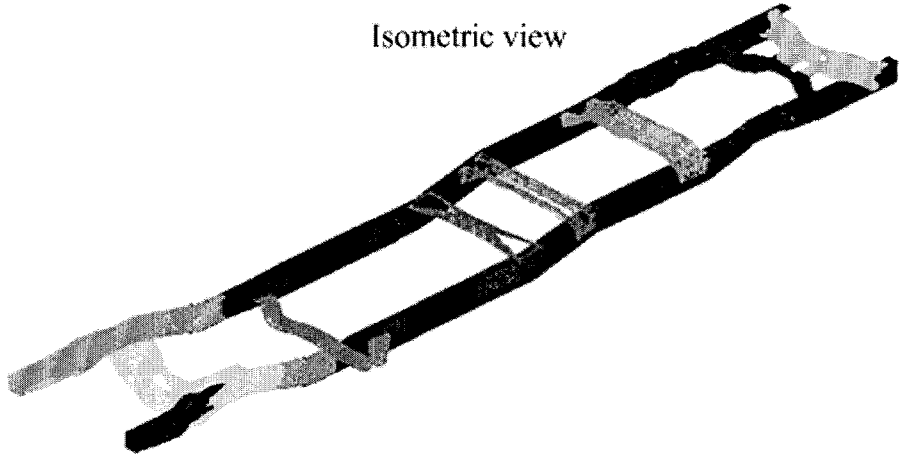
Figure 82. Detailed truck chassis model

Table 21. Detailed Truck Chassis Model Input Data

Material Properties	
Young's modulus (E)	2.07E5MPa
Density (ρ)	7830kg/m^3
Yield Stress (σ_y)	200MPa
Ultimate Stress (σ_u)	630MPa
Hardening modulus (E_{sn})	0
Poisson's ratio (ν)	0.3

Geometries	
Total length (L)	6215mm
Cross section (a,b)	Non-uniform cross section
Wall thickness (t)	Non-uniform thickness

Crash conditions	
Added mass (m)	236kg
Initial velocity (v_0)	15m/s
Crash time (t_c)	0.1sec
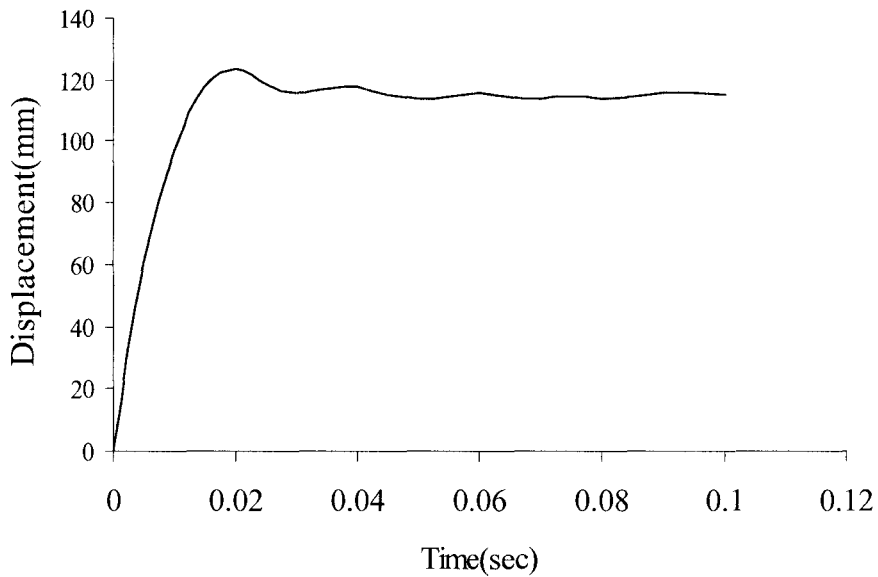
Figure 83. Global displacement for detailed truck chassis model

121
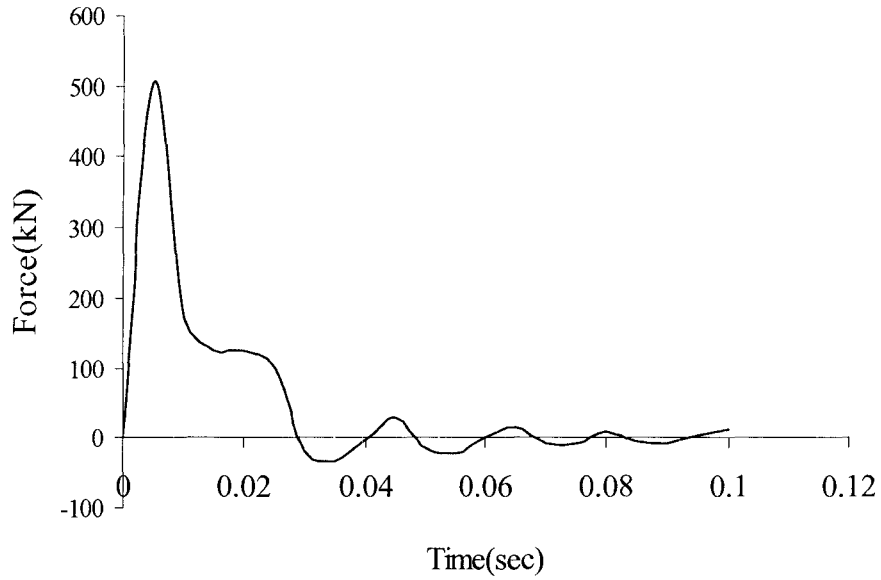
Figure 84. Crushing force for detailed truck chassis model
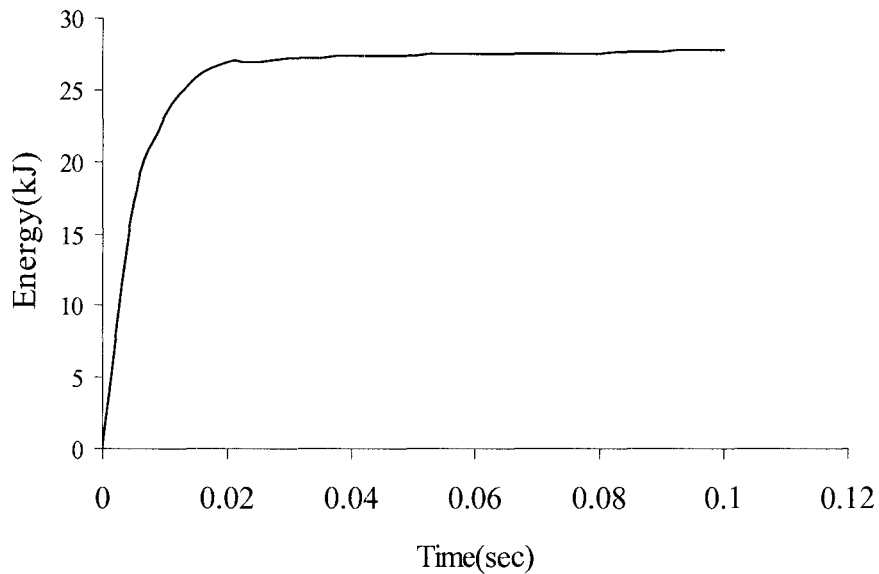
Figure 85. Absorbed energy for detailed truck chassis model

After the analysis, the crash behavior of the detailed model is observed from the

animation file. In comparison to the chassis model before and after the crash test, it is

found that during the crash, the side-rails of the chassis model deform mainly along their

longitudinal direction. However, for the cross members, it is observed that the frontal

member (member 1) undergoes a small bending because of the effects of the transferred impact force. Cross members 2, 5, and 6 almost keep their original shapes through the entire crash process because only a few impact forces are transferred to them. However, members 3 and 4 experience large displacements due to their weak structures. Figure 86 displays the original and the deformed truck chassis model; Figure 87 compares the configurations of the cross members before and after the analysis.

Original model
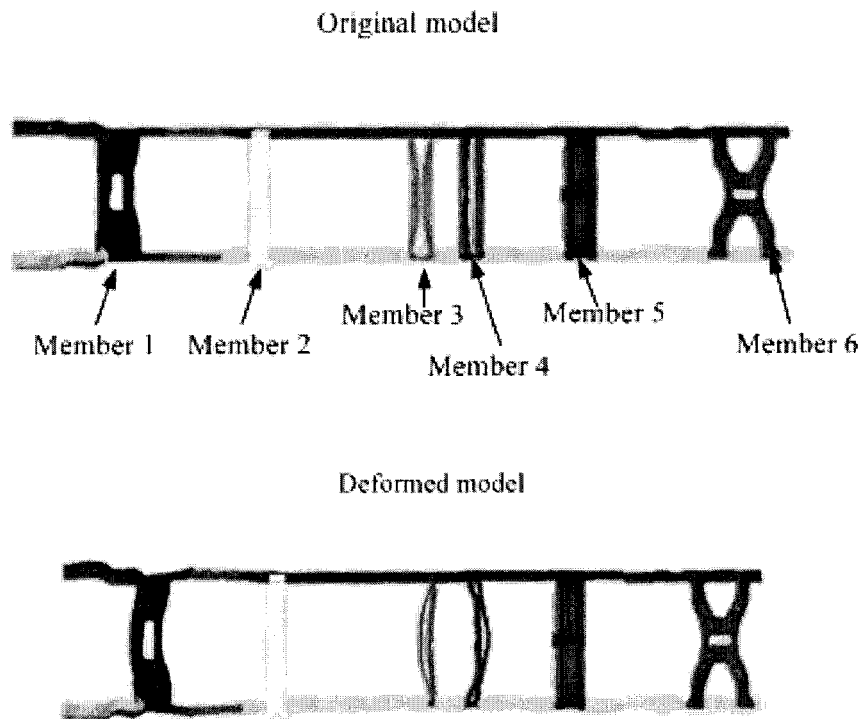
Deformed model

Figure 86. Original and deformed detailed truck chassis models

Cross member1
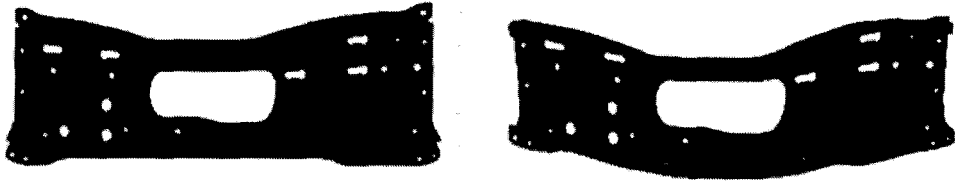
Cross member2

Cross member3

Cross member4

Cross member5

Cross member6
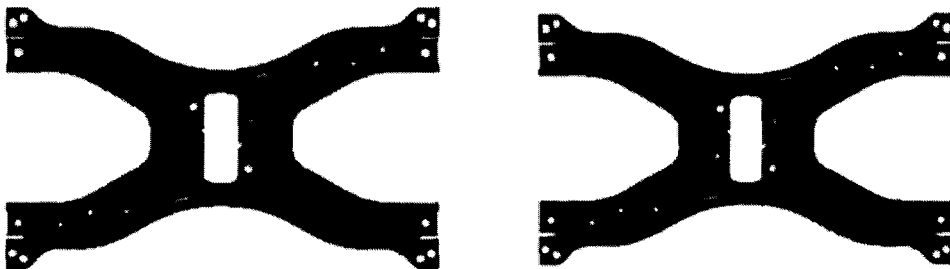
Original configurations   Deformed configurations

Figure 87. Original and deformed cross member models

4.3 Creating a Simplified Model for the Side-Rails Applying the Derived Bending Resistance

Viewing the truck chassis model, it is found that the entire chassis model is composed of two side-rails and six cross members. Simplified models are developed for each of them. From Figure 80, it is seen that the side-rails are composed of thin-walled box and channel section beams, and therefore, they are simplified by directly applying the modeling method and the derived bending resistance illustrated earlier. This section mainly describes how to create the simplified model for the side-rails, and the simplified modeling of the cross members is introduced in next section.

4.3.1 Detailed Model

Before creating the simplified side-rails model, the structure of detailed model is presented and studied. Figure 88 plots the left side-rail model; the right side-rail model has the same characteristics because the two side-rails are symmetric. From Figure 88, it is found that one side-rail model is analyzed as several segments because the varying geometries and features enable each segment to have its own cross section and wall thickness. A concise profile of the detailed model is drawn in Figure 89, which also indicates the related dimensions. Later, the simplified side-rails model is created using this profile.

Top view

Side view

Sec2   Sec4   Sec6
Sec1 Sec3   Sec5   Sec7

Isometric view
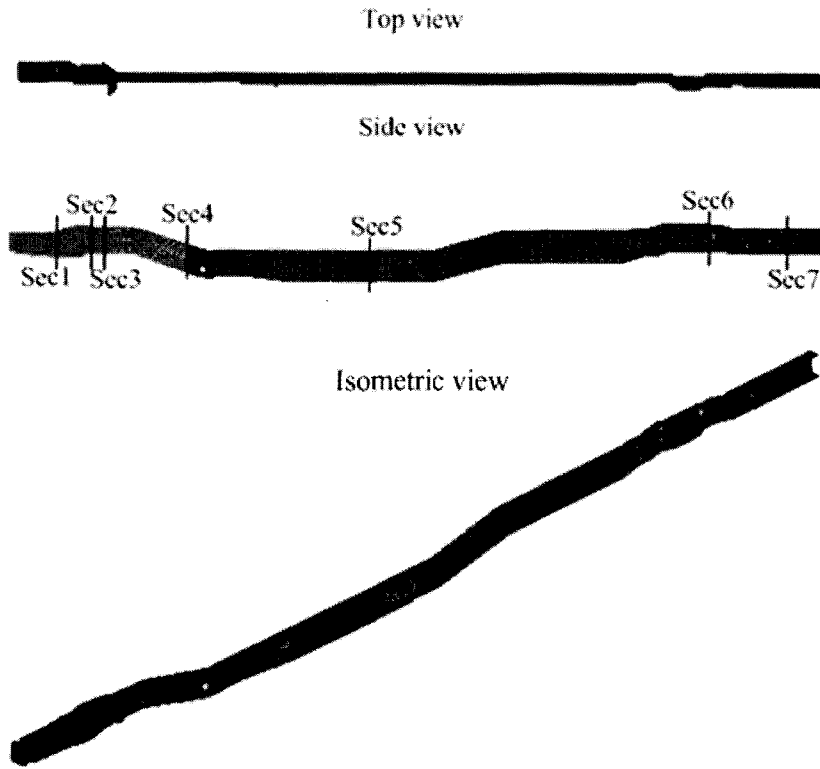
Figure 88. Detailed side-rail model

Top view

386   24

64

Side view

174   296   296   306

②   ④   115   ⑥   ⑦
③   40   32
337 ①   503 120   1735   552   922   228   678

188

Cross sectional area: Box   Channel   Unit: mm
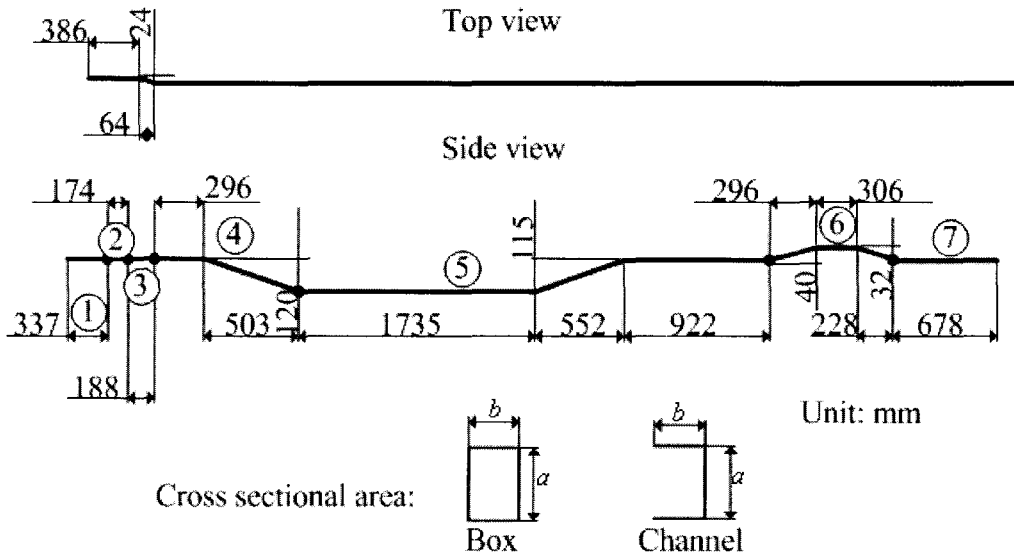
Figure 89. Profile of side-rail model

In Figure 89, segments 1 through 7 have different cross sections, which are

numbered from 1 to 7 in Figure 88. Because the cross section in the model changes

126

gradually, a median cross section is extracted from each segment and used as the

characteristic cross section of a segment. Table 22 lists the cross sectional geometries.

Table 22. Cross Sectional Geometries of Different Segments

Segment # (Figure 89)	Cross section # (Figure 88)	Cross sectional type	Web a (mm)	Flange b (mm)	Thickness t (mm)
1	1	Box	118.7	97.7	5.1
2	2	Box	155	97.7	5.1
3	3	Box	160.5	97.7	5.1
4	4	Channel	147.2	50	5.1
5	5	Channel	174.5	66.5	6.1
6	6	Channel	157.8	50	6.1
7	7	Channel	136.7	68	6.1

4.3.2 Simplified Modeling

After reviewing the configuration of the detailed side-rail model and the

characteristics of its cross sectional areas, the simplified side-rail model is developed. In

developing the simplified model, the modeling methods developed in earlier chapters are

applied here. Similar to the previous examples, the body of the simplified model is

modeled using the Hughes-Liu beam elements based on the plotted profile of the detailed

model (as shown in Figure 89). From analyzing the structure of the side-rail model, it is

found that the simplified model needs 10 plastic hinges to predict its bending behavior.

Those plastic hinges are modeled with nonlinear rotational spring elements (shown and

numbered in Figure 90), and the dimensions of the cross sections where the plastic hinges

are located is measured to calculate the nonlinear spring's bending resistance. As listed

in Table 22, the detailed side-rail model has 7 different cross sections along its length.

Table 23 lists all 10 nonlinear springs and their corresponding cross sections. Since the

cross sections include both box and channel sections, the equations presented in chapters

2 and 3 are applied to calculate the equivalent bending resistances, and some of the results of the calculations are also listed in Table 23.

Table 23. Characteristics of Nonlinear Springs used for Simplified Side-Rail Model

Nonlinear spring #	Related cross section # (see Table 22)	Bending resistance	Fully plastic moment M_p (kN*m)	Angle of fully plastic bending θ_P (degree)	Angle of jamming θ_J (degree)
1	2	Eq. 2-5	38.2	1.2	57
2	2	Eq. 2-5	38.2	1.2	57
3	4	Eq. 3-39	24.8	1.3	62
4	4	Eq. 3-39	24.8	1.3	62
5	5	Eq. 3-39	44.7	1.1	59
6	5	Eq. 3-39	44.7	1.1	59
7	5	Eq. 3-39	44.7	1.1	59
8	6	Eq. 3-39	32.4	1.7	61
9	6	Eq. 3-39	32.4	1.7	61
10	7	Eq. 3-39	32.1	1.2	65

With the calculated bending resistances of the nonlinear springs, the simplified side rail model is created by integrating the beam elements and the nonlinear springs. Figure 90 plots the simplified model, which has the same profiles shown in Figures 88 and 89.
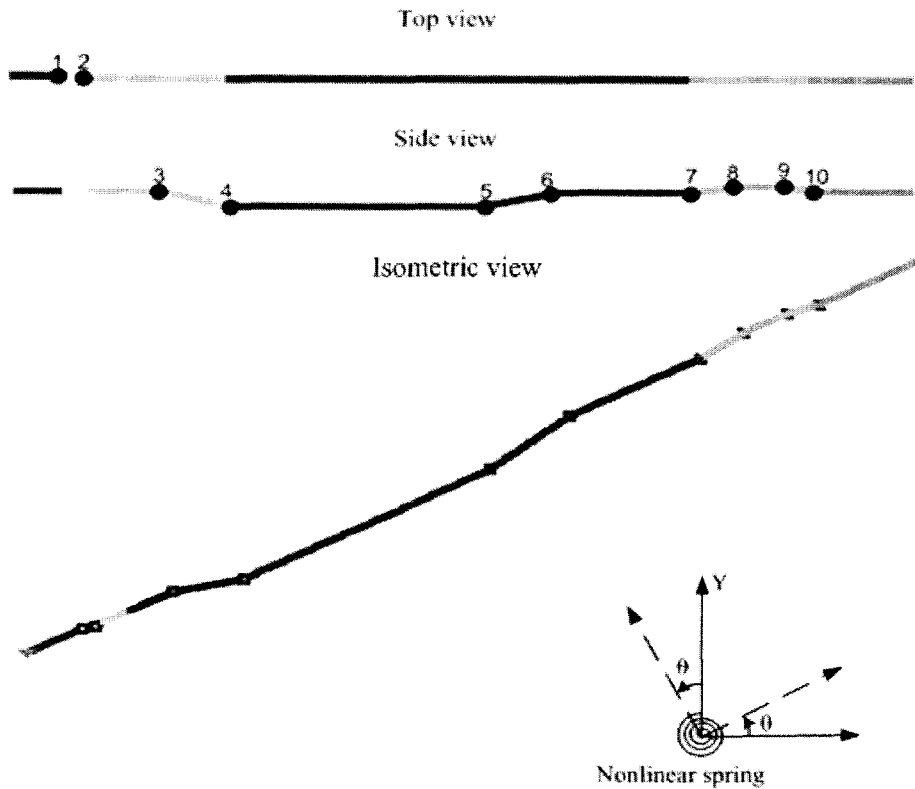
Figure 90. Simplified side-rail model

4.3.3 Crash Results and Comparisons

After creating the detailed and the simplified side-rail models, they are used for crashworthiness analysis. The crash conditions are the same as those for the detailed truck chassis model in section 4.2.1. Important crash results are recorded and compared to verify the efficiency of the simplified model. They are plotted and listed in the following Figures and table. Meanwhile, the deformed configurations of both models are also presented.
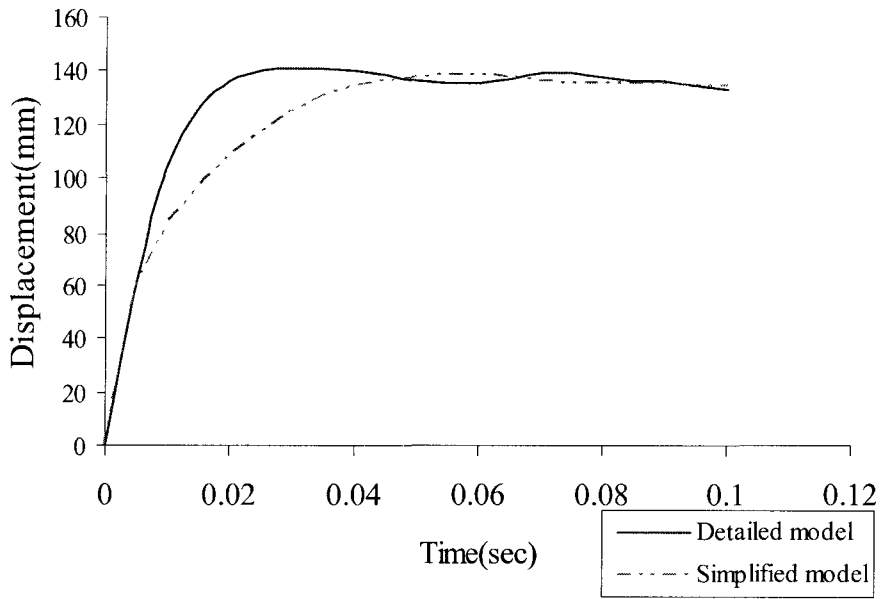
Figure 91. Displacements for side-rail models
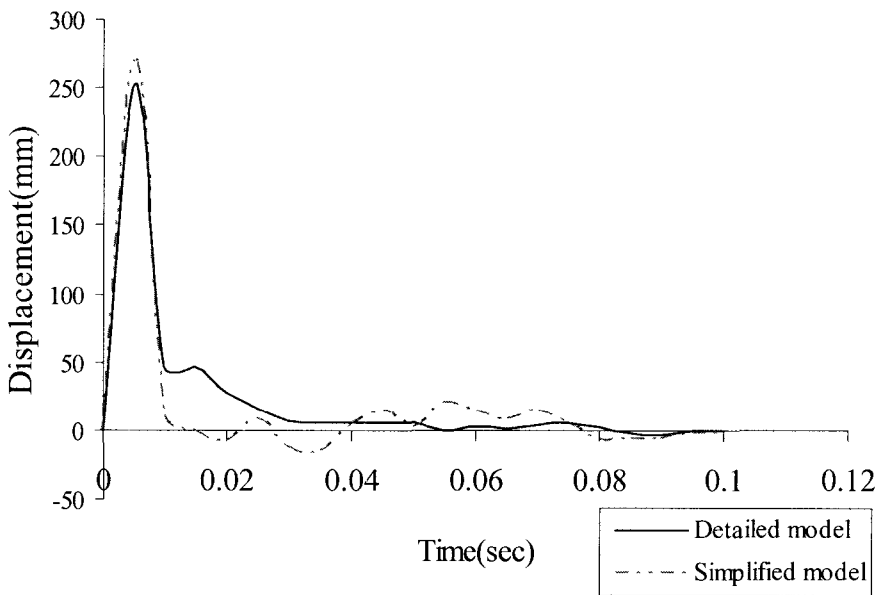
Figure 92. Crushing forces for side-rail models
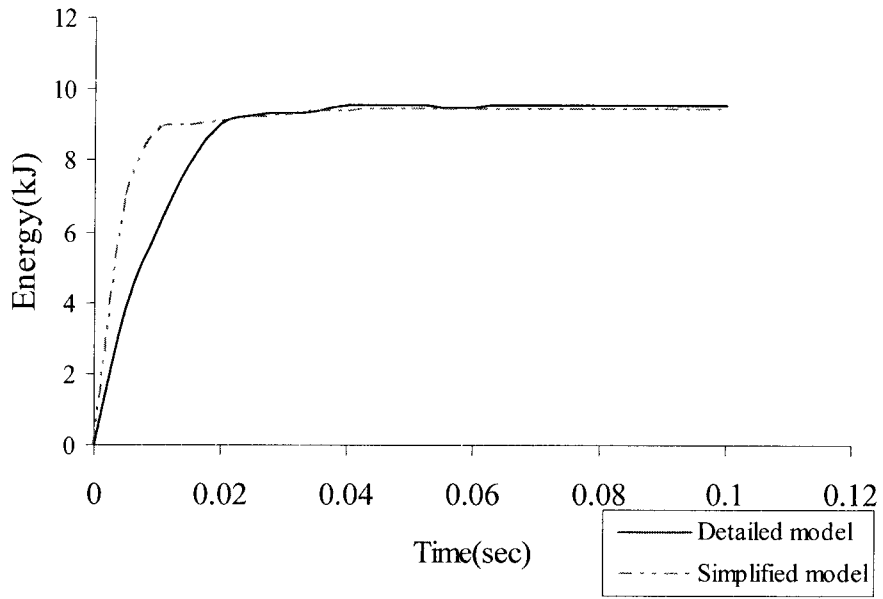
Figure 93. Absorbed energies for side-rail models

Top view

Side view

Isometric view
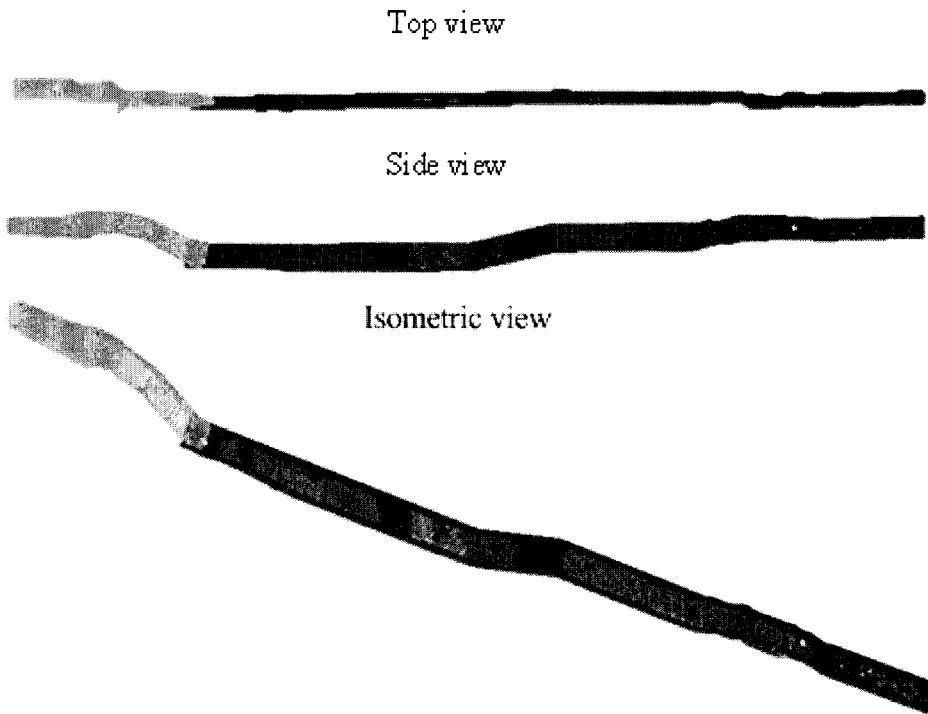
Figure 94. Deformed detailed side-rail model

Top view

Side view

Isometric view
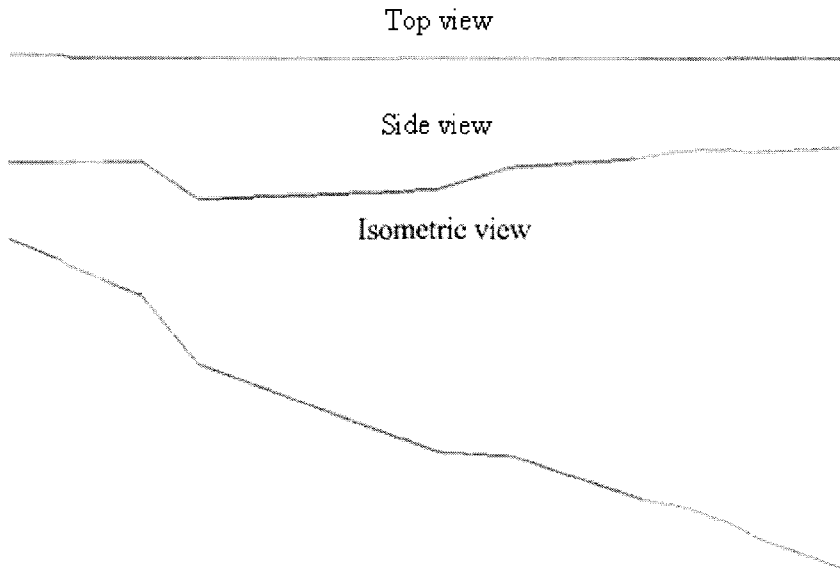
Figure 95. Deformed simplified side-rail model

Table 24. Comparison of Crash Results from Detailed and Simplified Side-Rail Models

	Detailed model	Simplified model	Difference (%)
Max. global displacement (mm)	141.3	138.8	-1.8
Peak crushing force (kN)	252.8	270.8	7.1
Absorbed energy (kJ)	9.6	9.4	-2
Computer time (sec)	60420	2580	-95.7

From Table 24, it is concluded that the developed simplified model can accurately simulate the crash behavior of the detailed model; all of the errors for the important crash results are below 10%. Meanwhile, the simplified model only takes about 4% as much computer time as the detailed model does. Thus, the efficiency of the simplified model is verified, and the simplified model is applied directly for the final simplified truck chassis model.

4.4 Develop Simplified Model for Cross Members

Apart from the two side-rails, the entire chassis model also has six cross members, which are plate parts with irregular shapes. A simplified modeling method for generating the simplified cross member models needs to be developed for use in the final simplified truck chassis model. Two possible options exist for simplifying the cross member models. The first is to generate a superelement for each of the cross members and to integrate these superelements with the developed simplified side-rails model to obtain the objective simplified chassis model. The other method is to calculate the original cross members' mass and stiffness and then, create equivalent beams that have the same mass and stiffness as the original cross members. These equivalent beams should have simple configurations, which are represented by beam element models with the specified cross sectional information. Next, the developed beam element models are connected to the simplified side-rails model and replace the original cross member models in the final simplified chassis model.

In this section, the two optional methods are introduced separately in sections 4.4.1 and 4.4.2. The corresponding simplified cross member models are developed by applying the two methods. In next section, the developed simplified cross member models are used to create the final simplified truck chassis model, and the efficiencies of the two modeling methods are compared and discussed.

4.4.1 Creating Superelements for Cross Members

A superelement is a single-matrix element condensed from a group of finite elements. In nonlinear analyses and analyses of structures containing repeated

133

geometrical patterns, the superelement is always applied in order to reduce computer time and to allow the solution of very large problems with limited computer resources [53]. In this section, six superelements are created to represent the cross members and are imported into the simplified side-rails model to complete the final simplified chassis model. In the simplified chassis model, each superelement works as a single element during the crashworthiness analysis significantly saving computer time.

Since LS-DYNA only recognizes the superelement in a NASTRAN format, the cross members are all re-written as NASTRAN input files. In creating the superelements for these members, the master nodes are selected at the center of the assembly holes through which they are connected to the side-rails. These master nodes are also the interface nodes shared by the super and nonsuperelement structures. All three translational DOF's of the master nodes are selected as the master DOFs. Figure 96 shows the master nodes from all six cross members. After running these input files, the corresponding superelements are created, and the condensed mass and stiffness matrices are generated and output. These matrices are put in the LS-DYNA model to replace those detailed cross member models and to simplify the overall model.
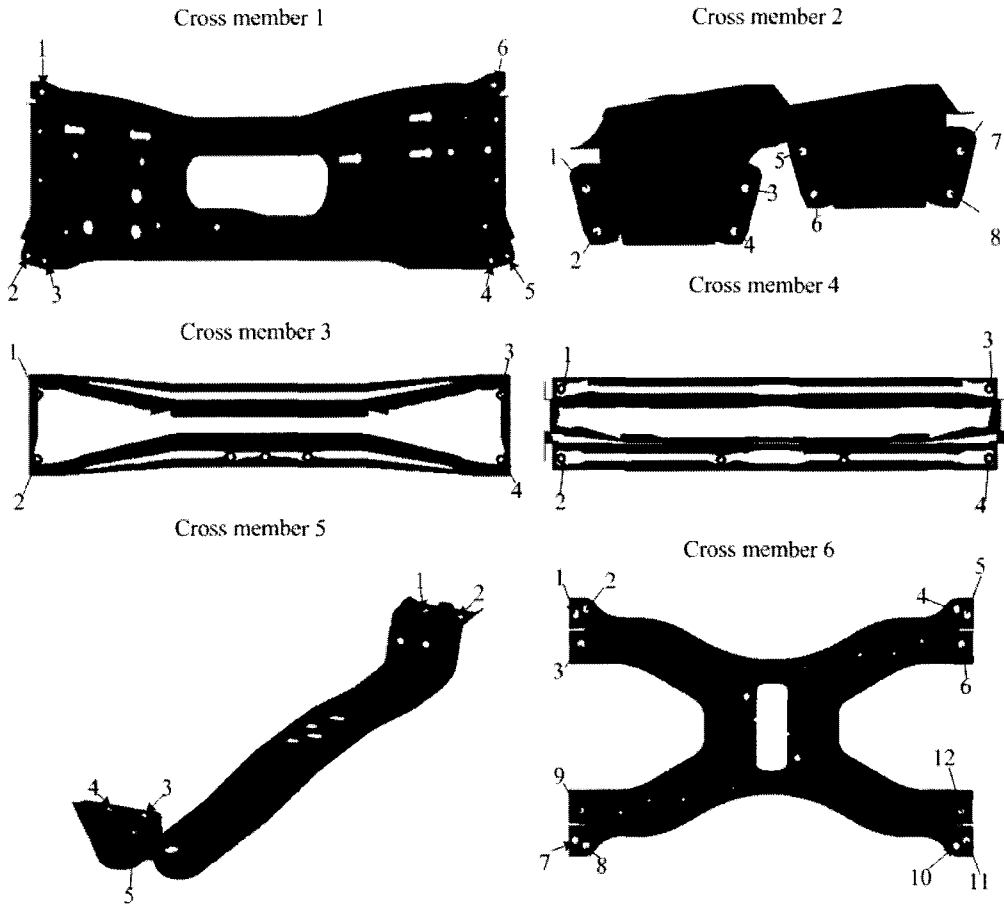
Figure 96. Master nodes from cross members 1 through 6

4.4.2 Developing Equivalent Beams for Cross Members

Apart from the superelement method, there is another scheme to simplify the

cross members. It uses equivalent beams to replace the original cross member models.

In the truck chassis model, the cross members are mainly used to support the side-rails

and to absorb the partial impact energy during the crashworthiness analysis. Therefore, it

is possible to calculate these cross members' masses and their moments of inertia and to

develop a series of equivalent beam models that have those same masses and moments of

inertia. Thus, the equivalent beams have the same masses and stiffness as the original

cross members and show similar crash behavior during the crashworthiness analysis. The

developed beam models are straight beams with uniform cross sections enabling easy representation by beam elements.

Table 25 lists the cross members' masses and moments of inertia, which are the same as those of the equivalent beams. Since the cross members and the equivalent beams have the same material, the volume of the equivalent beams is calculated by dividing the mass by the density. The length of the equivalent beams is measured as the distance between the two side-rails, which is 897mm. Then, the cross sectional areas of those beams are calculated and assigned as characteristic parameters of the beams to ensure that they have the same masses as the original cross members. The values of the cross sectional areas of the equivalent beams are also listed in Table 25.

In Table 25, the moments of inertia I_{xx}, I_{yy} and I_{zz} are calculated using a series of static analyses. For example, to find the I_{xx}, a testing moment, M_x, is applied on the ends of the cross members; after the analyses, the final bending angel θ_x is found. Thus, the I_{xx} is calculated using the formula $M_x = \dfrac{EI_{xx}}{L}\theta_x$, where E is material's Young's modulus and L is the cross member's length, which is 897mm. Similarly, the I_{yy} is found following the same steps. As for the I_{zz}, since it regards the torsional stiffness, in the analysis, one end of the cross member is fixed and a testing torque T_z is applied to the other end. After obtaining the final torsion angle ϕ, the moment of inertia I_{zz} is calculated using the formula $T_z = \dfrac{GI_{zz}}{L}\phi$, where the G is the material's shear modulus. It is determined using the given material's Young's modulus and Poisson's ratio, which is

136

$G = \dfrac{E}{2(1 + v)}$. Figure 97 uses cross member1 as an example and shows how the different

testing moments are applied to it.
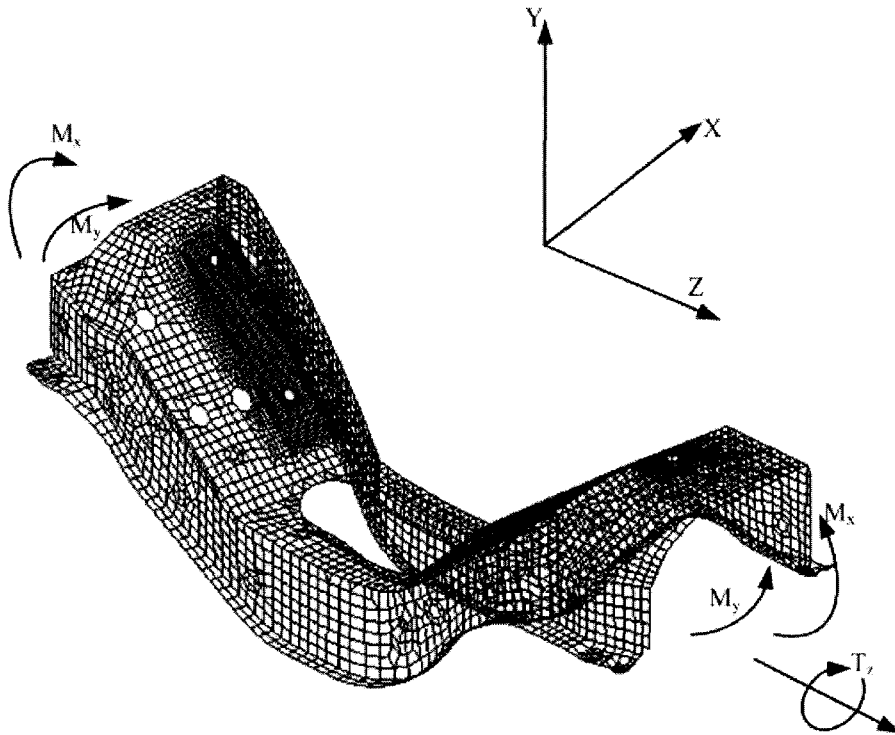
Figure 97. Applying testing moments to find moments of inertia

Table 25. Characteristic Inputs for Equivalent Beams

	Mass (kg)	Cross sectional area (mm^2)	I_{xx}(mm^4)	I_{yy}(mm^4)	I_{zz}(mm^4)
Equivalent beam1	23.7	3374	2108	2196	507
Equivalent beam2	8.2	1168	802	799	34
Equivalent beam3	2.8	399	178	187	9
Equivalent beam4	4.2	598	385	391	19
Equivalent beam5	8.7	1239	757	792	64
Equivalent beam6	10	1424	704	730	59

(Note: Original cross members have the same masses and inertias as the equivalent beams)

After obtaining the inertias and cross sectional areas, the equivalent beams are

modeled using beam elements with correct input moments of inertia and cross sectional

areas. Figure 98 shows the equivalent beams' I_{xx} and I_{yy} with respect to X and Y

directions.
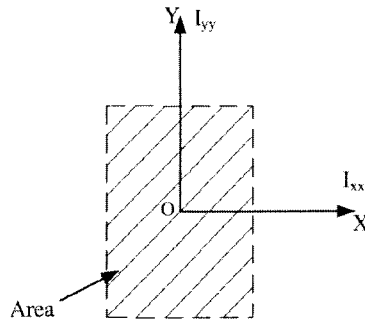
Figure 98. Cross sectional information of equivalent beams

As seen in Figures 86 and 87, some of the cross members buckle from their

middle portion during the crashworthiness analysis. To reproduce the buckling in the

simplified model, one hinge is applied at the middle of each cross member. The hinge is

a spring element whose stiffness is estimated as the bending stiffness $\dfrac{EI_{yy}}{L}$; thus, the new

rotational spring element is defined by inputting its bending stiffness. Figure 99 shows

the detailed model for cross member1 and its equivalent beam model with one hinge in

the middle.

Detailed model   Equivalent beam
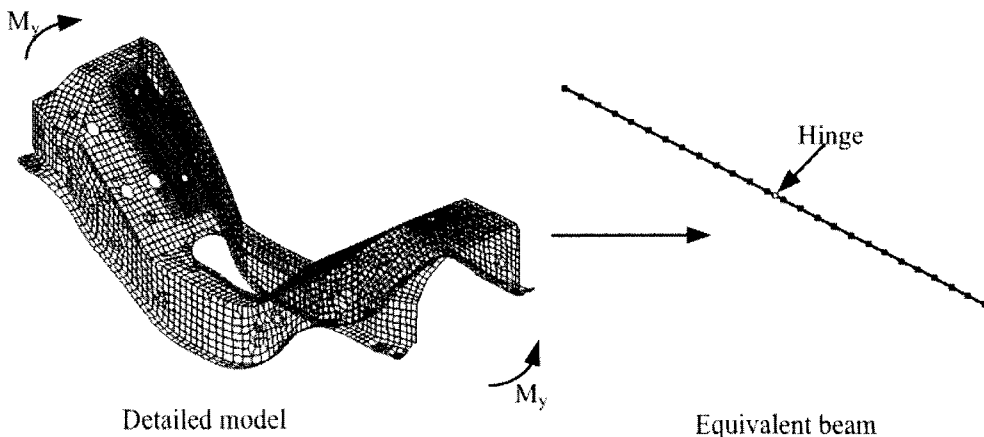
Figure 99. Detailed model and equivalent beam model for cross member1

4.5 Developing a Simplified Model for the Truck Chassis

4.5.1 Superelement Method

In this section, the superelements generated in 4.4.1 are imported into the simplified side-rails model, which is presented in 4.3, to complete the simplified truck chassis model. Then, this simplified model is used for the same crashworthiness analysis performed in 4.2 to verify its efficiency.

4.5.1.1 Simplified Modeling

With all the previous preparations, the simplified truck chassis model is easily completed by integrating the simplified side-rails model and the superelement models. The superelement method requires that the superelements and the non-superelement model share the same interface nodes. Therefore, auxiliary nodes are created in the simplified side-rails model at the same positions where the master nodes are defined for the superelements (see Figure 96). These auxiliary nodes are constrained to the side-rails model by coupling the related DOF's together (see Figure 100). Figure 100 displays the simplified truck chassis model that uses superelements to replace the original cross members.

Side view

Isometric view

The interface nodes are constrained to
the side-rails model
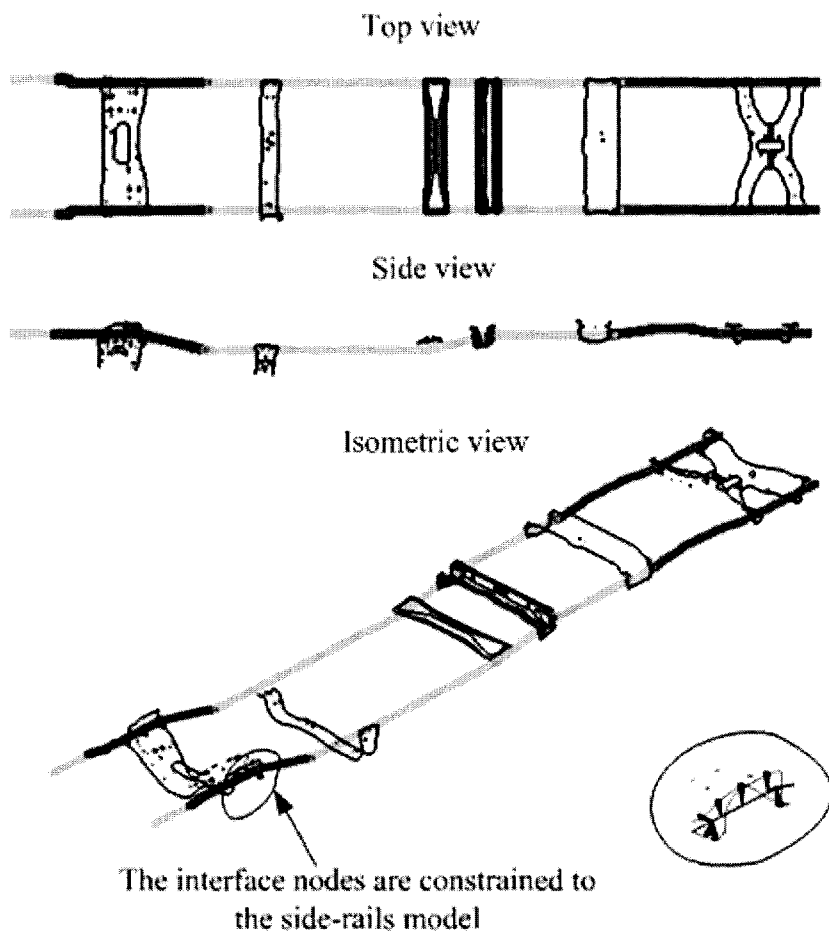
Figure 100. Simplified truck chassis model with superelements

4.5.1.2 Crash Results and Comparisons

The simplified model from 4.5.1.1 is used in the same crashworthiness analysis previously performed on the detailed chassis model. The crash results are compared to those from the detailed model to validate the simplified model and the superelement method. Additionally, a transitional model is also created and used in this analysis. The transitional model is composed of the detailed side-rails model and the superelements (as shown in Figure 101). The crash results of this transitional model are compared in order

to validate the generated superelements and to show the advantage of the developed

simplified model.

Top view

Side view

Isometric view
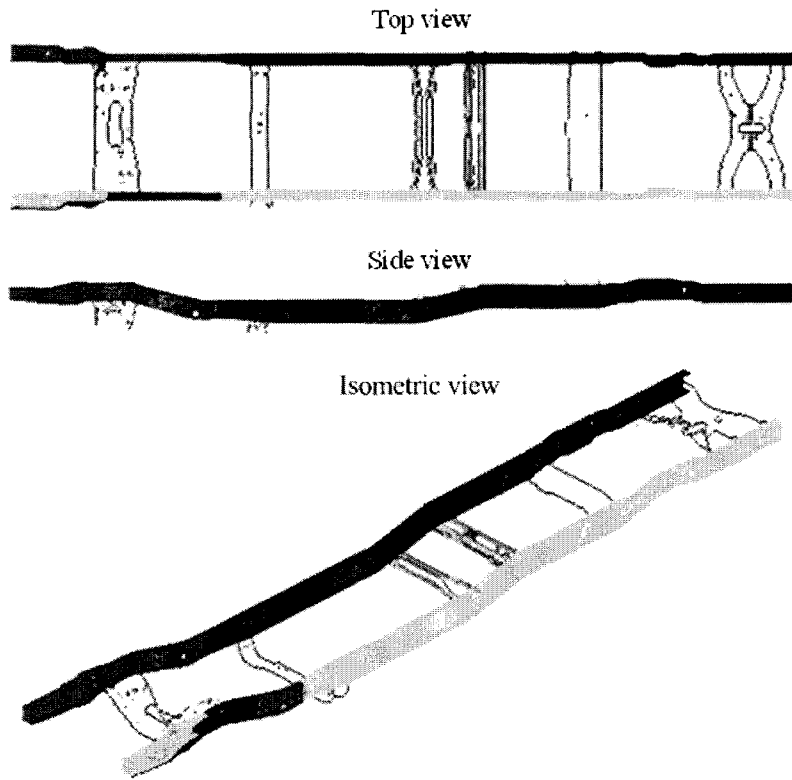
Figure 101. Transitional model with detailed side-rails and superelements

After finishing the crashworthiness analyses, all of the important crash results are

recorded and compared. The results of the comparisons are plotted in following Figures

along with the deformed geometries of both the detailed and the simplified chassis

models; Table 26 lists all of the numerical values.
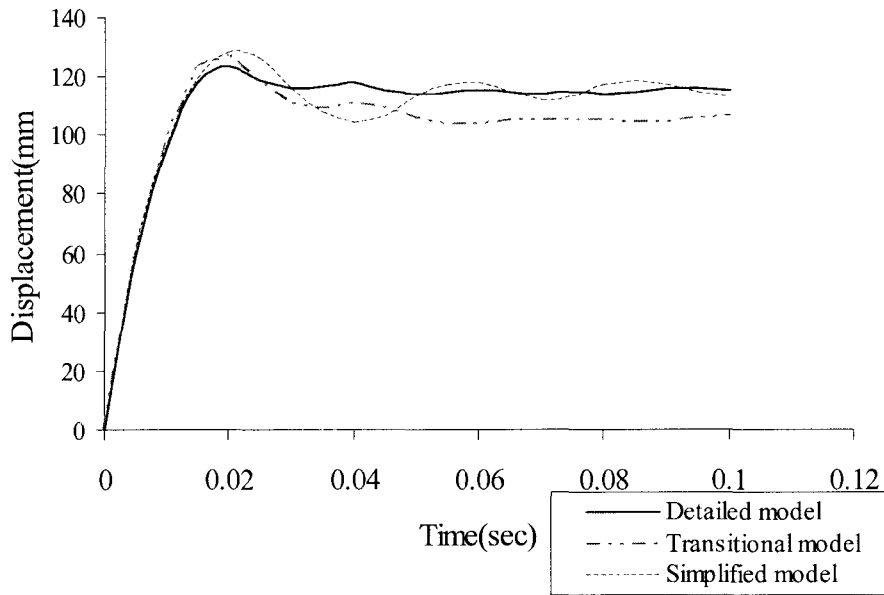
Figure 102. Global displacements for simplified chassis model with superelements
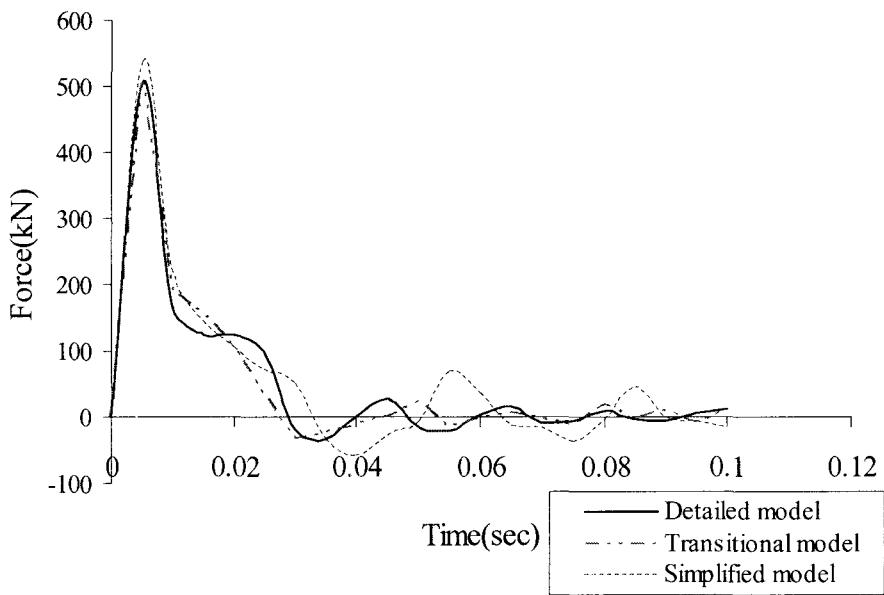
Figure 103. Crushing forces for the simplified chassis model with superelements
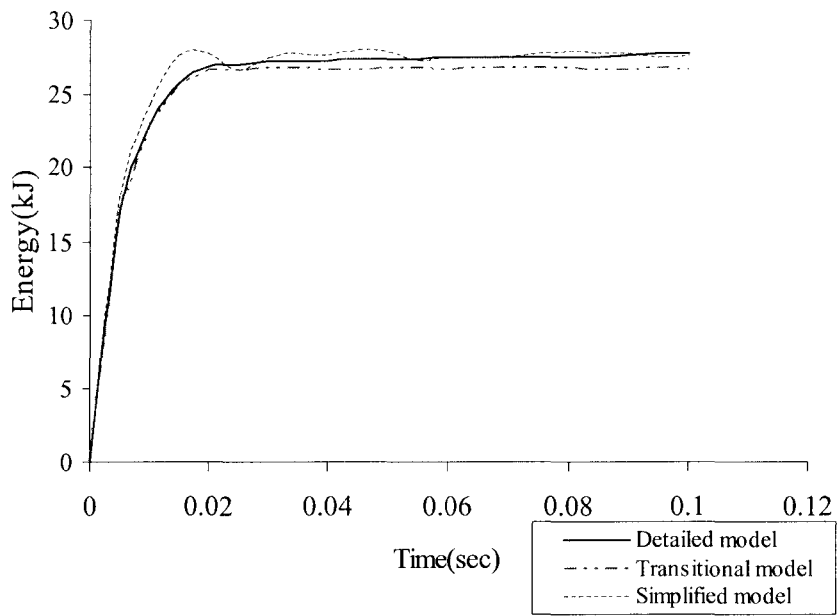
Figure 104. Absorbed energies for simplified chassis model with superelements

Top view

Side view
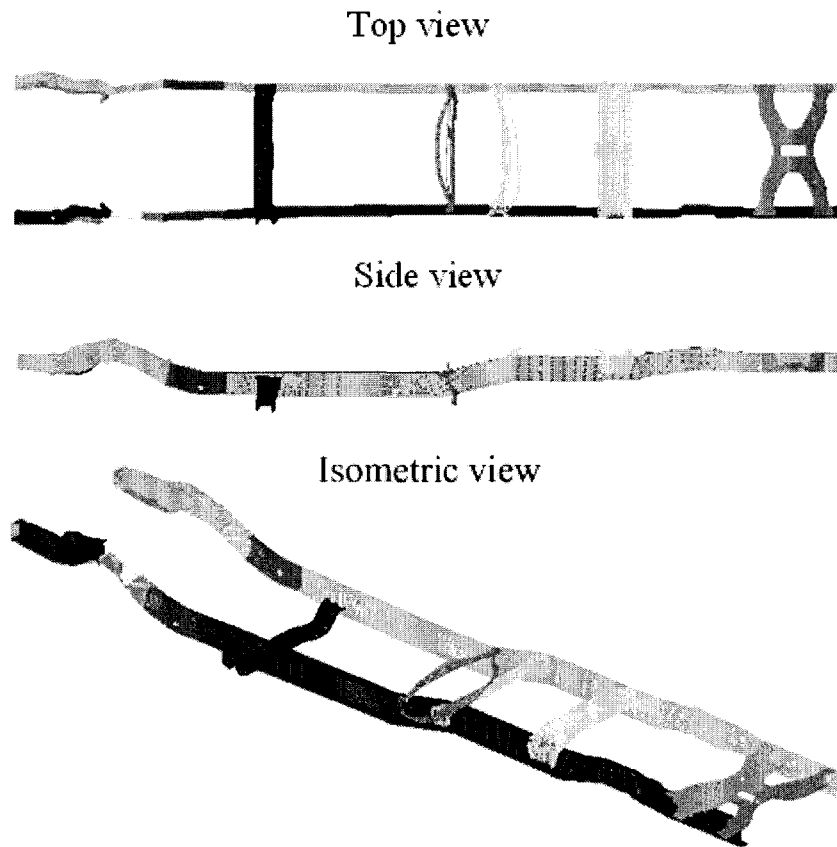
Isometric view

Figure 105. Deformed detailed truck chassis model

Top view

Side view

Isometric view

Figure 106. Deformed simplified truck chassis model with superelements

Table 26. Verification of Simplified Chassis Model with Superelements

	Detailed model	Detailed side-rails with superelements	Simplified model with superelements
Max. global displacement (mm)	123.7	127	128.7
Difference (%)		2.6	4.0
Peak force (kN)	505.5	505.4	540
Difference (%)		-0.02	6.8
Absorbed energy (kJ)	27.8	26.7	26.7
Difference (%)		-4.0	-4.0
Computer time (sec)	126420	81300	7860
Difference (%)		-35.7	-93.8

The comparison between the detailed model and the model composed of detailed side-rails and superelements verifies the accuracy and the efficiency of the generated superelements. From Table 26, it is found that the application of the superelements did not affect the accuracy of the crash results while reducing the computer time by 36%. The advantages of using simplified model with superelements is verified by the same table: the errors of all the crash results yielded from the simplified model are below 10% and the developed simplified model only uses 6% of the computer time of the detailed model.

4.5.2 Equivalent Beam Method

In this section, the equivalent beams of section 4.4.2 are applied to the simplified chassis model to replace the cross members. The same crashworthiness analysis is

performed on the simplified model, and the crash results are compared with those from the detailed model to verify the efficiency of the developed simplified model and the equivalent beams.

4.5.2.1 Simplified Modeling

Given the simplified side-rails model and developed equivalent beams, the simplified chassis model is easily created by assembling the equivalent beams onto the simplified side-rails model. The X-positions of connecting points between the equivalent beams and the side-rails are the X-positions of the cross members' centers of gravity (as shown in Figure 107).
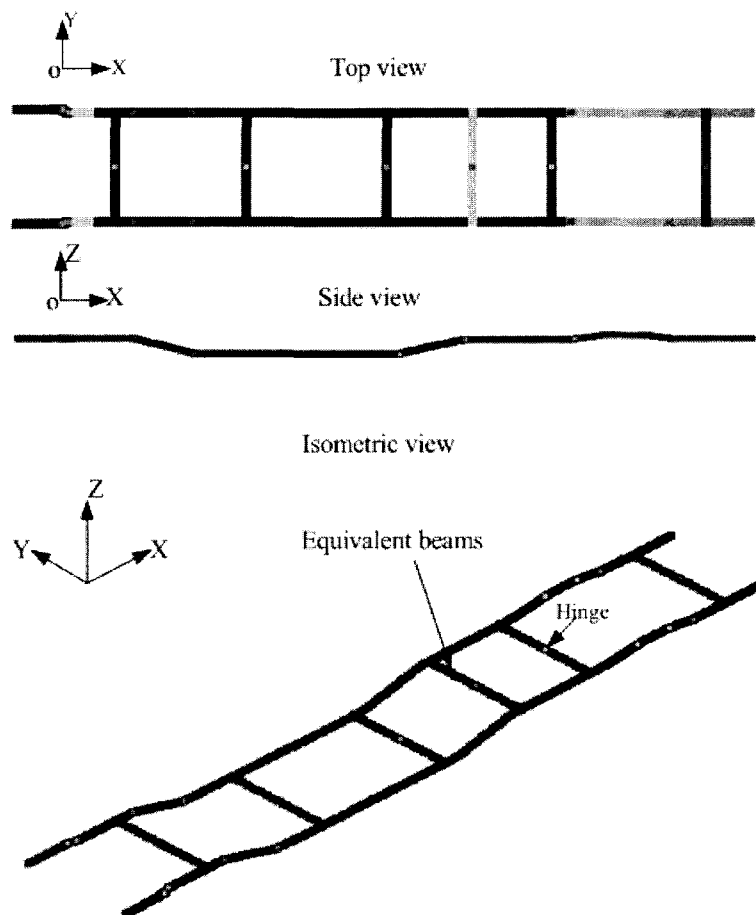
Figure 107. Simplified truck chassis model with equivalent beams

4.5.2.2 Crash Results and Comparisons

The developed simplified chassis model with equivalent beams is used in the crashworthiness analyses, and the crash results are compared with the detailed model to validate the developed simplified model and the equivalent beams. Figure 111 plots the deformed configuration of the simplified model; the results of the comparisons are plotted in Figures 108 through 110 and listed in Table 27.
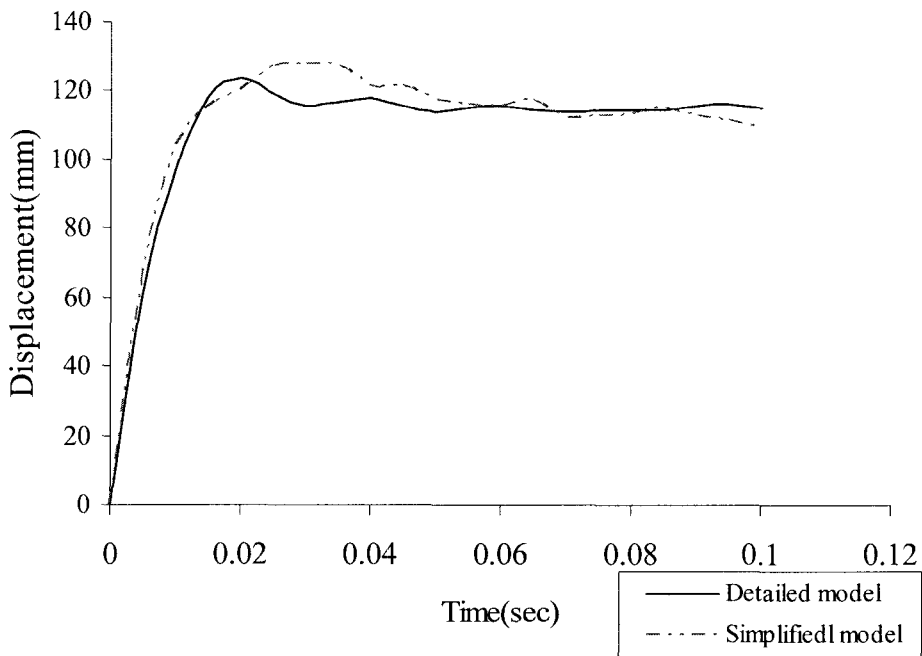
Figure 108. Global displacements for simplified chassis model with equivalent beams
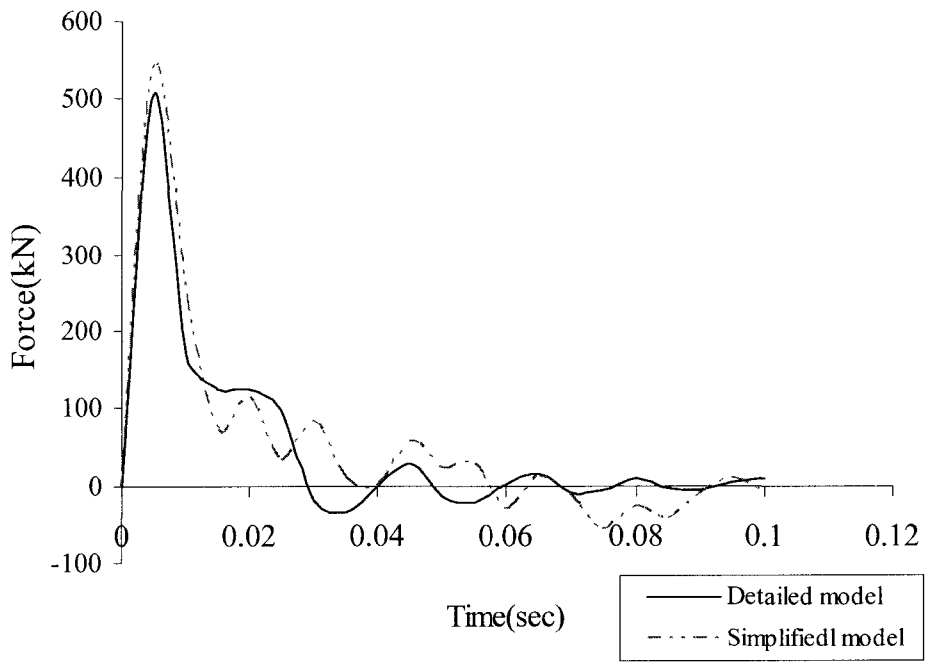
Figure 109. Crushing forces for simplified chassis model with equivalent beams
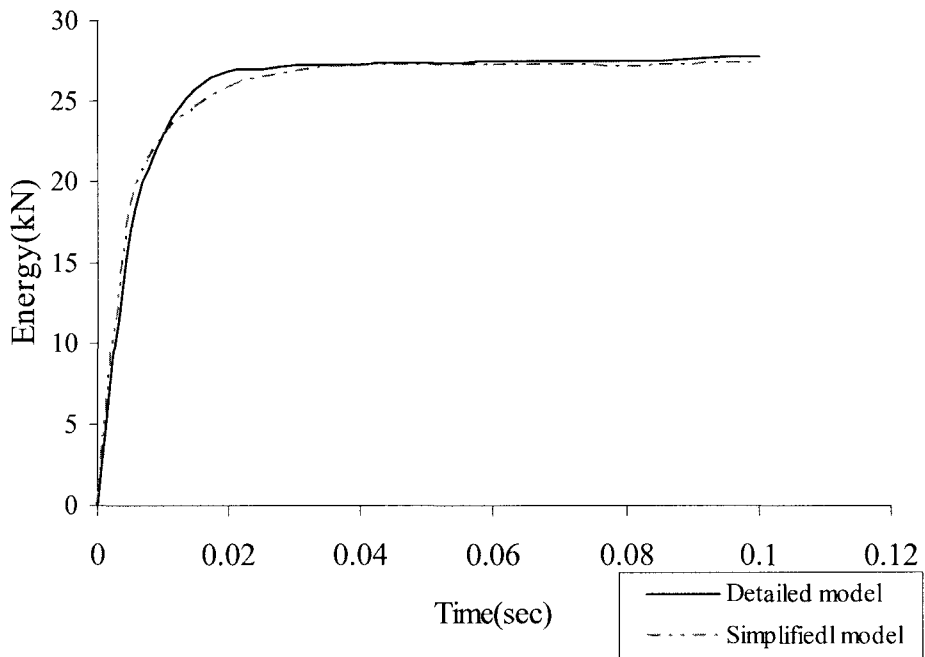
Figure 110. Absorbed energies for simplified chassis model with equivalent beams

Top view

Side view

Isometric view
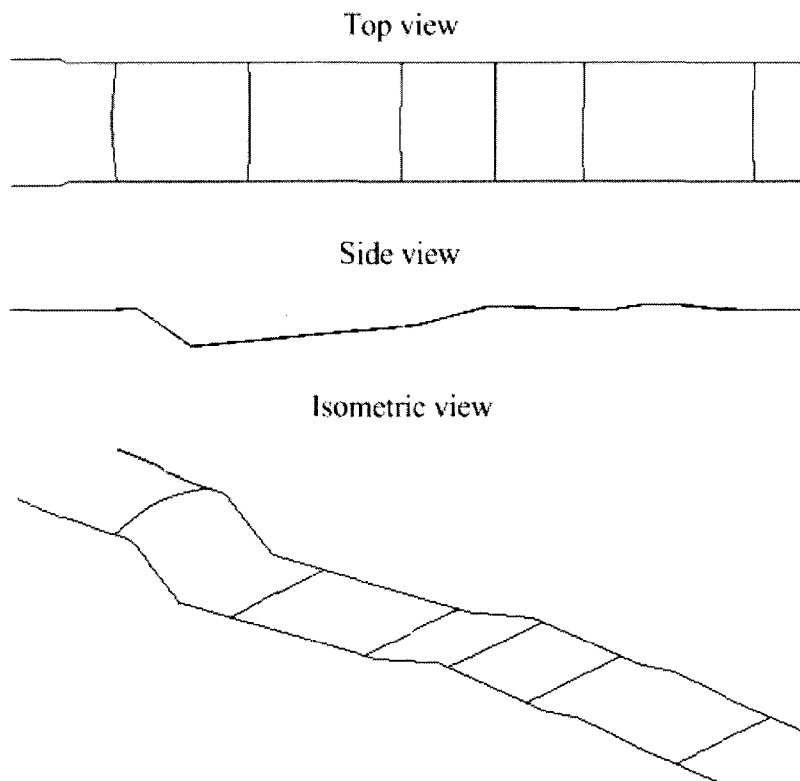
Figure 111. Deformed simplified truck chassis model with equivalent beams

Table 27. Verification of Simplified Chassis Model with Equivalent Beams

	Detailed model	Simplified model with equivalent beams	Difference (%)
Max. global displacement (mm)	123.7	127.6	3.2
Peak crushing force (kN)	505.5	540	6.8
Absorbed energy (kJ)	27.8	27.4	-1.4
Computer time (sec)	126420	10140	-92

The results of the comparisons show that the developed simplified model and the detailed model reach a close consensus in simulating the chassis's crash response. All the errors are below 10%, and the simplified model only requires 8% of the computer time of the detailed model to finish the analysis. Additionally, when comparing Figures

105 and 111, it is found that with the hinge at the middle of cross members, cross member1 in the simplified model experiences buckling similar to the detailed cross member model. From the output of the nodes' displacements, it is calculated that in the detailed model the deformation at the center of cross member1 is 62.2mm while, the value in the simplified model is 60.0mm; thus, they are very close to each other. The simplified chassis model with equivalent beams is validated, and the modeling method is verified as capable of creating further simplified crash models.

4.5.3 Discussion

The results of the comparisons show that the detailed model and both of the developed simplified models achieve similar results in simulating the chassis's crash response. All the errors are below 10%, and the simplified models took less than 10% of the computer time necessary for the detailed model to finish the crashworthiness analysis.

As in tables 26 and 27, both the superelement method and the equivalent beam method can efficiently simplify the cross members in the original detailed model. The two methods have similar principles: using a simplified model to transfer the mass and stiffness of the original cross members and integrating the correct mass and stiffness into the final simplified model, and simulating the crash behavior of the cross members.

Of the two methods, the equivalent beam method is recommended because it is easier to find the masses and moments of inertia of the cross members and create the equivalent beams by assigning these values than to generate the superelements for the cross members using some other software package. Unlike the superelement method, all the operations of the equivalent beam method are solvable in an LS-DYNA environment, and no other software package is necessary. Moreover, with the application of the middle

hinges, the simplified model with equivalent beams visually demonstrating the buckling of the cross members other than the side-rails.

4.6 Conclusions

This chapter develops the final simplified model for the truck chassis based on all the previous studies and preparations. The crash results and the comparisons show that the developed simplified model works very well in simulating low-speed impact problems and can replace the existing detailed model to save computer resources. In the simplified model, the bending resistance of the channel section beam from chapter 3 is applied to the development of the new nonlinear spring elements that model the plastic hinges of the side-rails. Again, the simplified modeling method in chapter 2 is used to create the simplified model for the side-rails that receive the majority of the impact loads and significantly contribute to the crash. Also, in simplifying the cross members, the equivalent beams are generated and applied to replace the detailed cross member models previously simulated by shell elements. As a result, following all of the steps significantly reduces the overall size of the chassis model.

The modeling method above develops the simplified truck chassis model very effectively and is extensively applicable to other engineering problems. The following chapters summarize and present a general simplified modeling methodology using earlier research. This methodology is thoroughly discussed and evaluated.

CHAPTER V

DEVELOPMENT OF A SIMPLIFIED MODELING METHODOLOGY

5.1 Simplified Modeling Methodology

Based on the simplified modeling of the truck chassis described in chapter 4, a general simplified modeling methodology is summarized and applicable to the development of simplified crash models for more structures.

The first step of creating a qualified simplified model is to carefully study the structure of the detailed model that requires simplification. Generally, most real crash models are composed of longitudinal thin-walled frame members and cross members. When investigating the formation of the detailed model, the features of these members are studied, recorded, and referenced in future simplified modeling.

Secondly, different modeling strategies are chosen for the modeling of each of the members. The simplified modeling method of chapters 2, 3, and 4 are applicable to the creation of simplified models for the longitudinal thin-walled frame members. As illustrated in previous chapters, in the creation of such simplified models, nonlinear spring elements are necessary for simulating the crash behavior of the plastic hinges. To develop the nonlinear spring elements, the researchers decide the possible positions of the plastic hinges in the original model, first. Using the cross section information from the plastic hinges, appropriate collapse theories are applied to determining the approximate moment – rotation characteristics of the nonlinear spring element. Afterwards, the

developed spring element is integrated with the beam element to build the simplified

model for the longitudinal thin-walled frame members. Beam-element models with the

same masses and moments of inertia replace the cross members of the original detailed

model. A spring element is applied at the middle of the members to simulate the

buckling behavior.

Finally, after developing the simplified models for all the members, these

developed simplified models are combined to accomplish the final simplified model.

Detailed steps of the simplified modeling methodology are described in section 5.2.

5.2 Detailed Steps of the Methodology

The detailed steps of creating the simplified crash models are summarized as:

1. Use beam elements with the correct cross sectional information to model the body
   of the longitudinal thin-walled frame members.

2. Use nonlinear spring elements with calculated bending resistance to model the
   plastic hinges.

3a. For the box section beams, the nonlinear spring's bending resistance is estimated
    based on given cross section information by using equations 2-5 to 2-10.

3b. For the channel section beams, the nonlinear spring's bending resistances
    regarding different $\lambda = \dfrac{a}{b}$ are derived applying equations 3-28 through 3-39

4. Calculate the transverse plate parts' masses, moments of inertia, and bending
   stiffness.

5. Use beam elements with the correct masses and moments of inertia to model the
   body of cross members.

6. Define a spring element with the cross members' bending stiffness at the middle of the beam models created in step 5 to simulate its buckling behavior.

7. Integrate the developed simplified models of the longitudinal thin-walled frame members and of the cross members to accomplish the final simplified crash model.

After creating the simplified model in LS-DYNA environment, boundary conditions and initial conditions are applied and crash time is set for analyses. Then the developed simplified model is exported into a *.dyn output file, which is used for crashworthiness analyses. The crash results are found and processed in postprocessor.

CHAPTER VI

SUMMARY

6.1 Evaluation

In this research, the simplified crash model for truck chassis is developed and validated through the analyses and comparisons. A systematic simplified modeling methodology is also presented. This methodology can help researchers create qualified simplified models that can replace existing detailed models in crashworthiness analyses. The results of the analyses and the comparisons verify that the developed simplified models save much more computer time than the detailed ones with the errors less than 10%. With the simplified model, designers can easily changes the model to attempt and compare different design ideas. Obviously, in comparison with the detailed model, the simplified model requires much less labor for modifications or for changing geometries. This is especially useful during the early product design stage.

Despite all its advantages, some limitations still exist in developed modeling methodology. As shown in previous results and comparisons, a simplified model developed following this modeling methodology can accurately simulate the structure's crash behavior in a low-speed impact problem (initial velocity is around 15m/s). If the initial velocity is increased to 30m/s or higher, the developed simplified model can not simulate the structure's crash response accurately, and a detailed model is still necessary under such conditions. One possible reason is that during a high-speed crash, much

higher impact loads are generated and transformed to the structure. Therefore, the crash

model collapses much more quickly and much more seriously than the low-speed crash

case. Thus, serious buckling and the phenomenon of "self-contact" (shown in Figure 112)

appear in this crash model and significantly complicate the crashworthiness analysis.

The current beam element used to model the structure's body in the simplified model can

not even approximately simulate the serious buckling itself due to the interactions among

the "self – contact" parts. Also, since a high instant impact load appears in the high-

speed crash problem, the nonlinear spring elements fail the first time and can not

correctly predict the plastic hinges' crash behavior. These two factors cause the failure of

the simplified model in simulating high-speed impact problems.
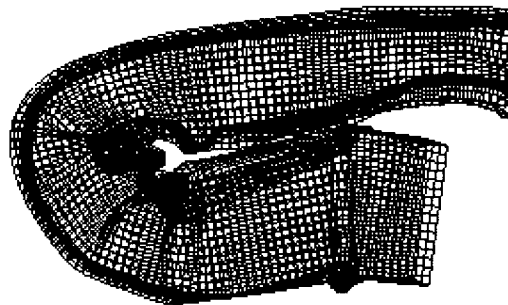
Figure112. "Self – contact" happens in the high-speed crash problem

In the developed simplified modeling methodology, the superelement models and

the equivalent beam element models are proposed to replace those transverse parts that

do not directly contact the impact objects. Nevertheless, the methodology does not

answer the question of how to simplify the transverse plate parts that are directly

impacted by other objects during the crash process. One example is the bumper of a

vehicle, during a crash, the bumper is impacted and seriously buckles; the impact loads

are transferred to the remaining parts of the vehicle through the bumper. Obviously, neither a single superelement nor a beam element can develop the simplified model for the bumper; the shell element can not be replaced in this case. One possible solution is to use several superelements or several equivalent beams connected through "plastic hinges" to represent the bumper. During the crash, the relative motions between these superelements or equivalent beams along the corresponding "plastic hinges" simulate the buckling behavior of the bumper. The difficulties involve how to accurately predict the buckling behavior of the bumper and how to determine the characteristics of the "plastic hinges" as well as the number of superelements or equivalent beams that represent the bumper.

According to the above discussion, the simplified modeling methodology and the simplified models developed in this research still need improvement to meet the higher-level requirements in simulating more crash problems.

6.2 Future Directions

As mentioned in 6.1, the current research about simplified crash modeling can be improved in at least three areas in the future. The first area is the development of a new beam element that can represent significantly collapsed structures during high-speed crash simulations. To fulfill this, the new beam element should be capable of accurately simulating the buckling and "self-contact" of the crashed structure usually involved in high-speed crashes that can currently only be reflected by a shell element.

Secondly, in order to develop qualified simplified models that can be used for high-speed crashworthiness analyses, it is necessary to improve the nonlinear spring

elements. They need to be capable of correctly predicting the crash behavior of the plastic hinges even after the jamming angle is reached.

The third area is to develop a new method to simplify the detailed models of the transverse parts, which directly contact the impact objects during crash tests, e.g. the bumper. As explained in section 6.1, such parts might be represented by several superelements or equivalent beams, which are connected through "plastic hinges." Using the current knowledge about the buckling behavior of the plate parts, researchers may develop a new element to model these parts in the improved simplified models.

REFERENCE

[1] Don O. Brush, Bo O. Almroth. "Buckling of Bars, Plates and Shells," McGraw-Hill, Inc. 1975.

[2] S. Ishiyama, T. Nishimura, and Y. Tsuchiya. "Impact Response of Thin-walled Plane Frame Structures," *International Journal of Impact Engineering*, Vol. 1, Issue 3 (1988) 227 – 247.

[3] N. Jones, T. Wierzbicki. "Structural Crashworthiness and Failure," Elsevier Science Publishers Ltd., 1993.

[4] A. G. Mamalis, D. E. Manolakos, G. A. Demosthenous, and M. B. Ioannidis. "Crashworthiness of Composite Thin-walled Structural Components," Technomic Publishing Company, Inc., 1998.

[5] H. S. Kim, T. Wierzbicki. "Crush Behavior of Thin-walled Prismatic Columns under Combined Bending and Compression," *Computers and Structures* 79 (2001) 1417 – 1432.

[6] A. A. A. Alghmadi. "Folding-crumpling of Thin-walled Aluminum Frusta," *International Journal of Crashworthiness*, Vol. 7, No. 1 (2002).

[7] T. Belytschko. "On Computational Methods for Crashworthiness," *Computers and Structures*, Vol. 42, No. 2 (1992) 271-279.

[8] A. Toyama, K. Hatano, and E. Murakami. "Numerical Analysis of Vehicle Frontal Crash Phenomena," SAE Technical Paper Series, 920357.

[9] U. N. Gandhi and S. J. Hu. "Data-based Approach in Modeling Automobile Crash," *International Journal of Impact Engineering*, Vol. 16, No. 1 (1995) 95 – 118.

[10] C. Cosme, A. Ghasemi, and J. Gandevia. "Application of Computer Aided Engineering in the Design of Heavy-duty Truck Frames," *Society of Automotive Engineers (SAE)*, 1999-01-3760.

[11] H. Nishigaki, S. Nishiwaki, T. Amage, Y. Kojima, and N. Kikuchi. "First Order Analysis – New CAE Tools for Automotive Body Designers," *SAE*, 2001-01-0768.

[12] O. C. Zienkiewicz. "The Finite Element Method in Engineering Science," McGraw-Hill, Inc., 1971.

[13] B. G. Prusty and S. K. Satsangi. "Finite Element Buckling Analysis of Laminated Composite Stiffened Shells," *International Journal of Crashworthiness*, Vol. 6, No. 4 (2001) 471 – 483.

[14] C. B. W. Pedersen, "Topology Optimization for Crashworthiness of Frame Structures," *International Journal of Crashworthiness*, Vol. 8, No. 1 (2003) 29 – 39.

[15] S. W. Kirkpatrick, J. W. Simons, and T. H. Antoun. "Development and Validation of High Fidelity Vehicle Crash Simulation Models," *International Journal of Crashworthiness*'98 – International Crashworthiness Conference.

[16] J. M. Gonzalez, C. D. Kan, and N. E. Bedewi. "Versatility and Limitations of a Fully Detailed Finite Element Model of a 1997 Dodge Grand Caravan for Crashworthiness Application," Society of Automotive Engineers, Inc., 2000-01-062.

[17] D. Lawver, L. Nicodym, D. Tennant, and H. Levine. "Nonlinear Numerical Modeling of Aircraft Impact," *International Journal of Crashworthiness*, Vol. 6, No. 4 (2001) 451 – 469.

[18] Z. Q. Chen, J. G. Thacker, W. D. Pilkey, W. T. Hollowell, S. W. Reagan, and E. M. Sieveka. "Experiences in Reverse-engineering of a Finite Element Automobile Crash Model," *Finite Elements in Analysis and Design*, 37 (2001) 843 – 860.

[19] A. Eghilmi and J. D. Yang. "Collapsible Signpost Design Optimization for Car Crash Impact and Wind Loading," http://www.atsb.gov.au/road/pdf/CANCES_Final.pdf.

[20] Y. M. Jin. "Analysis and Evaluation of Minivan Body Structure Finite Element Methods," http://www.mscsoftware.com/support/library/conf/auto00/p00500.pdf.

[21] M. H. Ray. "Impact Conditions in Side-impact Collisions with Fixed Roadside Objects," *Accident Analysis and Prevention*, 31 (1999) 21 – 30.

[22] J. A. Zukas and D. R. Scheffler. "Practical Aspects of Numerical Simulations of Dynamic Events: Effects of Meshing," *International Journal of Impact Engineering*, 24 (2000) 925 – 945.

[23] B. Canaple, G. P. Rungen, E. Markiewicz, P. Drazetic, J. H. Smith, B. P. Chinn, D. Cesari. "Impact Model Development for the Reconstruction of Current Motorcycle Accidents," *International Journal of Crashworthiness*, Vol. 7, No. 3 (2002) 307 – 320.

[24] P. Drazetic, E. Markiewicz, and Y. Ravalard. "Application of Kinematic Models to Compression and Bending in Simplified Crash Calculation," *International Journal of Mechanical Science*, Vol. 35, No. ¾ (1993) 179 – 191.

[25] Ford Motor Company. "Guidelines for Modeling an Automobile Body for NVH Analysis – Simplified Models" (1995).

[26] R. J. Brooks and A. M. Tobias. "Choosing the Best Model: Level of Detail, Complexity, and Model Performance," *Mathematical Computer Modeling*, Vol. 24, No. 44 (1996) 1 – 14.

[27] H. S. Kim, S. Y. Kang, I. H. Lee, S. H. Park, and D. C. Han. "Vehicle Frontal Crashworthiness Analysis by Simplified Structure Modeling using Nonlinear Spring and Beam Elements," *International Journal of Crashworthiness*, Vol. 2, No. 1 (1997) 107 – 117.

[28] A. K. Aaouk, N. E. Bedewi, C. D. Kan, and D. Marzougui. "Development and Evaluation of a C-1500 Pick-up Truck Model for Roadside Hardware Impact Simulation," http://www.ncac.gwu.edu/archives/papers/c-2500_FHWA.pdf.

[29] W. Abramowicz. "Simplified Crushing Analysis of Thin-walled Columns and Beams," *Rozprawy Inzynierskie*, Engineering Transactions, 29, 1 (1981) 5 – 26.

[30] D. Kecman. "Bending Collapse of Rectangular and Square Section Tubes," *International Journal of Mechanical Science*, Vol. 25, No. 9 – 10 (1983) 623 – 636.

[31] T. Wierzbicki and W. Abramowicz. "On the Crushing Mechanisms of Thin-walled Structures," *Journal of Applied Mechanisms*, 50 (1983) 727 – 734.

[32] W. Abramowicz and T. Wierzbicki. "Axial Crushing of Multicorner Sheet Metal Columns," *Journal of Applied Mechanisms*, 53 (1989) 113 – 120.

[33] T. Wierzbicki, L. Recke, W. Abramowicz, and T. Gholmai. "Stress Profiles in Thin-walled Prismatic Columns Subjected to Crush Loading – I. Compression," *Computers & Structures*, Vol. 51, No. 6 (1994) 611 – 623.

[34] T. Wierzbicki, L. Recke, W. Abramowicz, T. Gholami, and J. Huang. "Stress Profiles in Thin-walled Prismatic Columns Subjected to Crush Loading – II. Bending," *Computers & Structure*, Vol. 51, No. 6 (1994) 623 – 641.

[35] LS-DYNA Theoretical Manual, Livermore Software Technology Corporation.

[36] H. S. Kim and T. Wierzbicki. "Closed-form Solution for Crushing Response of Three-dimensional Thin-walled 'S' Frames with Rectangular Cross-sections," *International Journal of Impact Engineering*, Vol. 30, Issue 1 (2004) 87 – 112.

[37] L. C. Bank and E. Cofie. "A Hybrid Force/stiffness Matrix Method for the Analysis of Thin-walled Composite Frames," *Composite Structures*, Vol. 28, Issue 4 (1994) 391 – 404.

[38] O. P. Agrawal, K. J. Danhof, and R. Kumar. "A Superelement Model Based Parallel Algorithm for Vehicle Dynamics," *Computers & Structures*, Vol. 51, Issue 4 (1994) 411 – 423.

[39] L. D. Flippen. "Current Dynamic Substructuring Methods as Approximations to Condensation Model Reduction," *Computers & Mathematics with Applications*, Vol. 27, Issue 12 (1994) 17 – 29.

[40] V. V. Tkachev. "The Use of Superelement Approach for the Mathematical Simulation of Reactor Structure Dynamic Behavior," *Nuclear Engineering and Design*, Vol. 196, Issue 1 (2000) 101 – 104.

[41] Z. P. Mourelatos. "An Efficient Crankshaft Dynamic Analysis Using Substructuring with Ritz Vectors," *Journal of Sound and Vibration*, Vol. 238, Issue 3 (2000) 495 – 527.

[42] H. Shakourzadeh, Y. Q. Guo, and J. L. Batoz. "Modeling of Connections in the Analyses of Thin-walled Space Frames," *Journal Computers and Structures*, 71 (1999) 423 – 433.

[43] S. Mourad, A. Ghobarah, and R. M. Korol. "Dynamic response of hollow section frames with bolted moment connections," *Journal of Engineering Structures*, Vol. 17, No. 10 (1995) 737 – 748, 1995.

[44] D. H. Johnson, R. B. Englund, B. C. McAnlis, K. C. Sari, and D. Colombet. "Three-Dimensional Modeling of a Bolted Connection," http://www.ohiocae.com/bolt.htm.

[45] C. L. Li, K. M. Yu, and T. W. Lam. "Implementation and Evaluation of Thin-shell Rapid Prototype," *Computers in Industry* 35 (1998) 185 – 193.

[46] S. Toshiyuki, S. Yoshihito, and K. Shochi. "FEM Stress Analysis and Strength of Adhesive Butt Joints of Similar Hollow Cylinders under Static and Impact Tensile Loadings," *Journal of Adhesion Science and Technology*, Vol. 16, No. 11 (2002) 1449 – 1468.

[47] A. N. Palazotto, E. J. Herup, and L. N. B. Gummadi. "Finite Element Analysis of Low-velocity Impact on Composite Sandwich Plates," *Composite Structures*, Vol. 49, No. 2 (2000), 209 – 227.

[48] W. J. Kang and H. Huh. "Crash Analysis of Thin-walled Structures with an Elasto-plastic Finite Element Method," *Key Engineering Materials*, (2000) 177 – 180.

[49] R. D. Cook. "Finite Element Modeling for Stress Analysis," John Wiley & Sons, Inc. 1995.

[50] K. J. Bathe. "Finite Element Procedures," Prentice Hall, Inc. 1996.

[51] V. Adams and A. Askenazi. "Building Better Products with Finite Element Analysis," Onword Press, 1999.

[52] K. Schweizerhof, L. Nilsson, and J. O. Hallquist. "Crashworthiness Analysis in the Automotive Industry," *International Journal of Computer Application in Technology*, Vol. 5, Nos. 2/3/4 (1992) 134 – 156.

[53] ANSYS, Advanced Analysis Techniques Guide.

[54] F. P. Beer and E. R. Johnston, Jr.. "Mechanics of Materials," McGraw-Hill, Inc. 1981.

[55] W. Prager. "An Introduction to Plasticity," Addison-Wesley Publishing Company, Inc. 1959.

[56] J. B. Martin. "Plasticity: Fundamentals and General Results," *Massachusetts Institute of Technology Press*, 1975.

[57] R. Hill, "Extremal Paths of Plastic Work and Deformation," *Journal of Mechanical Physics and Solids*, Vol. 34, No. 5 (1986) 511 – 523.

[58] X. T. Chu, Z. M. Ye, R. Kettle, L. Y. Li, "Buckling Behavior of Cold-Formed Channel Sections under Uniformly Distributed Loads," *Thin-Walled Structures*, Vol. 43 (2005) 531 – 542

[59] P. Drazetic, F. Payen, P. Ducrocq, E. Markiewicz, "Calculation of the Deep Bending Collapse Response for Complex Thin-Walled Columns I. Pre-Collapse and Collapse Phases," *Thin-Walled Structures*, Vol. 33 (1999) 155 – 176

[60] E. Markiewicz, F. Payen, P. Ducrocq, P. Drazetic,"Calculation of the Deep Bending Collapse Response for Complex Thin-Walled Columns II. Post-Collapse and Collapse Phases," *Thin-Walled Structures*, Vol. 33 (1999) 177 – 210

[61] W. Abramowicz and N. Jones, "Dynamic Progressive Buckling of Circular and Square Tubes," *International Journal of Impact Engineering*, Vol. 4, No. 4 (1986) 243 – 270

[62] R. Hauptmann, S. Doll, M. Harnau, K. Schweizerhof, "Solid-Shell Elements with Linear and Quadratic Shape Functions at Large Deformations with Nearly Incompressible Material," *Computers & Structures*, 79 (2001) 1671 – 1685

[63] M. Kotelko, "Load-Capacity Estimation and Collapse Analysis of Thin-Walled Beams and Columns – Recent Advances," *Thin-Walled Structures*, 42 (2004) 153 – 175

APPENDICES

A. Implicit Code and Explicit Code

As mentioned in chapter 1, the LS-DYNA is an explicit code while ANSYS is an

implicit code. The differences between the two computer software packages are caused

by the different solution procedures and time integration methods they use. The ANSYS

is an implicit code, which uses the Newmark method. The LS-DYNA is an explicit code

that uses the central difference method. The basic procedures of both integration

methods are introduced below, and the features of each method are then discussed.

a) The Newmark method

for governing the equilibrium equation of a system of finite elements:

$$M\ddot{U} + C\dot{U} + KU = R.$$ A-1

The Newmark integration scheme assumes

$$\dot{U}_{i+1} = \dot{U}_i + [(1-\delta)\ddot{U}_i + \delta\ddot{U}_{i+1}]\Delta t$$ A-2

$$U_{i+1} = U_i + \dot{U}_i\,\Delta t + [(\frac{1}{2}-\alpha)\ddot{U}_i + \alpha\ddot{U}_{i+1}]\Delta t^2$$ A-3

where, α and δ are parameters that can be determined to obtain integration accuracy and

stability; in the Newmark method, $\alpha = \frac{1}{4}$, and $\delta = \frac{1}{2}$. Then, to solve the displacements,

velocities, and accelerations at time t + Δt, the equilibrium equation A-1 is written as:

$$M \ddot{U}_{i+1} + C \dot{U}_{i+1} + KU_{i+1} = R_{i+1}. \qquad \text{A-4}$$

In solving the equation, $\ddot{U}_{i+1}$ is first solved from A-3, which is in terms of U_{i+1}, and then,

substitutes $\ddot{U}_{i+1}$ into A-2. Then the equations for $\ddot{U}_{i+1}$ and $\dot{U}_{i+1}$ are obtained, each in

terms of the unknown displacements U_{i+1} only. The two relations for $\ddot{U}_{i+1}$ and $\dot{U}_{i+1}$ are

substituted into A-4 to solve for U_{i+1}. After that, $\ddot{U}_{i+1}$ and $\dot{U}_{i+1}$ are calculated using A-2

and A-3.

b) The central difference method

In this method, it is assumed that

$$\ddot{U}_i = \frac{1}{\Delta t^2}\left(U_{i-1} - 2U_i + U_{i+1}\right) \qquad \text{A-5}$$

$$\dot{U}_i = \frac{1}{2\Delta t}(U_{i+1} - U_{i-1}) \qquad \text{A-6}$$

for the governing equilibrium equation at time t

$$M \ddot{U}_i + C \dot{U}_i + KU_i = R_i. \qquad \text{A-7}$$

Substituting the relations for $\ddot{U}_i$ and $\dot{U}_i$ shown in A-5 and A-6 into A-7, we have

$$\left(\frac{1}{\Delta t^2} M + \frac{1}{2\Delta t} C\right)U_{i+1} = R_i - \left(K - \frac{2}{\Delta t^2} M\right)U_i - \left(\frac{1}{\Delta t^2} M - \frac{1}{2\Delta t} C\right)U_{i-1} \quad \text{A-8}$$

because the calculation of U_{i+1} involves U_i and U_{i-1}. Before starting the procedure,

U_{-1} is determined. The relations in A-5 and A-6 are used to obtain U_{-1}

$$U_{-1} = U_0 - \Delta t \dot{U}_0 + \frac{\Delta t^2}{2} \ddot{U}_0. \qquad \text{A-9}$$

When comparing the two solution procedures, it is found that the implicit solution

that uses the Newmark method requires matrix inversion to calculate U_{i+1} while, the

explicit solution does not. So compared to the implicit method, the explicit method can

save more on computational costs and can handle a dynamic problem faster. However,

unlike the implicit solution method, which is unconditionally stable for large time steps,

the explicit method is stable only if the time step size is smaller than the critical time step

size for the structure being simulated. The un-damped critical time step size is $2/\omega_n$

(where ω_n is the largest natural circular frequency), which is usually a very small value.

To show the stability problem clearly, a simple un-damping structure with the

equilibrium equation $\ddot{x}_i + \omega^2 x_i = r_i$ is used for the stability analysis of both integration

methods.

a) For the Newmark method related to the implicit analysis, the equations are

$$\ddot{x}_{i+1} + \omega^2 x_{i+1} = r_{i+1} \qquad\qquad\text{A-10}$$

and

$$\dot{x}_{i+1} = \dot{x}_i + [(1-\delta)\ddot{x}_i + \delta \ddot{x}_{i+1}]\Delta t \qquad\qquad\text{A-11}$$

$$x_{i+1} = x_i + \dot{x}_i \Delta t + [(\frac{1}{2} - \alpha)\ddot{x}_i + \alpha \ddot{x}_{i+1}]\Delta t^2 \qquad\qquad\text{A-12}$$

Substituting equations A-11 and A-12 into A-10 using $\alpha = \frac{1}{4}$ and $\delta = \frac{1}{2}$, the following

relation is established:

$$\begin{bmatrix} \ddot{x}_{i+1} \\ \dot{x}_{i+1} \\ x_{i+1} \end{bmatrix} = A \begin{bmatrix} \ddot{x}_i \\ \dot{x}_i \\ x_i \end{bmatrix} + L r_{i+1} \qquad\qquad\text{A-13}$$

166

where,

$$A = \begin{bmatrix} -0.25\beta & -\dfrac{\beta}{\Delta t} & -\dfrac{\beta}{\Delta t^2} \\[2ex] \Delta t[0.5 - 0.125\beta] & 1 - 0.5\beta & -\dfrac{\beta}{2\Delta t} \\[2ex] \Delta t^2[0.25 - 0.0625\beta] & \Delta t[1 - 0.25\beta] & 1 - 0.25\beta \end{bmatrix} \qquad \text{A-14}$$

$$\beta = (\frac{1}{\omega^2 \Delta t^2} + \frac{1}{4})^{-1}, \qquad \text{A-15}$$

which is used to analyze the stability.

If substituting A into the eigenvalue problem Au = λu, λ is solved. For stability, it is required that $|\lambda| \leq 1$. After solving the equation, it is found that for any Δt, the inequality $|\lambda| \leq 1$ is satisfied. Thus, the implicit analysis is unconditionally stable.

b) For the central difference method related to the explicit analysis, the equations are

$$\ddot{x}_i + \omega^2 x_i = r_i \qquad \text{A-16}$$

and

$$\ddot{x}_i = \frac{1}{\Delta t^2}(x_{i-1} - 2x_i + x_{i+1}) \qquad \text{A-17}$$

$$\dot{x}_i = \frac{1}{2\Delta t}(x_{i+1} - x_{i-1}) \qquad \text{A-18}$$

Substituting A-17 and A-18 into A-16 and solving for x_{i+1}, it is obtained that

$$x_{i+1} = (2 - \omega^2 \Delta t^2)x_i - x_{i-1} + \Delta t^2 r_i. \qquad \text{A-19}$$

Solution A-19 is written in the form of A-13 as

$$\begin{bmatrix} x_{i+1} \\ x_i \end{bmatrix} = A \begin{bmatrix} x_i \\ x_{i-1} \end{bmatrix} + Lr_i \qquad \text{A-20}$$

where,

$$A = \begin{bmatrix} 2 & -1 \\ 1 & 0 \end{bmatrix}. \qquad \text{A-21}$$

Substituting this A into the equation $Au = \lambda u$ and solving for the inequality $|\lambda| \leq 1$, it is

found that the inequality is satisfied only when $\Delta t \leq 2/\omega_n$ (where ω_n is the largest natural

circular frequency). Thus, the explicit analysis is conditionally stable.

From the above explanation, it is concluded that for a high-speed impact problem

with small Δt, the computational cost increases dramatically when using implicit analysis,

which includes matrix inversions and may cause divergence. Compared to the implicit

analysis, the explicit analysis is more appropriate for this kind of problem due to its

advantage in saving the computational cost. Its disadvantage of conditional stability can

be ignored because of the small Δt involved. At last, a simple un-damped, two degrees of

freedom system is presented as an example to show how the Newmark method and the

central difference method solve a real problem. The example is taken from Bathe's book,

"Finite Element Procedures," page 773 [50].

Example: Given a simple mass-spring system as shown in figure1,
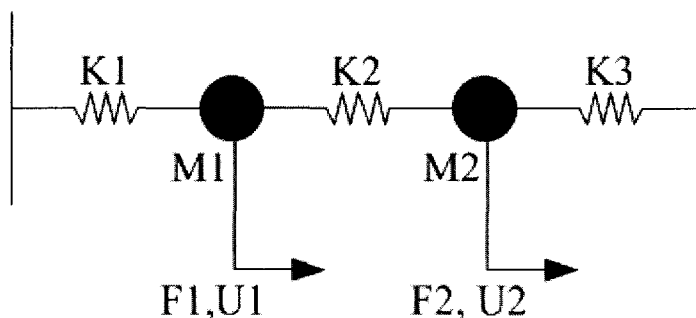
Figure A1. Simple mass-spring system

where, $K_1 = 4N/m$, $K_1 = 2N/m$, $K_1 = 2N/m$, $M_1 = 2kg$, $M_2 = 1kg$, $F_1 = 0$, and $F_2 = 10N$.

The governing equilibrium equation for the system:

$$\begin{bmatrix} M_1 & 0 \\ 0 & M_2 \end{bmatrix} \begin{bmatrix} \ddot{U}_1 \\ \ddot{U}_2 \end{bmatrix} + \begin{bmatrix} K_1 + K_2 & -K_2 \\ -K_2 & K_2 + K_3 \end{bmatrix} \begin{bmatrix} U_1 \\ U_2 \end{bmatrix} = \begin{bmatrix} F_1 \\ F_2 \end{bmatrix},$$

which is

$$\begin{bmatrix} 2 & 0 \\ 0 & 1 \end{bmatrix} \begin{bmatrix} \ddot{U}_1 \\ \ddot{U}_2 \end{bmatrix} + \begin{bmatrix} 6 & -2 \\ -2 & 4 \end{bmatrix} \begin{bmatrix} U_1 \\ U_2 \end{bmatrix} = \begin{bmatrix} 0 \\ 10 \end{bmatrix}.$$

To calculate the response of the system for 12 steps, use the Newmark method and the central difference method separately.

Before solving the problem, the Δt is determined. As the same Δt is used for both methods, an appropriate Δt needs to be calculated to ensure the stability of the central difference method. First, the generalized eigenvalue problem is solved as

$$\begin{bmatrix} 6 & -2 \\ -2 & 4 \end{bmatrix} \phi = \omega^2 \begin{bmatrix} 2 & 0 \\ 0 & 1 \end{bmatrix} \phi \Rightarrow \omega_1^2 = 2, \omega_2^2 = 5 \Rightarrow T_1 = 4.45, T_2 = 2.8.$$

Then, Δt is established as $T_2/10 = 0.28$, which is far below the critical value $2/\omega_n = 0.89$.

Solution:

a) Using the Newmark method

The first step is to calculate $\ddot{U}_{t=0}$. Assume that $U_{t=0} = 0$, and $\dot{U}_{t=0} = 0$. Use

$$\begin{bmatrix} 2 & 0 \\ 0 & 1 \end{bmatrix} \ddot{U}_{t=0} + \begin{bmatrix} 6 & -2 \\ -2 & 4 \end{bmatrix} \begin{bmatrix} U_1 \\ U_2 \end{bmatrix} = \begin{bmatrix} 0 \\ 10 \end{bmatrix} \Rightarrow \ddot{U}_{t=0} = \begin{bmatrix} 0 \\ 10 \end{bmatrix}.$$

Substitute K, M, R and Δt into equations A-2, 3, and 4, to obtain

$$\dot{U}_{i+1} = \dot{U}_i + 0.14 \ddot{U}_i + 0.14 \ddot{U}_{i+1}.$$

Performing these calculations, the final results are

Time	Δt	2Δt	3Δt	4Δt	5Δt	6Δt	7Δt	8Δt	9Δt	10Δt	11Δt	12Δt
U_1	0.00673	0.0505	0.189	0.485	0.961	1.58	2.23	2.76	3.00	2.85	2.28	1.40
U_2	0.364	1.35	2.68	4.00	4.95	5.34	5.13	4.48	3.64	2.90	2.44	2.31

b) Using the central difference method

Similarly, substituting K, M, R, and Δt into equations A-8 and A-9 obtains

$$\begin{bmatrix} 25.5 & 0 \\ 0 & 12.8 \end{bmatrix} U_{i+1} = \begin{bmatrix} 0 \\ 10 \end{bmatrix} + \begin{bmatrix} 45.0 & 2 \\ 2 & 21.5 \end{bmatrix} U_i - \begin{bmatrix} 25.5 & 0 \\ 0 & 12.8 \end{bmatrix} U_{i-1}.$$

The solution for each time step and the final results are

Time	Δt	2Δt	3Δt	4Δt	5Δt	6Δt	7Δt	8Δt	9Δt	10Δt	11Δt	12Δt
U_1	0	0.0307	0.168	0.487	1.02	1.70	2.40	2.91	3.07	2.77	2.04	1.02
U_2	0.392	1.45	2.83	4.14	5.02	5.26	4.90	4.17	3.37	2.78	2.54	2.60

The two sets of results are compared, and the following two Figures plot the

corresponding results. From the figures, it is apparent that both methods provide very

similar results.
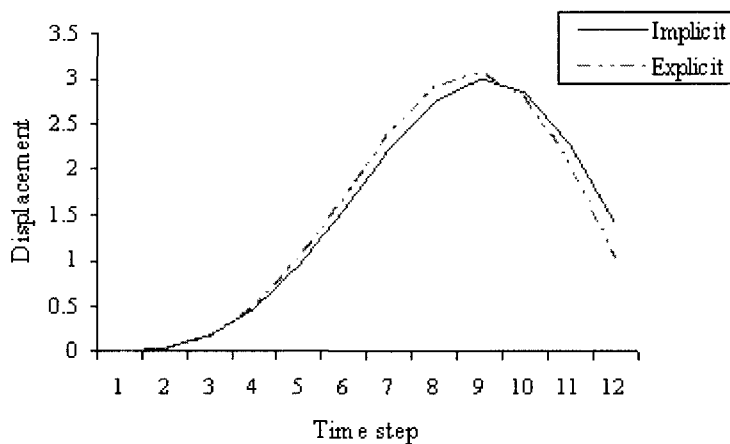
Figure A2. Displacement for first degree of freedom
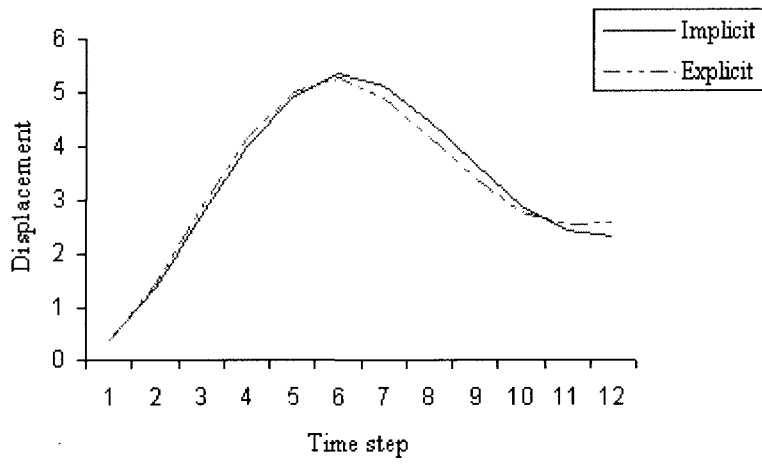
Figure A3. Displacement for second degree of freedom

Note: the subscripts $i, i+1$, and $i-1$ represent the varying parameters at times $t, t+\Delta t$, and $t - \Delta t$ respectively.

B. Dynamic Results Generated by Simplified Models for Thin-walled "Z" Shaped
   Square Section Beam with Different Mesh Densities.
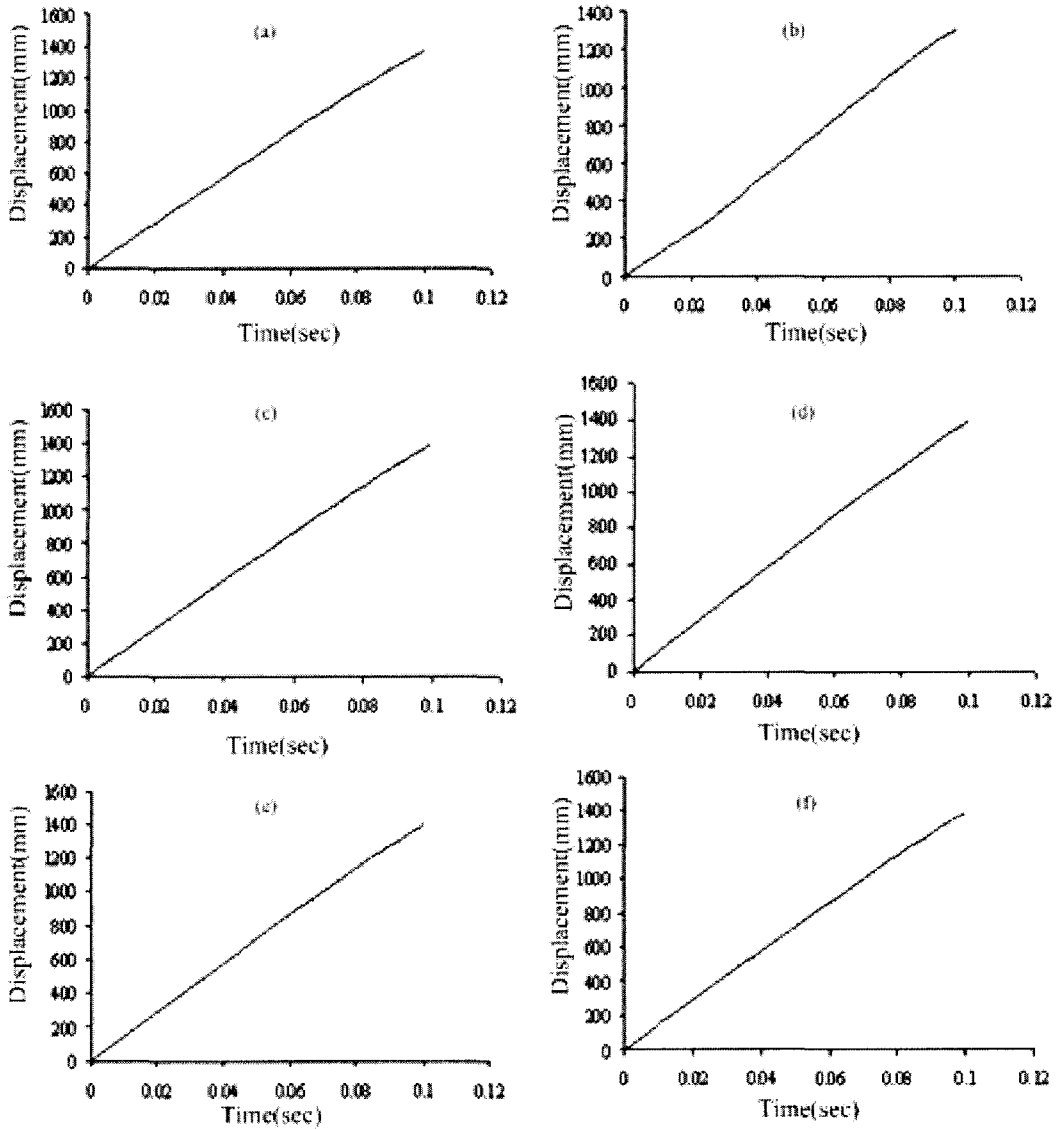
Figure B1. Displacements at end of beam, a) 1-element, b) 2-element, c) 4-element,
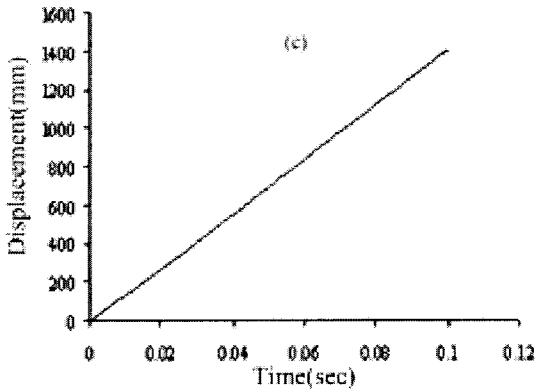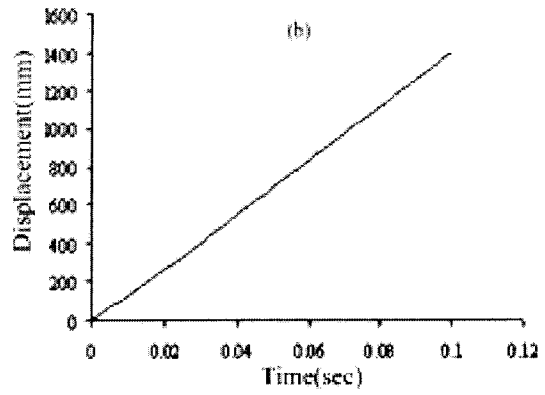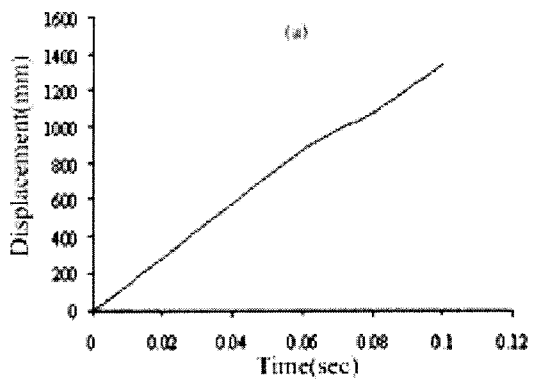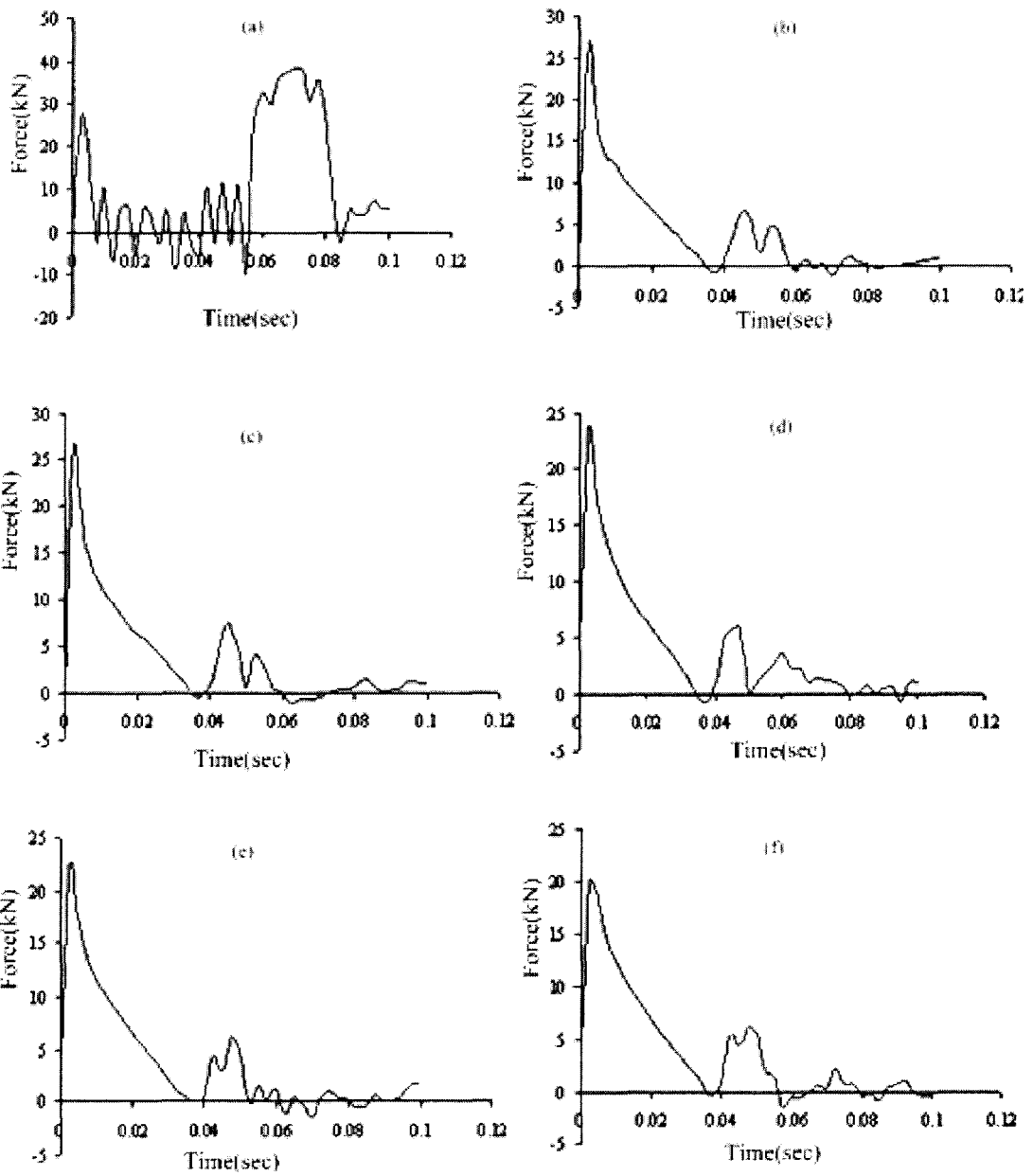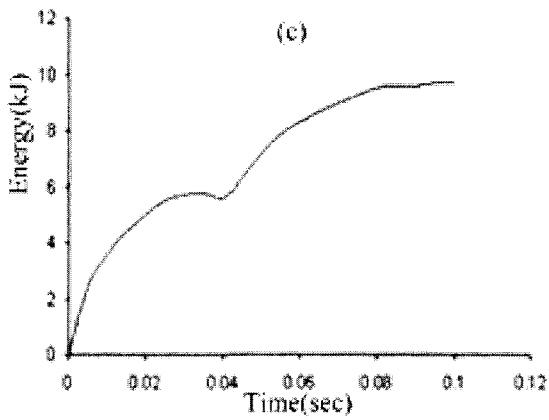d) 8-element, e) 16-element, f) 32-element
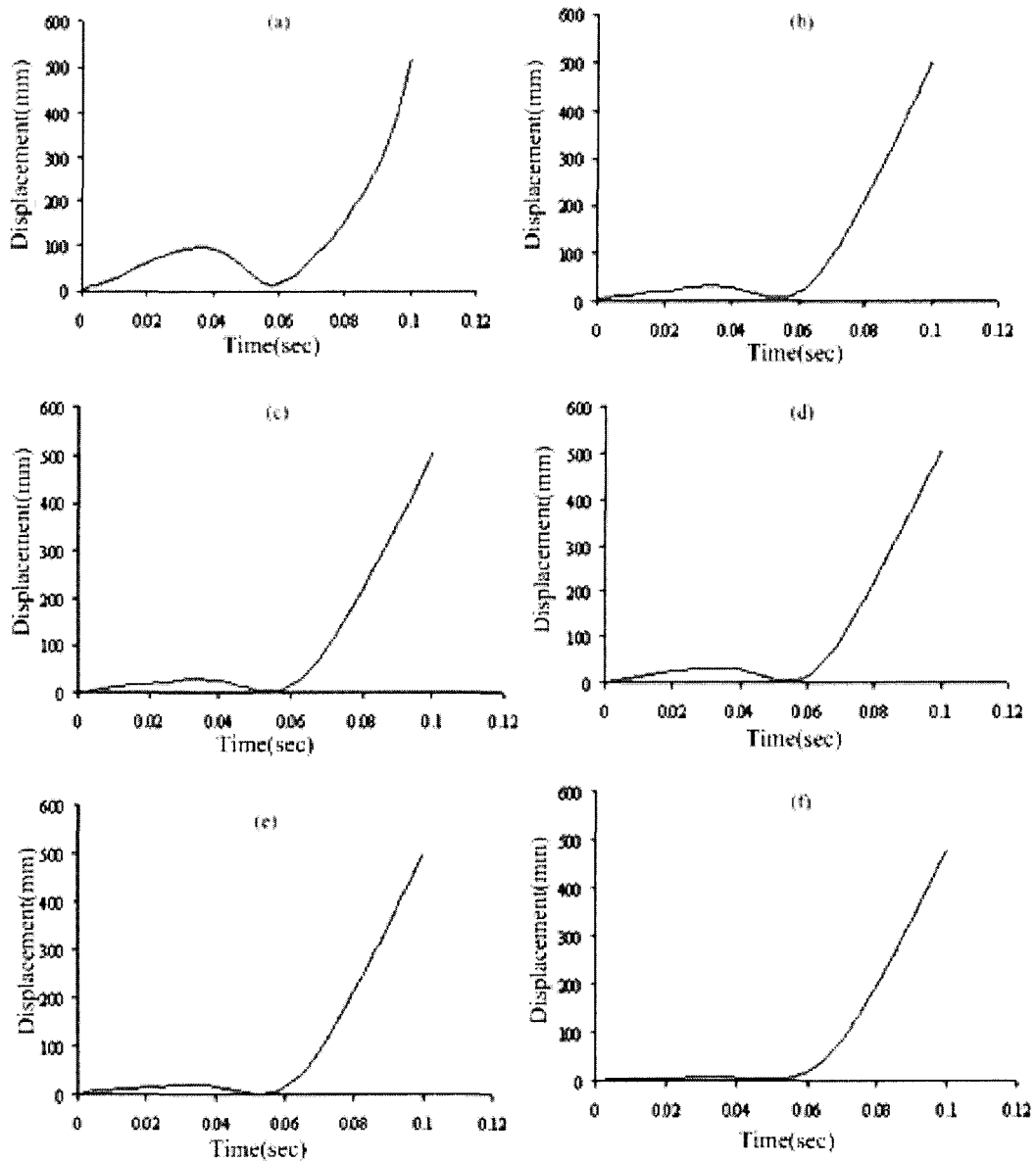
Figure B2. Displacements at hinge1 of beam, a) 1-element, b) 2-element, c) 4-element, d) 8-element, e) 16-element, f) 32-element
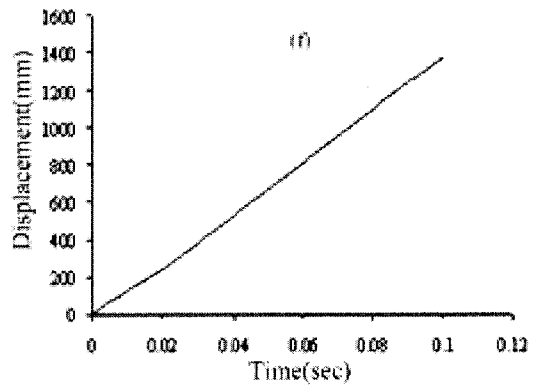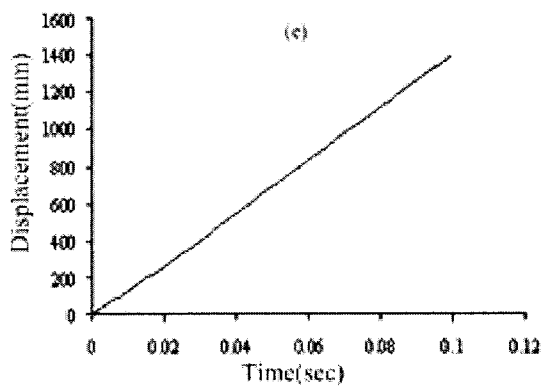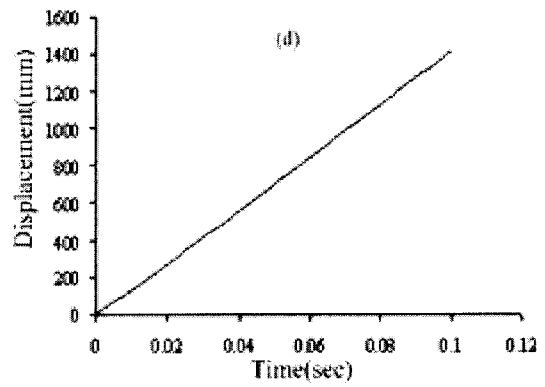
Figure B3. Displacements at hinge2 of beam, a) 1-element, b) 2-element, c) 4-element, d) 8-element, e) 16-element, f) 32-element

Figure B4. Crushing forces of beam, a) 1-element, b) 2-element, c) 4-element, d) 8-element, e) 16-element, f) 32-element
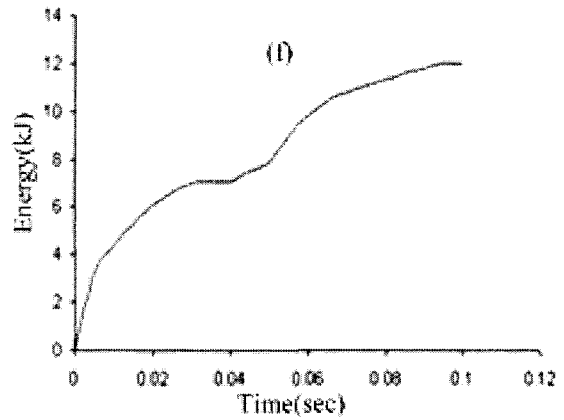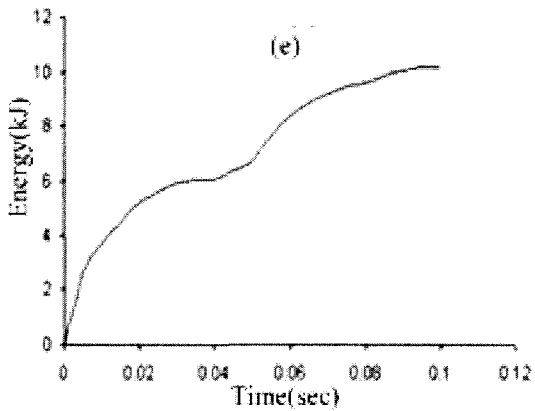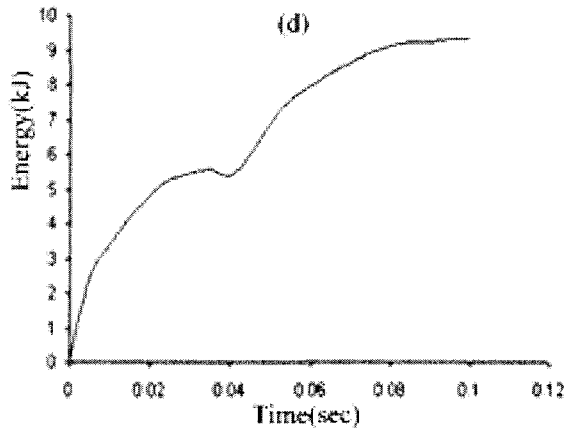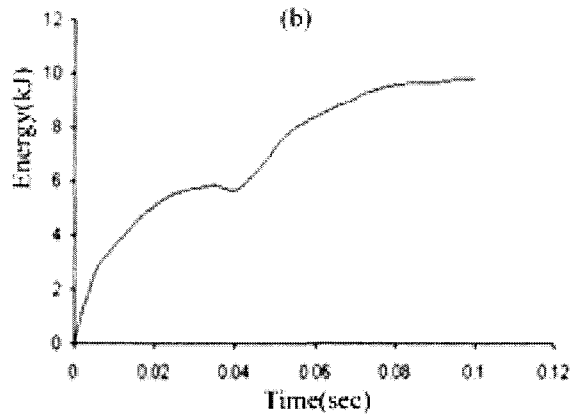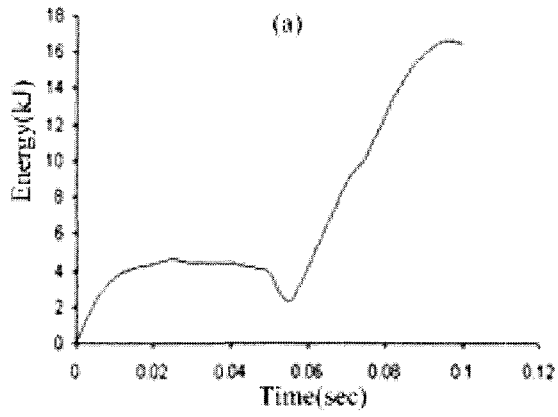
Figure B5. Absorbed energies of beam, a) 1-element, b) 2-element, c) 4-element, d) 8-element, e) 16-element, f) 32-element

C. Dynamic Results Generated by Simplified Models for Thin-walled "S" Shaped Rectangular Section Beam with Different Number of Nonlinear Spring Elements
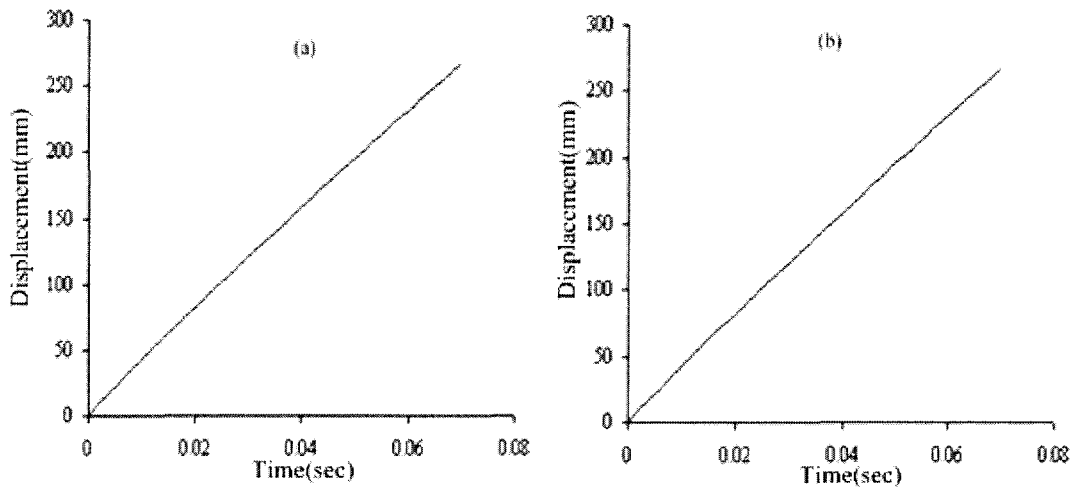

Figure C1. Displacements at end of beam, a) 3-body-3-spring, b) 6-body-6-spring
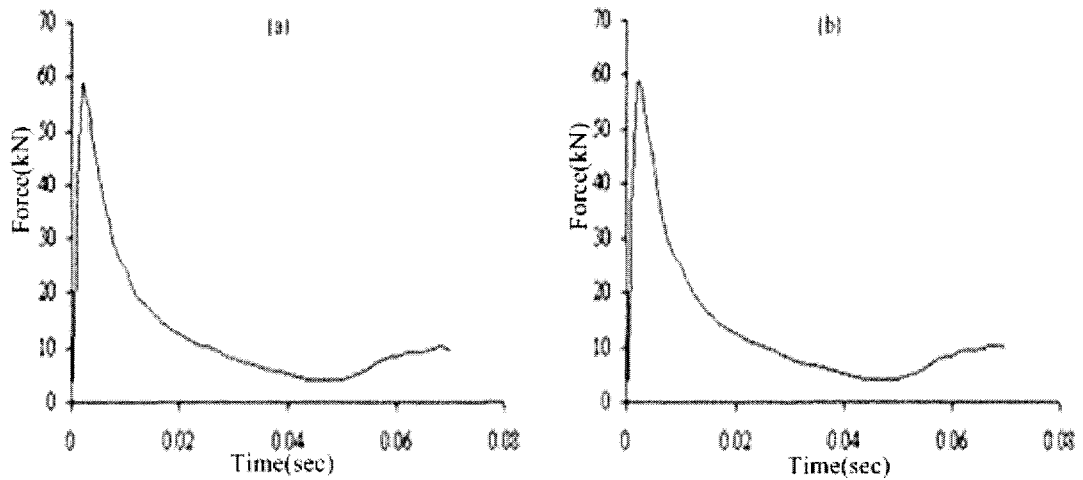

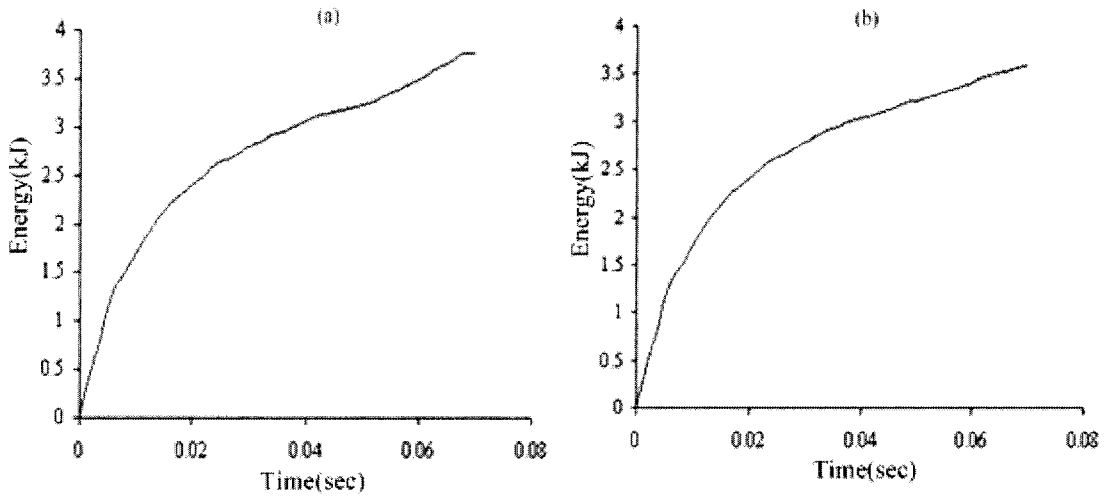Figure C2. Crushing forces of beam, a) 3-body-3-spring, b) 6-body-6-spring

Figure C3. Absorbed energies of beam, a) 3-body-3-spring, b) 6-body-6-spring

D. Dynamic Results Generated by Simplified Models for Thin-walled "Z" Shaped Channel Section Beam with Different Mesh Densities.
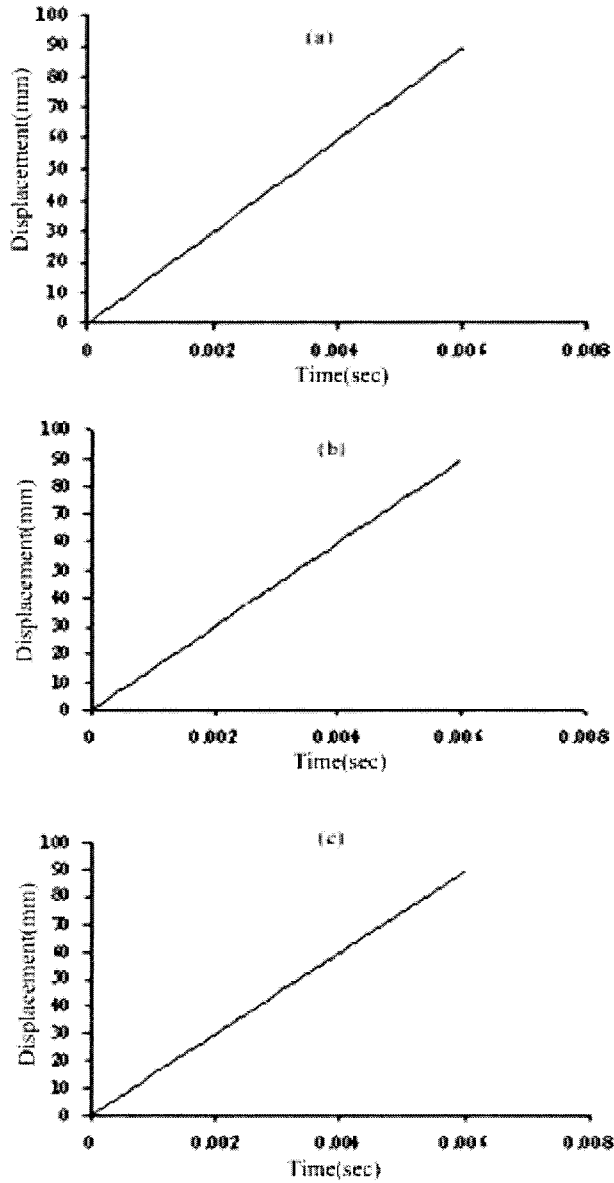

Figure D1. Displacements at end of beam, a) 4-element, b) 8-element, c) 16-element
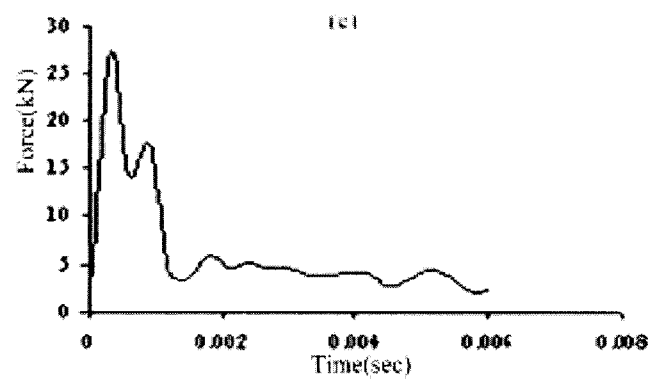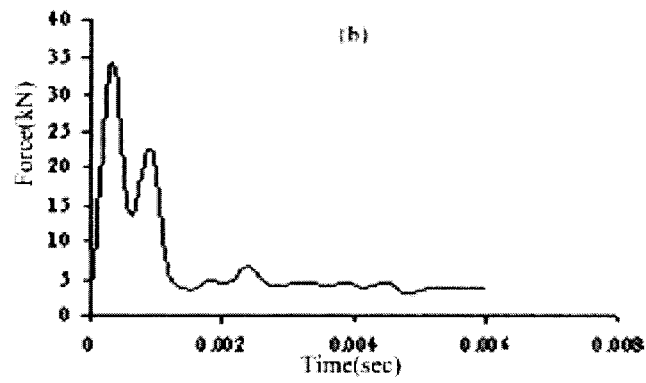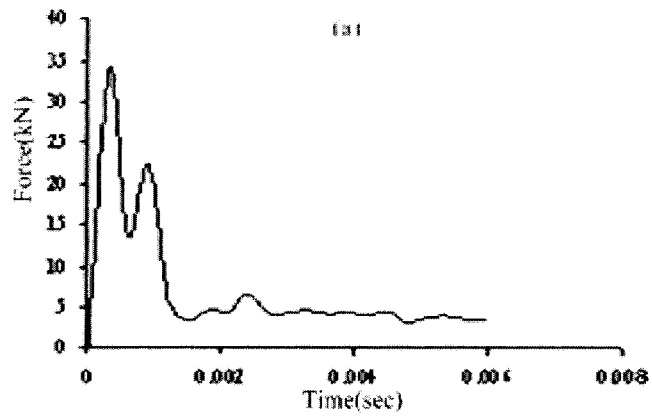
179

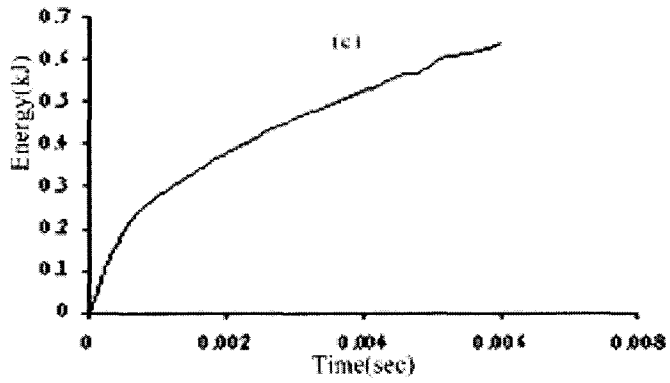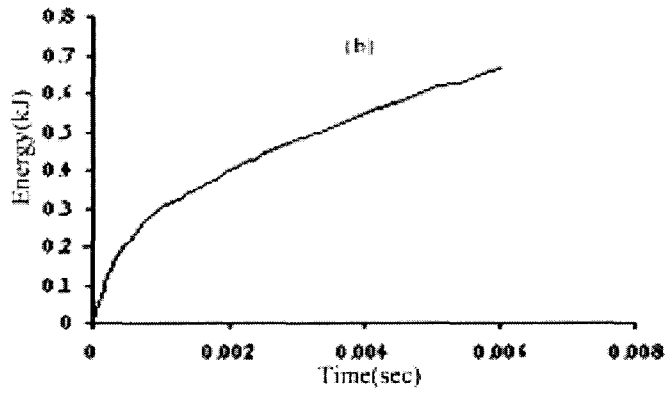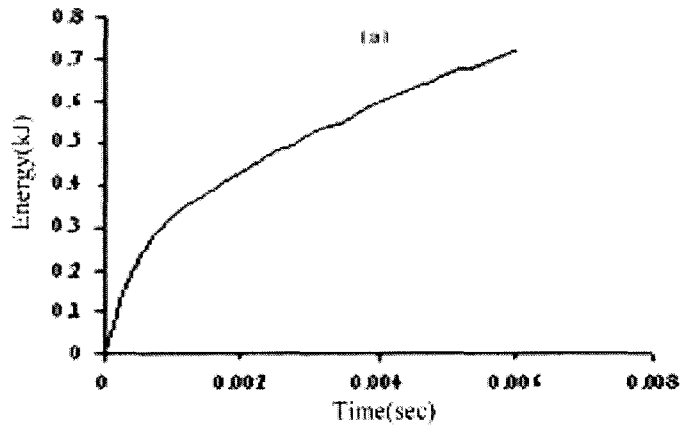Figure D2. Crushing forces of beam, a) 4-element, b) 8-element, c) 16-element

Figure D3. Absorbed energies at end of beam, a) 4-element, b) 8-element, c) 16-element

E. Nomenclature

a	Width of cross-section (web)
b	Depth of cross-section (flange)
C	Average edge length of cross-section
E_{comp}	Energy dissipated along compressive flange
E_{ext}	Total external energy
E_{int}	Total internal energy
E_{ten}	Energy dissipated along tensile flange
E_{web}	Energy dissipated along web
H	Half length of plastic fold
ℓ_i	Length of hinges
$M(\theta)$	Bending moment
M_0	Fully plastic moment per unit length of section wall
M_p	Fully plastic moment of a section
P	Instantaneous crushing force
P_m	Mean crushing force
r	Small rolling radius
s	Web coordinate
t	Wall thickness
u	In-plane displacement along a
α	Folding angle
δ	Axial shortening
θ	Rotation angle
θ_i	Initial angle
θ_J	Angle of jamming
σ_0	Energy equivalent flow stress
σ_u	Ultimate stress
$\dot{\psi}_i$	Relative rotation rate at the i th hinge
ϕ	Out of plane bending
λ	Aspect ratio of cross-section
η	Position of neutral axis

F. List of Abbreviations

2D	Two-dimensional
BC	Boundary condition
CAD	Computer aided design
CAE	Computer aided engineering
DOF	Degree of freedom
FE	Finite element
FEA	Finite element analysis
FOA	First order analysis
MSS	Multi-body system simulation
CMS	Component mode synthesis

CURRICULUM VITAE

NAME: Yucheng Liu

ADDRESS: Department of Mechanical Engineering
            J. B. Speed School of Engineering
            University of Louisville
            Louisville, KY 40292

DOB: Hefei, Anhui, China – January 9, 1976

EDUCATION:

2002-2005   University of Louisville, Doctor of Philosophy degree in Mechanical
            Engineering granted July 2005

2000-2002   University of Louisville, Master of Science degree in Mechanical
            Engineering granted July 2003

1993-1997   Hefei University of Technology, Bachelor of Science degree in
            Mechanical Engineering granted July 1997

EXPERIENCE:

2004-present University of Louisville
            Research Assistant, Development of Software Tools Supporting Structural
            Assessment of Wheeled Tactical Vehicles Project (CMTS)

2000-2002   University of Louisville
            Research Assistant, FORD Improved Materials & Powertrain Architecture
            for 21st Century Trucks Project (IMPACT)

1997-2000   Engineer, Shanghai Yanfeng Automobile Trim Products Co., Ltd.

AWARDS:

2002-2004   University of Louisville, Grosscurth Fellowship

    2001   University of Louisville, Hsing Chuang Award for Excellence in Graduate
            Study

1995-1996   Hefei University of Technology, Scholarship Awarded

1995-1996   Hefei University of Technology, Scholarship Awarded

1993-1994   Hefei University of Technology, Scholarship Awarded

1993-1994   Hefei University of Technology, Scholarship Awarded